Luyao Wang

Structure-Property Correlation on Solvent-Fractionated Lignin to Functional Materials

Åbo Akademi University

Luyao Wang

Born 1992, Jiamusi, Heilongjiang, P.R. China

Previous studies and degrees

B.Sc. Chemical Processing of Forest Products, 2011, Northeast Forestry University, Harbin, Heilongjiang, China

M.Sc. Chemical Engineering, 2015, Qingdao Institute of Bioenergy and Bioprocess Technology, Chinese Academy of Sciences, Qingdao, Shandong, China

Ph.D. studies at the Laboratory of Natural Materials Technology from November of 2018, Åbo Akademi University, Turku/Åbo, Finland

Structure-Property Correlation on Solvent-Fractionated Lignin to Functional Materials

Luyao Wang

Laboratory of Natural Materials Technology
Faculty of Science and Engineering
Åbo Akademi University
Åbo, Finland, 2023

Supervised by

Dr. Xiaoju Wang
Laboratory of Natural Materials Technology
Åbo Akademi University, Åbo, Finland

Co-supervised by

Professor Chunlin Xu
Laboratory of Natural Materials Technology
Åbo Akademi University, Åbo, Finland

Professor Patrik Eklund
Laboratory of Molecular Science and Engineering
Åbo Akademi University, Åbo, Finland

Professor Thomas Rosenau
Department of Chemistry
University of Natural Resources and Life Sciences (BOKU University),
Vienna, Austria

Professor Stefan Willför
Laboratory of Natural Materials Technology
Åbo Akademi University, Åbo, Finland

Pre-examined by

Professor Orlando J. Rojas
Department of Chemical and Biological Engineering
The University of British Columbia, Vancouver, Canada

Associated Professor Olena Sevastyanova
Division of Wood Chemistry and Pulp Technology
KTH Royal Institute of Technology, Stockholm, Sweden

Opponent for the public defense

Professor Orlando J. Rojas
Department of Chemical and Biological Engineering
The University of British Columbia, Vancouver, Canada

ISBN 978-952-12-4313-4 (printed)
ISBN 978-952-12-4314-1 (digital)
Painosalama Oy – Åbo, Finland 2023

Abstract

The abundance of lignin in combination with its impressive properties, *i.e.*, a macromolecule with multifunctional groups, an amphiphilic molecular structure, and a unique nanotechnological advantage of forming nanospheres, have attracted an intensified interest in engaging this natural polyphenol in functional materials. However, native lignin is not the lignin that is available for applications, and the structure of lignin may significantly change during pulping or other biorefinery processes. In this scenario, a given sample of lignin possesses significant variability concerning impurities (*e.g.*, extractives and carbohydrates) and has heterogeneous structural features. These aspects, together with the underlying analytical challenges, have substantially constrained the valorization of lignin. Therefore, fractionation of lignin to produce fractions with decreased heterogeneity and well-defined properties is of utmost importance, leading to breakthroughs in efficiently integrating lignin in functional materials. This thesis is dedicated to using a sequential solvent fractionation approach (isopropyl alcohol, ethanol, and methanol) to establish correlations between the structural characteristics of the lignin fractions and material properties of lignin and to reveal the determining factors of lignin utilization in certain applications. Furthermore, the lignin structure-property correlation will be used to tailor the properties of lignin-integrated functional materials.

The effectiveness of this strategy was validated in the fractionation of birch and spruce alkaline lignin, where lignin fractions with well-defined properties, *e.g.*, molar mass, content of functional groups, and degree of condensation, were obtained. The deployed lignin solvent fractionation strategy revealed fundamental insights into the correlation between the molar-mass-dependent differences of lignin fractions and the chemical accessibility to synthesize a thermosetting lignin-containing phenol-formaldehyde adhesive. In the current work, up to 70% of phenols could be replaced by birch alkaline lignin fractions.

Nano-sized lignin, such as lignin nanoparticles (LNPs), is rising as a class of sustainable nanomaterials, which can function as a template to modulate surface functionalization *via* interfacial interactions. This thesis proposed a high-efficacy route to integrate lignin as a bioplastic in poly (butyl acrylate-*co*-methyl methacrylate) acrylic latex formulation by fabricating polymerization-active LNPs with surface-arranged allyl groups. The interfacial-modulating function on the LNPs regulated the core-shell emulsion polymerization of

acrylate monomers and successfully produced a multi-energy dissipative latex film structure containing a lignin-dominating core. Depending on the surface chemistry metrics of LNPs, such as the abundance of polymerization-active anchors, polymeric flexibility, and surface hydrophobicity, the LNP-integrated latex film could achieve a high toughness almost three times higher than that of the neat latex film.

In addition to chemical functionalization, this thesis also upgraded lignin through a biochemical functionalization strategy. First, a lignin solvent fractionation approach was successfully applied to reveal fundamental insights on the correlation between the lignin structural characteristics and the laccase-assisted oxidation/polymerization properties. The fractionation-dependent lignin polymerization kinetics also brought new insights into *in situ* polymerization of lignin fractions on nanocellulose templates, where the dispersion of nanocellulose with its fiber evenly decorated by aligned LNPs was obtained. Moreover, the cellulose-lignin nanocomposite film exhibited enhanced water barrier properties when compared to the neat cellulose film, which provides a sustainable solution for the development of functional bio-based packaging materials. Second, the lignin reactivity could be fine-tuned using solvent fractionation in combination with the laccase-catalyzed polymerization approach, which endowed LNPs from laccase-polymerized lignin (L-LNPs) with dispersion durability and surface functionality in highly alkaline conditions. Subsequently, the L-LNP was utilized as a highly dispersible and nano-sized polymeric template for *in situ* reduction of Ag^+ from silver ammonia solution (pH 11), which resulted in a uniform surface-embedded hierarchical nanostructure of lignin-silver nanosphere. The durable dispersibility and optical properties of lignin-silver nanospheres endowed the photo-crosslinkable resin of methacrylated *O*-acetyl-galactoglucomannan with improved printing fidelity in three-dimensional printing. In general, this thesis provides green solutions for upgrading lignin with desired properties for efficient chemical integration in functional materials.

Abstrakt

Överskottet av lignin i kombination med dess imponerande egenskaper, det vill säga en makromolekyl med multifunktionella grupper, amfifila egenskaper och en unik nanoteknisk fördel vid bildandet av nanosfärer, har väckt ett intensifierat intresse att dra nytta av denna naturliga polyfenol i funktionella material. Naturligt lignin finns dock inte tillgängligt för dessa applikationer, och strukturen hos lignin kan förändras avsevärt under massatillverkning eller andra bioraffinaderiprocesser. Tekniskt lignin har betydande variationer i avseende på föroreningar (till exempel extraktivämnen och kolhydrater) och har heterogena strukturella egenskaper. Dessa aspekter, tillsammans med de analytiska utmaningarna, har väsentligt begränsat valoriseringen av lignin. Därför är fraktionering av lignin för att producera ligninfraktioner med minskad heterogenitet och väldefinierade egenskaper av största vikt för att leda till genombrott i att effektivt integrera lignin i funktionella material. I denna avhandling användes en fraktioneringsstrategi med sekventiell lösningsmedelsextraktion (isopropylalkohol, etanol och metanol) för att fastställa korrelationer mellan de strukturella egenskaperna hos ligninfraktionerna och materialegenskaperna hos fraktionerna, och för att avslöja de avgörande faktorerna för ligninanvändning i vissa applikationer. Vidare användes ligninstrukturegenskaps-korrelationen för att skräddarsy egenskaperna hos ligninintegrerade funktionella material.

Effektiviteten av denna strategi validerades genom fraktionering av alkaliskt lignin utvunnet från björk eller gran. Ligninfraktionerna som erhölls hade väldefinierade egenskaper, som till exempel molmassa, innehåll av funktionella grupper och kondensationsgrad. Den använda fraktioneringsstrategin med olika lösningsmedel gav grundläggande insikter i korrelationen mellan molmassa hos fraktionen och den kemiska tillgängligheten för att syntetisera ett värmehärdande ligninnehållande fenolformaldehydlim. I detta arbete visades att upp till 70 % fenolerna kunde ersättas med alkaliska ligninfraktioner från björk.

Lignin i nanostorlek, till exempel ligninnanopartiklar (LNP), blir allt viktigare som en klass av hållbara nanomaterial. Dessa kan fungera som en mall för att modulera ytfunktionaliseringen via gränssnittsinteraktioner. I denna avhandling beskrivs en högeffektiv väg att integrera lignin som bioplast i poly(butylakrylat-co-metylmetakrylat)akryllatex genom att tillverka polymerisationsaktiva LNP med allylgrupper på ytan. Genom att modifiera gränsytan på ligninnanopartiklarna kunde kärnemulsionspolymerisationen av

akrylatmonomerer regleras och en multienergidissipativ latexfilmstruktur innehållande en lignindominerande kärna framgångsrikt produceras. Beroende på de ytkemiska egenskaperna för LNP, såsom överskottet av polymerisationsaktiva ankare, polymerflexibilitet och ythydrofobicitet, kan den LNP-integrerade latexfilmen uppnå en hög seghet som är nästan tre gånger högre än den ursprungliga latexfilmens.

I tillägg till kemisk funktionalisering, visar denna avhandling också att lignin kan uppgraderas genom en biokemisk funktionaliseringsstrategi. För det första tillämpades fraktioneringsmetoden av lignin med olika lösningsmedel framgångsrikt för att avslöja grundläggande insikter om korrelationen mellan ligninets strukturella egenskaper och prestandan för lackasassisterad ligninoxidation och -polymerisation. Den fraktioneringsberoende ligninpolymerisations-kinetiken gav också nya insikter i in situ polymerisering av ligninfraktioner på nanocellulosamallar, där en dispersion av nanocellulosa på vars fibrer LNP förekom regelbundet, erhölls. Dessutom uppvisade nanokompositfilmen av cellulosa-lignin förbättrade vattenbarriäregenskaper jämfört med den ursprungliga cellulosafilmen, vilket ger en hållbar lösning för utveckling av funktionella biobaserade förpackningsmaterial. För det andra kunde ligninreaktiviteten finjusteras med hjälp av lösningsmedelsfraktionering i kombination med en lackaskatalyserad polymerisationsmetod, som gav LNP från lackaspolymeriserat lignin (L-LNP) med hög dispersionshållbarhet och ytfunktionalitet vid extrema alkaliska förhållanden. Därefter användes L-LNP som en polymermall i nanostorlek med hög dispergerbarhet för ”in situ”-reduktion av Ag^+ från en silverammoniaklösning (pH 11), vilket resulterade i en enhetlig ytinbäddad hierarkisk nanostruktur av lignin-silvernanosfärer. Den durabla dispergerbarheten och de optiska egenskaperna hos nanosfärer av lignin-silver gav det fototvärbindningsbara hartset av metakrylerad O-acetyl-galaktoglukomannan en förbättrad tillförlitlighet vid tredimensionell utskrift. Generellt ger denna avhandling gröna lösningar för uppgradering av lignin med önskade egenskaper för effektiv kemisk integration i funktionella material.

List of included publications

The thesis is based on the following 4 publications. The publications are reprinted here with permission from the publishers.

I. Tailored thermosetting wood adhesive based on well-defined hardwood lignin fractions

L. Wang, L. Lagerquist, Y. Zhang, R. Koppolu, T. Tirri, I. Sulaeva, S. von Schoultz, L. Vähäsalo, A. Pranovich, T. Rosenau, P. Eklund, S. Willför, C. Xu, X. Wang. *ACS Sustainable Chem. Eng.* **2020**, 8 (35), 13517–13526.

The author planned the experimental work together with the co-authors. The author carried out the main experiment work and drafted the manuscript.

II. Template-directed polymerization of binary acrylate monomers on surface-activated lignin nanoparticles in toughening of bio-latex films

L. Wang, Q. Wang, E. Rosqvist, J-H. Smått, Q. Yong, L. Lassila, J. Peltonen, T. Rosenau, M. Toivakka, S. Willför, P. Eklund, C. Xu, X. Wang. *Small* **2023**, 19 (24), 2207085.

The author planned the experimental work together with the co-authors. L. Wang performed the main experiment work and data interpretation and drafted the manuscript. Q. Wang carried out the lab work on DMA analysis of film samples. E. Rosqvist contributed to the AFM measurement.

III. On laccase-catalyzed polymerization of biorefinery lignin fractions and alignment of lignin nanoparticles on the nanocellulose surface *via* one-pot water-phase synthesis

L. Wang, L. Tan, L. Hu, X. Wang, R. Koppolu, T. Tirri, B. van Bochove, P. Ihalainen, L. S. Seleenmary Sobhanadhas, J. V. Seppälä, S. Willför, M. Toivakka, C. Xu. *ACS Sustainable Chem. Eng*. **2021**, 9 (26), 8770–8782.

L. Wang, L. Tan, and L. Hu equally contributed to the data collection, analysis, and interpretation. L. Tan initially validated the laccase-polymerization parameters. L. Wang carried out the lignin fractionation and the multiple-instrumental characterizations on the polymerized samples. L. Hu carried out the lab work on the *in situ* polymerization of lignin with nanocellulose and further film-making and its characterizations. L. Wang and X. Wang drafted the manuscript together.

C. Xu and X. Wang are the main principal scientists who conceptualized and cosupervised the work.

IV. Digital light processing (DLP) 3D-fabricated antimicrobial hydrogel with a sustainable resin of methacrylated woody polysaccharides and hybrid silver-lignin nanospheres

L. Wang, Q. Wang, A. Slita, O. Backman, Z. Gounani, E. Rosqvist, J. Peltonen, S. Willför, C. Xu, J. M. Rosenholm, X. Wang. *Green Chem*. **2022**, 24, 2129–2145.

L. Wang, C. Xu, and X. Wang conceived and initiated the work. All the authors contributed to experimental design, planning, execution, and data analysis. L. Wang carried out the main experiment work and drafted the manuscript.

List of supporting publications

I. Fractionation of lignin with decreased heterogeneity: Based on a detailed characteristics study of sequentially extracted softwood kraft lignin
R. Liu, A. Smeds, **L. Wang**, A. Pranovich, J. Hemming, S. Willför, H. Zhang, C. Xu. *ACS Sustainable Chem. Eng.* **2021**, 9 (41), 13862–13873.

II. Functional lignin nanoparticles with tunable size and surface properties: Fabrication, characterization, and use in layer-by-layer assembly
N. Alipoormazandarani, T. Benselfelt, **L. Wang**, X. Wang, C. Xu, L. Wågberg, S. Willför, P. Fatehi. *ACS Appl. Mater. Interfaces* **2021**, 13 (22), 26308–26317.

III. AqSO biorefinery: a green and parameter-controlled process for the production of lignin-carbohydrate hybrid materials
D. Tarasov, P. Schlee, A. Pranovich, A. Moreno, **L. Wang**, D. Rigo, M. H. Sipponen, C. Xu, M. Balakshin. *Green Chem*. **2022**, 24, 6639–6656.

IV. Synthesis of galactoglucomannan-based latex *via* emulsion polymerization
Q. Yong, J. Xu, **L. Wang**, T. Tirri, H. Gao, Y. Liao, M. Toivakka, C. Xu. *Carbohydrate Polymers* **2022**, 291, 119565.

Selected conference and seminar contributions

I. **L. Wang**, Q. Wang, A. Slita, C. Xu, J. M. Rosenholm, X. Wang. All-wood-based antimicrobial hydrogel fabricated by digital light processing (DLP) printing, oral presentation at *TAPPI Nano*, Virtual Conference, 15–16 June **2021**

II. **L. Wang**, L. Hu, X. Wang, C. Xu. On laccase-catalyzed polymerization of alkaline lignin fractions in aqueous alkaline solution, proceeding and oral presentation at *International Conference on Polyphenols (ICP)*, Virtual Conference, 13–15 July **2021**

III. **L. Wang**, S. Willför, P. Eklund, T. Rosenau, C. Xu, X. Wang. Solvent-fractionated alkaline lignins: from analysis and structure-property correlations to functional materials, oral presentation at *Lignin Valorisation Conference* in Wageningen, Netherlands, 1–3 June **2022**

IV. **L. Wang**, L. Hu, S. Willför, M. Toivakka, X. Wang, C. Xu. Laccase-catalyzed polymerization of lignin towards their chemical integration to functional materials, oral presentation by C. Xu at *Nordic Polymer Days* in Gothenburg, Sweden, 1–3 June **2022**

V. **L. Wang**. Tailored thermosetting wood adhesive based on well-defined lignin fractions: Lignin structure-property-performance correlation, oral presentation at *16th European Workshop on Lignocellulosics and Pulp (EWLP)* in Gothenburg, Sweden, 28 June–1 July **2022**

VI. **L. Wang**, T. Rosenau, M. Toivakka, S. Willför, P. Eklund, C. Xu, X. Wang. Lignin-Nanoparticle-Integrated core-shell latex colloids towards sustainable coating, oral presentation at *CA17128 LignoCOST Working Groups meeting (physical)* in Reims, France, 1–2 February **2023**

VII. **L. Wang**, T. Rosenau, M. Toivakka, S. Willför, P. Eklund, C. Xu, X. Wang. Lignin-Nanoparticle-Integrated core-shell latex colloids towards sustainable coating, oral presentation at *21st International Symposium on Wood, Fiber and Pulping Chemistry* (iswfpc) in Venice, Italy, 4–7 July **2023**

List of abbreviations

3D	Three-dimensional
AL	Alkaline lignin
A-LNPs	Allylated LNPs
AFM	Atomic force microscopy
APS	Ammonium persulfate
α_0	Lattice constant
BA	Butyl acrylate
CNF	Cellulose nanofibers
$Cr(acac)_3$	Chromium(III) acetylacetonate
$CDCl_3$	Deuterated chloroform
$C_{Ar\text{-}H}$	Methine carbons
$Đ$	Dispersity
$Đ_M$	Molar mass dispersity
DC	Degree of condensation
$D_{1/2}$	Decomposition temperature at 50% weight loss
DLP	Digital light processing
DSC	Differential scanning calorimetry
DMSO	Dimethyl sulfoxide
DMSO-d_6	Deuterated DMSO
DMA	Dynamic mechanical analyzer
d_{inter}	Average interfacial domain boundary size
E'	Extensional storage modulus
E''	Extensional loss modulus
EtOH	Ethanol
EtOAc	Ethyl acetate
FID	Flame ionization detector
G-subunit	Guaiacyl subunit
GC	Gas chromatography
GGM	*O*-acetyl-galactoglucomannan
GGMMA	Methacrylated GGM
H-subunit	*p*-hydroxyphenyl subunit
HSQC	Multiplicity-edited heteronuclear single quantum coherence
H_2SO_4	Sulfuric acid
HPLC	High-performance liquid chromatograph
i-PrOH	Isopropyl alcohol
ICP-OES	Inductively coupled plasma-optical emission spectroscopy

LPF	Lignin-containing phenol-formaldehyde
LNPs	Lignin nanoparticles
L-LNPs	LNPs from laccase-polymerized lignin
L-LNP@Ag	L-LNPs with surface-embedded silver nanoparticles
LAP	Lithium phenyl-2,4,6-trimethylbenzoylphosphinate
L/P	Lignin to phenol mass ratio
Macro-CT	Macromolecular chain-transfer agent
MeOH	Methanol
MMA	Methyl methacrylate
MTBE	Methyl tert-butyl ether
MFC	Microfibrillated cellulose
M_W	Weight-average molar mass
NaOH	Sodium hydroxide
NMR	Nuclear magnetic resonance
N_2	Nitrogen
O_2	Oxygen
PMMA	Poly(methyl methacrylate)
PHWE	Pressurized hot water extraction
Py/GC-MS	Pyrolysis-gas chromatography-mass spectrometry
pBM	Poly(butyl acrylate-*co*-methyl methacrylate)
PF-QNM	PeakForce quantitative nanomechanical mapping
RCF	Reductive catalytic fractionation
RED	Relative energy difference between solvent and lignin
S-subunit	Syringyl subunit
SEC	Size exclusion chromatography
SDS	Sodium dodecyl sulfate
SAXS	Small-angle X-ray scattering
THF	Tetrahydrofuran
Tg	Glass transition temperature
TEM	Transmission electron microscopy
WCA	Water contact angle
WVTR	Water vapor transmission rate
XPS	X-ray photoelectron spectroscopy
XRD	X-ray diffraction
Z-average	Intensity-weighted average hydrodynamic diameter

Table of contents

1. Introduction

1.1. Lignin valorization: Importance and challenges

As the most abundant aromatic biopolymer in nature, lignin is exploited in many prospective products, such as thermosets, thermoplastics, lignin-based functional supports/carriers, nanoscale and microscale applications, and advanced three-dimensional (3D) printing materials. Conventional fiber-based biorefinery in combination with ethanol-based biorefinery processes that have been commissioned in recent years, such as Cellunolix® biorefinery and Formicobio™ technology, and *in situ* lignin functionalization biorefinery processes, such as Ecohelix technology for the production of lignin-carbohydrate polymer, and LigniOx process for ready-to-use water-soluble alkaline lignin (AL) production, are expected to expand the market of lignin and maximize the revenue of potential applications *vs.* lignin production costs.[1]

Lignin utilization in material applications is crucial from the perspective of biorefinery profitability and future circular economy. However, technical lignin imposes significant challenges to replacing most petrochemical-based feedstocks and integrating them into functional materials. These challenges affecting industrial lignin valorization are mainly: (i) lignin is not valued in the fiber-based and/or ethanol-based lignocellulose fractionation processes, (ii) lignin is inherently heterogeneous in terms of impurities, structural characteristics, functionalities, and molar mass dispersity ($Đ_M$), and (iii) the exaggerated understanding of lignin, such as lignin from any process is suitable for any application.

1.2. Hypothesis and research objectives

The hypotheses of this thesis were as follows:

i) Lignin can be covalently integrated into advanced materials (*e.g.*, phenolic resins) since the phenolic macromolecular backbone has the chemical characteristics required for chemical and biochemical functionalization. The heterogeneity of lignin can be decreased using fractionation strategies, which can further improve material properties.

ii) An efficient fractionation approach can refine lignin in terms of molar mass, $Đ_M$, structural properties, and functionalities, which may result in differences in the reactivity of lignin in chemical and biochemical integration to functional materials. Therefore, it is expected to obtain

lignin-containing materials with tailored properties, which can facilitate the establishment of correlations between lignin structural characteristics and the properties of the resulting materials.

iii) Lignin can be transferred from bulk material to lignin nanoparticles (LNPs) due to its amphiphilic structural properties. Lignin molecules with different structural characteristics can affect their self-assembly process in water and result in LNPs with application-specific properties, such as particle size, tailored surface functionality, and stability in chemically demanding conditions. The application of LNPs can then be extended to surface-active structural templates for devising functional nanomaterials through surface reactions (*e.g.*, emulsion polymerization and redox reactions). The molecular-scale differences on the LNPs surfaces can be recognized during the chemical integration and may result in nanocomposites with tailored properties.

iv) Chemical and biochemical functionalization of lignin should also be effective tools for modulating the nucleation-and-growth process of lignin molecules on other bio-based nanostructured templates (*e.g.*, nanocellulose fibers). This hypothesized mechanism may result in bio-based nanomaterials with tailored interfacial interactions and physiochemical properties, and open up possibilities to obtain processable dispersions for different application forms, such as functional films and coatings.

The overall objective of this thesis is the development of methodologies (*e.g.*, lignin fractionation and lignin chemical and biochemical functionalization) for upgrading technical lignin with desired properties for efficient chemical integration to functional materials. Bio-based alternatives will be developed for fossil-based thermosets, thermoplastics, and nanomaterials in different applications. More specifically, this thesis targeted to establish lignin structure-material property correlations for understanding the determining factors of lignin utilization in thermosets (*e.g.*, phenolic wood adhesives), thermoplastics (*e.g.*, acrylate latex), and nanomaterials (*e.g.*, nanocellulose-LNPs) at the molecular level and provide future perspectives on the best niche for specific lignin in specific application fields. This thesis also aimed to explore facile and green solutions for tailoring LNPs to structural templates with well-defined surface chemistry metrics for efficient surface reactions to prepare hybrid nanomaterials and bio-latex colloids with high lignin content.

1.3. Research overview

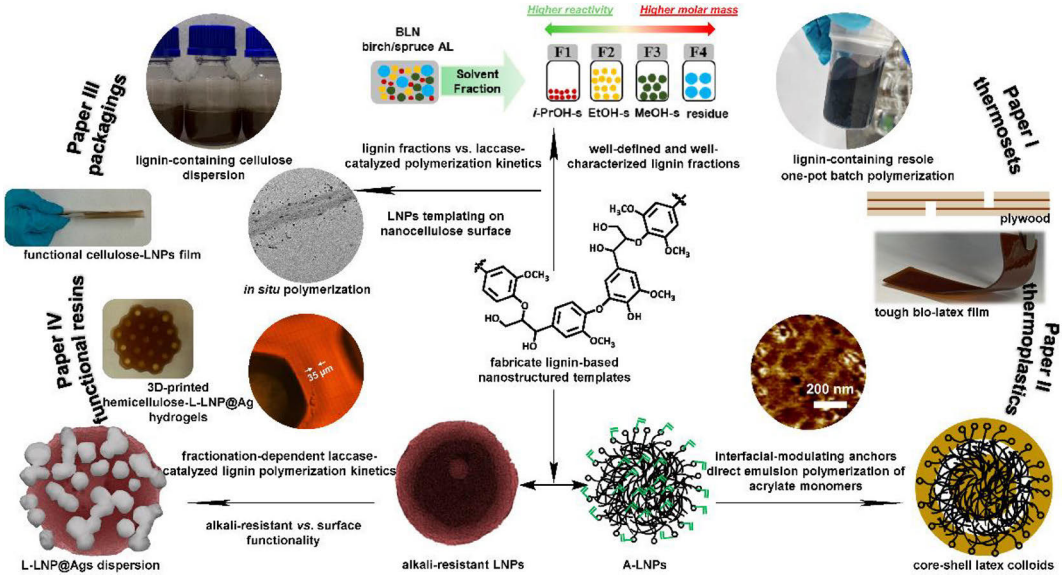

Figure 1.1. *Overview of the thesis work.*

The research overview of this thesis (**Figure 1.1**) and the research tasks to achieve the main objective are as follows:

i) To develop efficient lignin fractionation strategies for hardwood (*i.e.*, birch) and softwood (*i.e.*, spruce) AL and to prepare well-characterized lignin fractions with well-defined properties for lignin structure-property correlation studies (Paper I)

ii) To determine the correlation of lignin structural characteristics (*e.g.*, chemical reactivity and steric accessibility of reactive sites) with the efficiency of lignin phenolation and polymerization in phenolic resins to tailor the wet bonding strength of thermosets (Paper I)

iii) To develop lignin-based nanostructured templates (*e.g.*, LNPs with surface-distributed allyl groups) with different surface accessibility in emulsion polymerization for efficient integration of LNPs into thermoplastic latex colloids and to evaluate the potential for dispersion coating applications (Paper II)

iv) To develop sustainable processing approaches, such as enzymatic lignin valorization strategies, to tailor the properties of lignin as polymeric materials and to provide fundamental insights on the

correlation between lignin structural characteristics and laccase-catalyzed lignin polymerization kinetics (Paper III)

v) To utilize fractionation-dependent lignin polymerization kinetics to modulate the morphology and dispersibility of *in situ* laccase-polymerized lignin (nanoscale lignin) on nanocellulose structural templates (Paper III), and to trade off the alkali resistance and surface functionality of LNPs for *in situ* reduction of Ag^{+} in highly alkaline conditions (Paper IV)

vi) To demonstrate the value-added potential of lignin-based nanomaterials and other wood-derived polymers, such as lignin-cellulose dispersions for sustainable packaging applications (Paper III), and lignin-hemicellulose photo-crosslinkable resins for constructing antimicrobial hydrogels *via* additive manufacturing approaches, *e.g.*, 3D printing (Paper IV)

vii) To propose feasible strategies to control the physiochemical properties of LNPs for specific applications, *e.g.*, surface accessibility of LNPs for core-shell emulsion polymerization (Paper II) and the nanomorphology and crystalline characteristics of hybrid lignin-silver nanoparticles (Paper IV)

2. Background

2.1. Lignocellulosic biomass

2.1.1. Sources and structural composition

Lignocellulosic biomass is the organic matter produced by plants through photosynthesis. Lignocellulose is characterized by its main components being polysaccharides, *e.g.*, cellulose (40 – 55%) and hemicelluloses (20 – 40%), and an aromatic biopolymer, lignin (8 – 30%), as well as a wide variety of low molar mass compounds known as extractives (1 – 10%).[2] Terrestrial plants (*e.g.*, trees, bushes, grasses), agriculture wastes (*e.g.*, sugarcane bagasse, corn stover, cereal straw), forest residues (*e.g.*, wood chips, sawdust), and perennial energy crops (*e.g.*, switchgrass) are all viable sources of lignocellulosic biomass. Nevertheless, the content of the main chemical compounds in lignocellulosic biomass varies depending on the plant source (**Table 2.1**).

Table 2.1. Structural composition of representative lignocellulosic feedstocks.[3–7]

sources	compositions (% of total dry weight)		
	cellulose	hemicelluloses	lignin
softwood stems	45 – 50	25 – 35	25 – 35
hardwood stems	40 – 50	24 – 40	18 – 25
grasses	25 – 40	35 – 50	10 – 30
wheat straw	33 – 40	20 – 25	15 – 20
switchgrass	30 – 50	10 – 40	5 – 20

Plant-derived cellulose is a linear homopolysaccharide composed of β-(1→4)-D-glucopyranose units in a $^4C_1$ chair conformation (**Figure 2.1**).

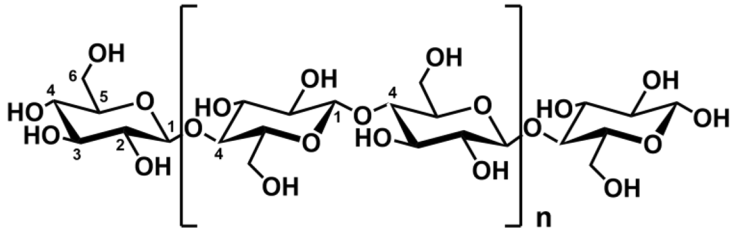

Figure 2.1. *The structure of cellulose drawn as a chair conformation demonstrating the cellobiose unit joint by the β-(1→4) glycosidic linkages.*

Wood has long been used for pulp and paper production. The cellulose polymers from wood pulp have typical chain lengths of 300 to 1700 glucose units.[8] Multiple hydroxyl groups on the cellulose chain can form intra- and inter-molecular hydrogen bonds, which can control the assembly of cellulose molecules.[9] The hierarchical levels of the cellulose fiber, *i.e.*, elementary fibril

composed of supramolecular cellulose chains (~ 1 nm), microfibril (~ 3 nm), microfibril bundle (~ 10 nm), macrofibril (~1 μm), and fiber (~10 μm),[10] contribute to the formation of lamella structures of the wood cell wall.

Hemicelluloses in plants are closely associated with cellulose and contribute to cell wall development, but they do not have a well-defined structure as cellulose. Hemicelluloses are a collective term for heteropolysaccharides. The structural backbone of hemicelluloses is monosaccharides of pentoses (*e.g.*, xylose) and/or hexoses (*e.g.*, glucose, mannose, galactose) connected with *β*-(1→4) glycosidic bonds and their acidic units. The main structural characteristics of hemicelluloses include branching and *in situ* functionalization of hydroxyl groups with acetyl and methyl groups during biosynthesis (**Figure 2.2**). Hemicelluloses vary considerably among plant species. In softwood (gymnosperm) secondary cell wall, *O*-acetyl galactoglucomannans (GGM, 20 – 25%), followed by arabino-4-*O*-methylglucuronoxylans (5 – 10%) being the most abundant hemicelluloses. *O*-acetyl-4-*O*-methylglucuronoxylans (15 – 30%) are the primary hemicelluloses in hardwood (angiosperm) secondary cell wall, followed by glucomannans (2 – 5%).[11]

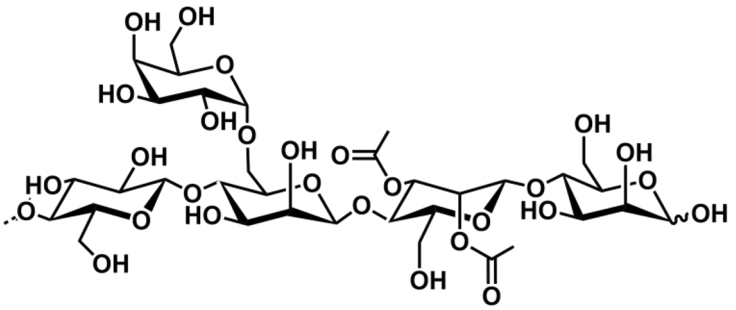

Figure 2.2. *The structure of GGM demonstrating branching and acetylation.*

Lignin is an amorphous and branched aromatic biopolymer composed of phenyl propane units as the main building block, which is predominantly found around arrays of cellulose and hemicelluloses to form secondary cell walls (**Figure 2.3**).[12] In 1839, Anselme Payen discovered lignin in wood, which was considered as the incrusting material that must be removed to isolate cellulose fibers.[13] In plants, the hydrophobic nature of lignin endows it with diffusion barrier properties, which is crucial for the transport of water and nutrition. Since lignin is abundant in the middle lamella of wood cells, functioning as

internal 'glue' between cell walls,[14] it can also provide mechanical strength of plant organs and resistance to biotic degradation.

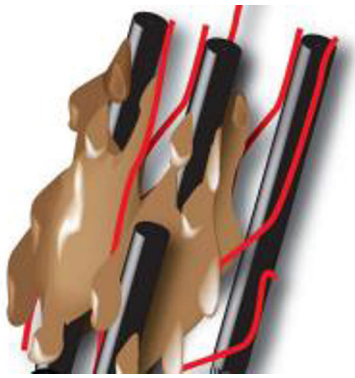

Figure 2.3. *Plant cells are surrounded by a recalcitrant cell wall mainly composed of cellulose (black). The microfibrils of cellulose are crosslinked by hemicelluloses (red) and the resulting polysaccharide network is embedded in lignin (brown).*[15]

2.1.2. Lignin biosynthesis and structural features

Lignin is synthesized *via* biosynthetic pathways from monolignols in the plant cell walls. It is generally accepted that lignin biosynthesis involves three basic propylphenol derivatives: *p*-coumaryl alcohol, coniferyl alcohol, and sinapyl alcohol (**Figure 2.4a–c**).[16] These three monolignols are widely known as *p*-hydroxyphenyl (H), guaiacyl (G), and syringyl (S) subunits (**Figure 2.4d–f**). In plant cell walls, phenoloxidases (*e.g.*, laccase and peroxidase) initiate phenoxy radicals that generate resonances in lignin molecules (**Figure 2.4g**). The oxidative radical-radical coupling of monolignols *via* the quinone methide intermediate results in a lignin macromolecular backbone with irregularly connected ether and carbon-carbon interunit linkages. The native lignin linkages include arylglycerol *β*-aryl ether (*β*-O-4'), phenylcoumaran (*β*-5'), resinol (*β*-*β'*), dibenzodioxocin (5-5'/*β*-O-4'), and spirodienone (*β*-*1'*) (**Figure 2.5**), while the structural alternations in lignin upon chemical pulping and biorefinery lead to the formation of enol ether, aryl glycerol, stilbene, episesinol (*β*-*β'*), 5-5', 4-O-5', and *α*-5' interunit linkages (**Figure 2.6**).[17] Extensive research has been devoted to understanding the kinetics of phenoxy radical coupling in lignin macromolecules. Sangha *et al*. computed the reaction enthalpies for the initial self- and cross-coupling reactions of monolignol radicals to form dimeric intermediates.[18] The *β*-O-4', *β*-*β'*, and *β*-5' couplings were computed to be the most favorable, whereas the *β*-1', 5-5', and 4-O-5' linkages were less favorable.[18]

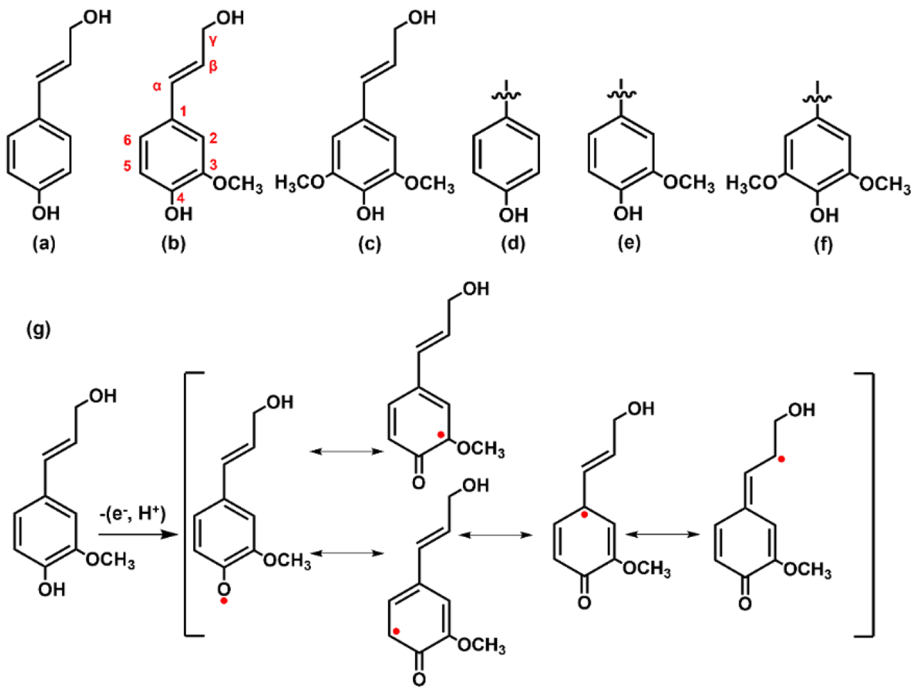

Figure 2.4. *Monolignol of (a) p-coumaryl alcohol, (b) coniferyl alcohol, and (c) sinapyl alcohol. 1–6 and α–γ in (b) denote aromatic and aliphatic carbons, respectively. (d) H-subunit, (e) G-subunit, and S-subunit of lignin. (g) Resonance structures of phenoxy radicals.*

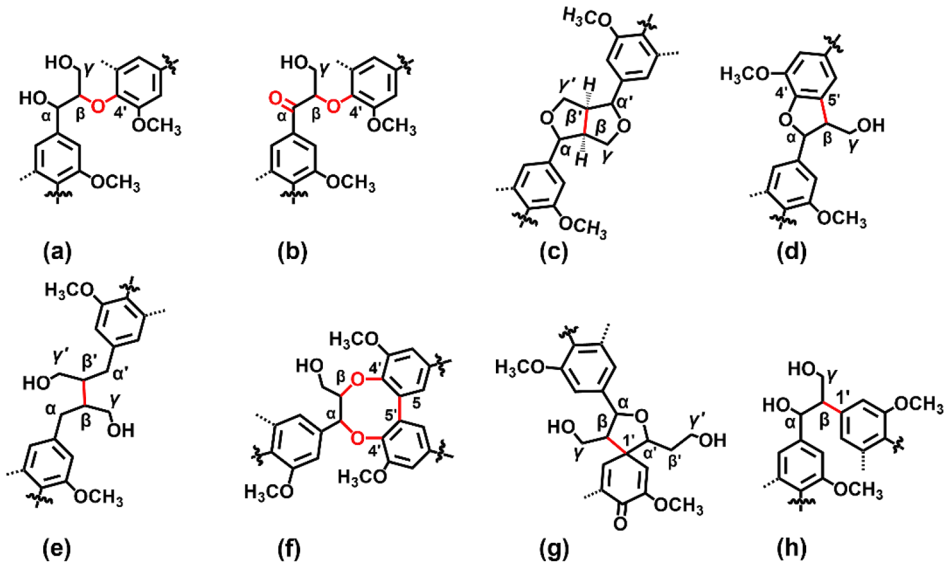

Figure 2.5. *Native lignin interunit linkages: (a) β-O-4', (b) C_α-oxidized β-O-4', (c) β-β' (resinol), (d) β-5', (e) β-β' (secoisolariciresinol), (f) dibenzodioxocin, (g) β-1' (spirodienone), and (h) β-1'.*

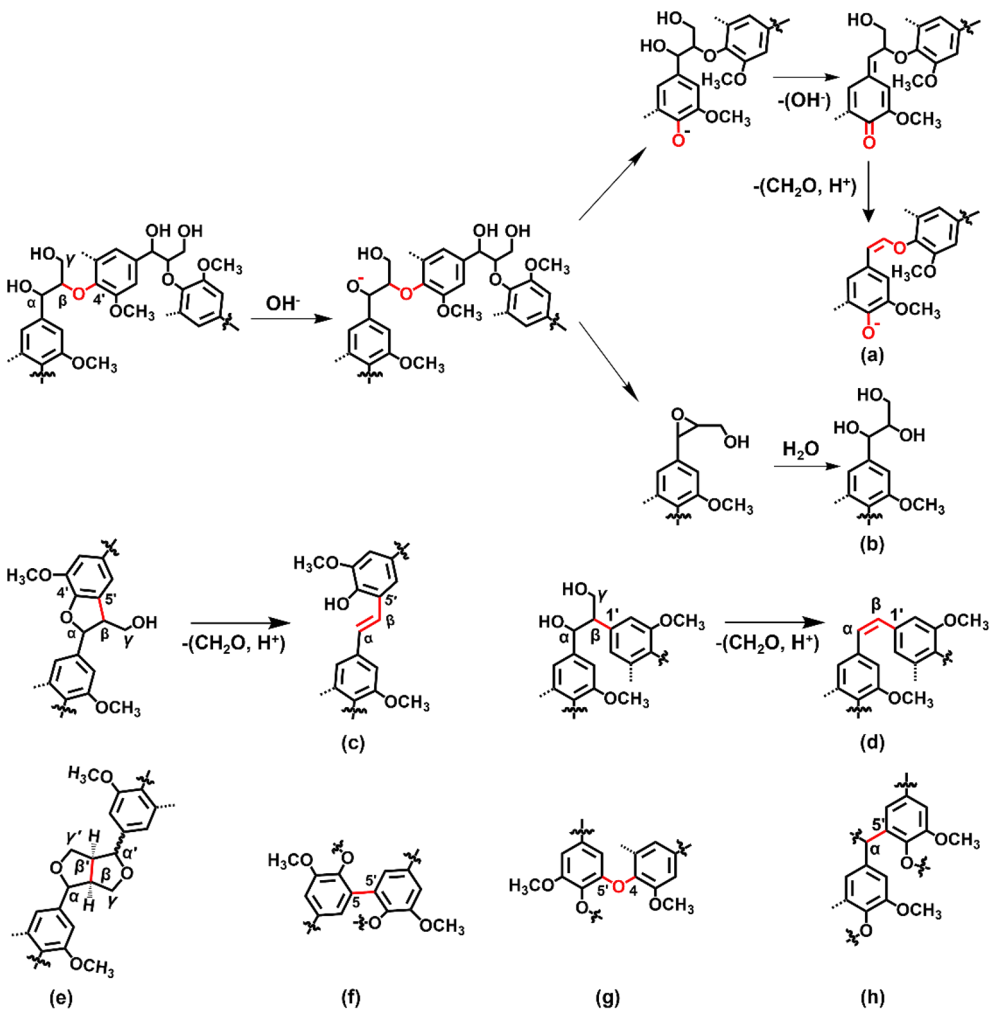

Figure 2.6. *Reaction scheme for the formation of (a) enol ether, (b) aryl glycerol, (c) stilbene from β-5' moieties, and (d) stilbene from β-1' moieties. Lignin structures linked by (e) β-β' (epiresinol), (f) 5-5', (g) 4-O-5', and (h) α-5' linkages.*

In addition to the significant variability in interunit linkages, lignin is also characterized with heterogeneous features concerning constituent aromatic units and the degree of condensation (DC) at the aromatic ring, which have significant impacts on lignin reactivity in terms of chemical accessibility and steric hindrance of functional groups (*e.g.*, phenolic-OH groups).[19] Lignin composition is species-dependent, *i.e.*, the ratio of monolignols is related to the plant type. Genetically, lignified cells of different wood species have different capacities to accumulate specific monolignols. Thus, lignin from softwood contains more G-subunits, lignin from hardwood presents a mixture of S- and G-subunits, and lignin from herbaceous plants bears a mixture of all three

monolignols, with higher content of H-subunits.[20] The lignin from softwood is supposed to have a higher DC value compared with that from hardwood, which arises from the notion that G-subunits are prone to form stubborn carbon-carbon linkages during lignin biosynthesis.[19]

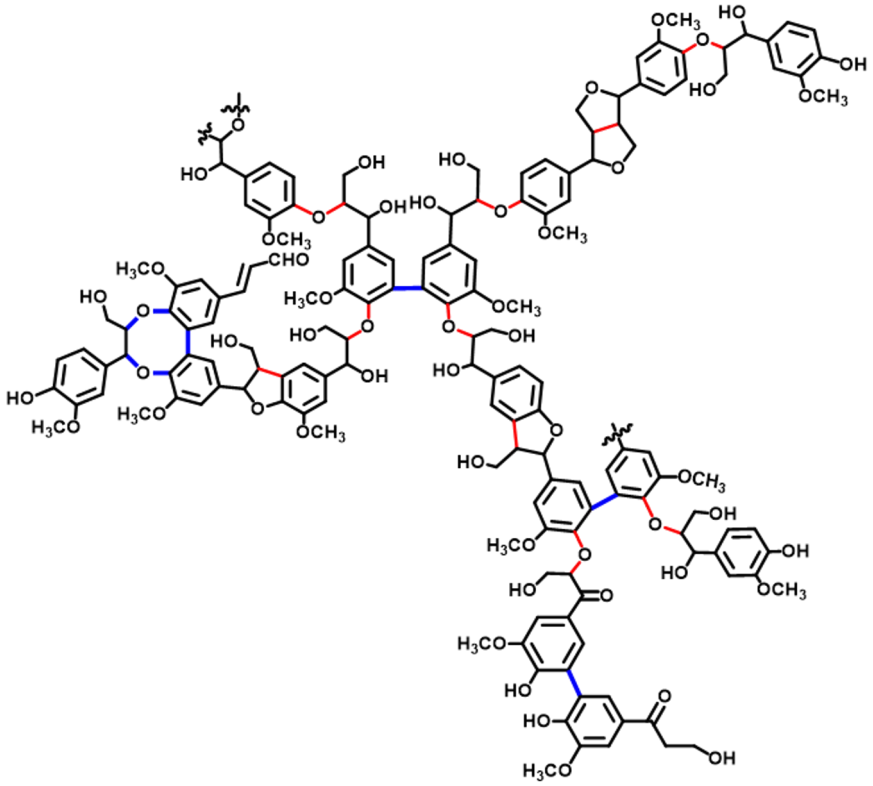

Figure 2.7. *Proposed structure of spruce milled wood lignin.[21] The structure delineates possible branch points (highlighted in blue) rather than insisting on a precise structure.*

The structural characteristic of lignin molecules in terms of branching or linear is one of the crucial metrics for assessing their properties and applications as advanced polymers or precursors for depolymerization. Recent reports pertaining to the feature of lignin macromolecular backbone have proposed a significant branched interunit linkage pattern of Norway spruce (*Picea abies*) milled wood lignin.[21] The main potential branching/cross-linking points at aromatic rings were determined to be 5-5', dibenzodioxocin (5-5'/β-O-4'), and etherified 4-O-5' moieties (**Figure 2.7**). In addition, the successful isolation of a linear homopolymer of catechyl lignin (C-lignin) bearing caffeyl alcohol subunits and benzodioxane (α-O-5'/β-O-4') linkages from vanilla and cactaceae seed coats has also been reported.[22,23] Intriguingly, the homogeneity of C-lignin allows it to be depolymerized into catechol monomers in high yield,[24] and

moreover, its high linearity makes it a suitable feedstock for carbon fiber production.[22]

Overall, the complexity of lignin polymer chemistry is predominantly derived from the different combinations of oxidative enzymes embedded in the plant cell wall since different enzymes have different active sites toward lignin biosynthesis.[25] The structural complexity of lignin molecules hinders their structural elucidation but creates the possibility of deriving lignin fractions with different structural characteristics from the same parent lignin.

2.1.3. Interaction of biomass components with lignin

In plant cell walls, the interaction of lignin with other biomass components, such as the covalent interactions between lignin and hemicelluloses, has a substantial impact on the recalcitrance of lignocellulosic biomass to enzymatic hydrolysis and biomass fractionation.[26] For instance, the recalcitrance of grasses to enzymatic digestion arises from a complex array of crosslinking between hemicelluloses, as well as lignin and hemicelluloses in the cell wall, especially for the glucuronoarabinoxylans in the presence of ferulic and *p*-coumaric acid residues as cross-linkers, as depicted in **Figure 2.8**.[27,28] The arabinosyl substitution in gymnosperms (*i.e.*, softwood) secondary cell walls may not be feruloylated. In this case, the nucleophilic groups of xylan and galactoglucomannan have been proposed to re-aromatize the quinone methide intermediate of lignin and generate ether or ester linkages.[28]

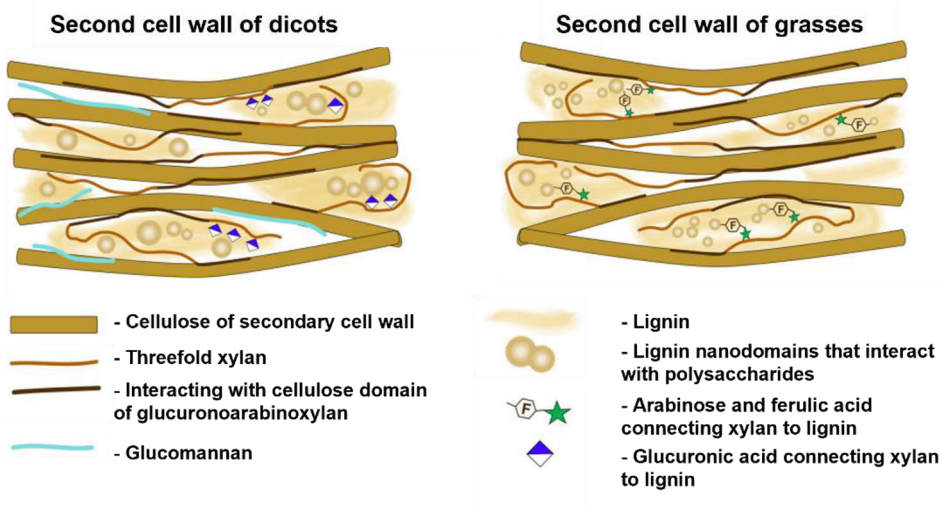

Figure 2.8. *Plant secondary cell wall model structures demonstrating complex crosslinking between hemicelluloses and lignin via glucuronic acid and feruloylated glucuronoarabinoxylan.*[35]

The inherited affinity of biomass components can also be exploited to enhance material properties. The beneficial synergistic effects between lignin and hemicelluloses as well as lignin and cellulose matrices have been demonstrated in different applications, such as Pickering emulsion stabilization,[29] lignin-containing phenol-formaldehyde (LPF) wood adhesives,[1] and lignin-containing cellulose dispersions and films.[30–34]

Lignin-containing cellulose dispersion is strategically advantageous in paper coating and packaging applications due to its sustainability. In recent research focused on the preparation of lignin-containing cellulose film, two major categories of processing strategies have been extensively studied, *i.e.*, either preserving the residual lignin in biomass pretreatments or mixing isolated lignin in various formats with dispersed cellulose. In the former category, the preserved residual lignin was beneficial to the defibrillation when treating bagasse fibers with improved nanofibril yield but reduced energy consumption and it also significantly improved the wet tensile strength of the obtained composite film prepared from tobacco stalk.[30,31] In the latter category, the importance of fine-tuning the interfacial interactions to result in the efficient integration of lignin into the nanocellulose matrix has been highlighted. In cases where lignin with different charge groups was directly mixed with nanocellulose as nanoparticles[32,33] or the dissolved lignin was *in situ* precipitated on the surface of nanocellulose in a nucleation-and-growth fashion *via* solvent shifting method,[34] the mechanical properties and surface wettability of the resultant nanocellulose films significantly varied, mainly depending on the interfacial interactions in the matrix. Farooq *et al*.[32] demonstrated that a direct mixing of the cationic lignin in the form of colloidal nanoparticles with the negatively charged cellulose nanofiber (CNF) matrix prior to vacuum filtration resulted in a nanocomposite film with an enhanced tensile strength of 162 MPa and strain at break of 16.2% at a lignin content of 10 wt%, in comparison to the corresponding values of 132 MPa and 9.4% for the neat CNF films. Meanwhile, a decreased but non-significant Young's modulus of the nanocomposite film was observed upon the mixing of negatively charged LNPs in the CNF matrix. The authors also concluded that the nanomorphology of lignin present in the CNF matrix played an essential role in enhancing film toughness, whereas films processed with soluble cationic lignin and anionic kraft lignin showed deteriorated mechanical properties, most likely due to the aggregation of lignin fragments during film formation.[32] From this perspective, strategies that can modulate the nanoscale spatial localization of lignin in the nanocellulose fiber network are needed.

2.2. Biomass fractionation process

Biomass fractionation processes can be subdivided into three categories, *i.e.*, fiber-based, ethanol-based, and lignin-first strategies. In pursuit of a more sustainable and competitive biorefinery, effective valorization of lignin is the key. The reactivity of lignin towards functionalization is generally determined by three factors: (i) the structural features of native lignin, (ii) the biomass fractionation method and underlying chemistries, and (iii) the severity of the fractionation method.[36]

2.2.1. Fiber-based biorefinery

Fiber-based biorefinery processes mainly focus on the production of fibers used in pulp and paper. A selective fractionation approach of the major structural components to overcome the recalcitrance of lignocellulosic biomass to pulping plays an important role on the physiochemical properties of the fiber and its subsequent conversion. In this scenario, cellulose fibers can be preserved by the preferential fragmentation and dissolution of at least one of the structural components, *i.e.*, lignin and hemicelluloses. The most predominant fiber-based biorefinery process is kraft/sulfate pulping, followed by sulfite pulping. In a typical kraft pulping process, wood chips are cooked in an aqueous solution of sodium hydroxide (NaOH) and sodium sulfide at 140 – 170 °C for a few hours. Lignin is extensively fragmented by the hydrosulfide ions under strongly alkaline conditions (pH-range 13 – 14), hemicelluloses undergo partial degradation and dissolution, while the cellulose fibers are isolated.[37,38] Consequently, a substantial amount of sulfur (1 – 3 wt%) is usually covalently bonded to kraft lignin in the form of thiol groups. In addition, competition between lignin degradation reactions (*e.g.*, aryl ether cleavage) and condensation reactions (*e.g.*, conjugate addition of carbanions to quinone methide intermediates) can lead to a rather heterogeneous lignin from kraft pulping.[37,39] The potential kraft lignin market is projected to reach 3.5 – 14 million tons per year, promoted by newly commissioned lignin recovery technologies (*e.g.*, LignoBoost and LignoForce), combined with the demand to not only burn the lignin to obtain heat and energy but to produce high-value products.[40]

Sulfite pulping is the second largest pulping process, while it is currently the only process that provides commercial lignin products, *i.e.*, lignosulfonate, in a significant volume, approximately 1.2 million tons per year.[1,41] Sulfite pulping is carried out at 130 – 160 °C using salts of sulfurous acid (sulfites or bisulfites) of diverse cations (*e.g.*, sodium, calcium, potassium, magnesium, ammonium)

as pulping chemicals, and the pH varies within a wide range.[42] Currently, acid sulfite pulping (pH-range 1 – 2) is almost exclusively used for dissolving pulp production, where hemicelluloses are extensively hydrolyzed and lignin is highly sulfonated, but the lignin macromolecules are not as fragmented as in kraft pulping. One of the major obstacles to the acid sulfite process is the need for extensive treatment to separate high-purity lignosulfonate from pulping effluent containing hemicellulose-derived sugars and vice versa.[42] The challenges mentioned above also create opportunities for various biorefinery concepts, such as the Ecohelix technology based on side streams of sulfite pulping. More specifically, lignosulfonate and polymeric hemicelluloses obtained in the early stages of sulfite pulping are refined by membrane filtration and polymerized through reactive phenolic moieties by consecutive laccase treatments, and the main product is lignosulfonate-carbohydrate complex, which is a valuable biopolymer.[43]

Softwoods are the main feedstock for kraft and sulfite pulping, while alkaline pulping (also known as soda pulping) is another versatile pulping process that is effective on hardwood and non-woody annual plants, as well as agricultural harvest residues (mainly straw-derived).[44] During alkaline pulping, biomass is usually treated with an aqueous alkali solution (*e.g.*, 13 – 16 wt% NaOH) at 140 – 160 °C, which causes hydrolytic cleavage of native lignin into fragments that are soluble in the alkaline pulping liquor. Lignin from alkaline pulping is sulfur-free, chemically unmodified, and has high purity, low molar mass, and considerable reactivity.[44]

Over the last few years, various alternative fiber-based biorefinery concepts have been developed, such as steam explosion, ionic liquid method, and organosolv fractionation processes using alcohol-water mixtures or organic acid mixtures such as formic acid and acetic acid.[45,46] However, most of the processes mentioned above are limited to laboratory scale. To translate laboratory-scale technologies into commercial-scale operations, process optimization, development of techno-economic models, simulations on cost and risk analysis, and life cycle assessments are required. It should be noted that benzylic functionalization readily occurs in the fiber-based biorefinery processes, such as benzylic thiolation, benzylic sulfonylation, and benzylic etherification during kraft, sulfite, and organosolv processes, respectively. Sulfur in lignin can poison many transition metal catalysts, and the benzylic functionalization can limit reactivity for reactions requiring benzyl alcohol.[47]

2.2.2. Ethanol-based biorefinery

The bio-ethanol biorefinery concept has gained increasing interest due to the fact that the feedstock and process conditions of fiber-based pulping processes are usually constrained to achieve the target properties of the fibers. The bio-ethanol biorefinery process is characterized by three stages, *i.e.*, feedstock selection, pretreatment to liberate cellulose and hemicelluloses for enhancing their digestibility, saccharification of carbohydrates to fermentable sugars *via* enzymatic hydrolysis and then fermentation of these monomeric sugars to bio-ethanol.[48] Nevertheless, the conversion of lignocellulosic biomass to bio-ethanol is complex and expensive, thus the price of bio-ethanol cannot compete with petroleum-derived fuels.[49] To address this challenge, integrated biorefining or multifunctional conversion processes are required to produce a wide range of high-value bio-based products from bio-ethanol production. First, residues (*i.e.*, enzymatic hydrolysis lignin) from the bio-ethanol biorefinery process can be utilized. It has previously been demonstrated that lignin and cellulose (10 – 20%) in enzymatic hydrolysis lignin have a beneficial synergistic effect in enhancing the mechanical properties of thermosets and thermoplastics.[50,51] Moreover, ethanol-based biorefinery processes are more flexible in engineering lignin than fiber-based pulping processes.[1] Second, novel concepts are being developed for cost-effective and integrated biorefining processes. Recently, the LigniOx biorefinery concept based on the alkali-oxygen (alkali-O_2) oxidation technology has been demonstrated for the feasible production of versatile lignin dispersants and high-performance concrete plasticizers at a kraft pulp mill.[52] In addition, the alkali-O_2 oxidation of enzymatic hydrolysis lignin obtained from the Cellunolix® process developed by the Finnish company St1 has been reported to convert lignin into carbohydrate-rich residue, leading to enhanced bio-ethanol production.[53] However, the feasibility of the LigniOx process to be *in situ* integrated into the bio-ethanol biorefineries remains to be demonstrated. Formicobio™ technology is another case of integrated bio-ethanol biorefinery, which is developed from Chempolis's biorefining platform based on organosolv fractionation, using formic acid as the solvent and fractionation chemical. The Formicobio™ process enables the selective production of multiple value-added products from bamboo structural components, such as bio-ethanol from cellulose, acetic acid and furfural from hemicelluloses, and bio-coal from lignin.

2.2.3. Lignin-first biorefinery

The lignin-first concept is defined as an active stabilization approach that solubilizes lignin from native lignocellulosic biomass during pulping while

minimizing undesired lignin condensation reactions that lead to the formation of recalcitrant carbon-carbon linkages. The concept of lignin-first biorefinery arose from the realization that lignin valorization needs to be considered in the design phase of biomass refining. The main focus of lignin-first research is to provide a high yield of monophenolics and oligomers from lignin. Two strategies are actively involved in stabilizing reactive intermediates of lignin during the biomass fractionation and depolymerization stages: (i) depolymerization-stabilization of native lignin, such as reductive catalytic fractionation (RCF) and diol-assisted fractionation to produce lignin monomers, and (ii) preservation of β-O-4' moieties using aldehyde-assisted fractionation to yield stabilized lignin macromolecules that can be deconstructed into lignin oligomers through RCF processes.[54] RCF strategies rely on the use of metal catalysts and hydrogen. Moreover, RCF is more effective on hardwood than on softwood and herbaceous biomass because hardwood typically possesses a high ratio of S- to G-subunits (S/G), which translates into a high proportion of easily cleavable β-O-4' linkages, whereas the latter feedstocks have more recalcitrant carbon-carbon linkages.[55] Photocatalytic deconstruction of lignocellulose to aromatic hydrocarbons is a state-of-the-art paradigm in lignin-first biorefining.[56]

Lignin-first biorefinery not only means lignin valorization but rather a holistic approach that delivers values from both lignin and polysaccharides. Hemicelluloses have mainly been hydrolyzed to glucose, xylose, galactose, and mannose.[54] Polysaccharides retention in residual solids (cellulose-rich fraction) and susceptibility of polysaccharides to enzymatic digestion for bio-ethanol production are important metrics for assessing the economic viability of lignin-first biorefinery.[57] To achieve holistic biomass valorization and fulfill alternative energy demands, residual polysaccharides could be converted to hydrogen for hydrodeoxygenation of lignin oil to produce gasoline and kerosene/diesel drop-in fuels.[58]

2.2.4. BLN biorefinery

The lignin and hemicelluloses investigated in this thesis originate from a novel biomass fractionation technology developed by CH-Bioforce, known as the BLN biorefinery process. This process is characterized by two stages, *i.e.*, a pressurized hot water extraction (PHWE) followed by an alkaline pulping process (**Figure 2.9**).[59,60] A polymeric hemicellulose fraction can be obtained by the PHWE process. The process efficiency and hemicellulose purity are tailored through the following parameter control: (i) biomass impregnation, (ii)

oxygen-starved condition, and (iii) closed-loop water circulation. Lignin fractionation is then performed on the residue after displacing the hemicellulose extract with plain water and using NaOH as pulping chemical under oxygen-starved conditions. Removal of O_2 from the reactor will reduce lignin oxidation and condensation.[61] The lignin black liquor, after circulating, is then filtered with a membrane (*e.g.*, 300 Da molar mass cut-off) to recover pulping chemicals and to concentrate lignin. The lignin is isolated from the black liquor by acid precipitation to pH 2.5 using hydrochloric acid (HCl). The BLN biorefinery technology yields sulfur-free, reactive, and low molar mass lignin. The remaining cellulose fraction is also isolated with high purity without peeling and is easy to bleach and fibrillate.

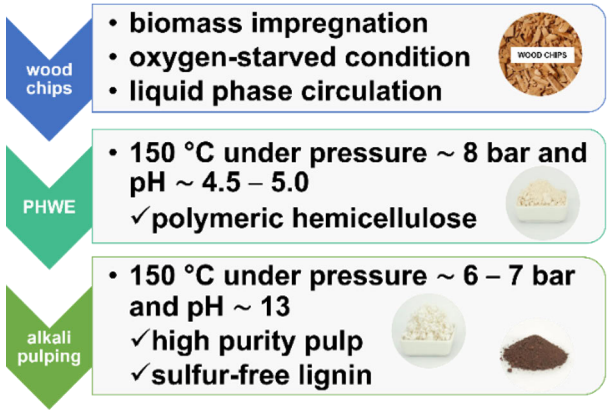

Figure 2.9. *Schematic illustration of the BLN biorefinery process.*[59,60]

2.3. Lignin fractionation methodology

Lignin-based by-products from biorefinery processes have significant variability in physiochemical properties, which not only depend on the fractionation process but also due to batch-to-batch variation.[62] Simple and potentially cost-efficient methods producing lignin fractions with consistent characteristics are highly demanded to upgrade lignin into high-value materials.[62] Therefore, it is vital to develop reliable and reproducible protocols to separate homogeneous lignin fractions with narrow $Đ_M$ and also well-defined specifications. To date, various lignin fractionation methodologies have been developed and extensively investigated, which can be subdivided into three categories, *i.e.*, solvent-tailored, pH-controlled, and membrane-mediated (**Figure 2.10**). Transforming bulk lignin into nanoscale lignin with narrow particle size dispersity ($Đ$) is another way to decrease the heterogeneity of lignin. Lignin fractionation strategies have aided our

understanding of its fundamental manufacturing chemistries,[63] chemical composition and structure elucidation of lignin,[64–66] profiles of functional heterogeneity (including nanoscale surface functionality)[67,68] and even laccase-lignin enzymatic chemistry.[69] Solvent fractionation strategies have also been utilized in understanding lignin micro- and nanoparticle nucleation and growth in aqueous dispersions.[70]

2.3.1. Sequential fractionation in organic solvents

The strategy of lignin fractionation in organic solvents can be achieved through (i) successive extraction with organic solvents or organic solvent–water mixture and (ii) dissolution followed by controlled lignin precipitation with the addition of extra water in organic solvent–water mixture (**Figure 2.10a-b**). A rational solvent sequence for lignin fractionation depends on the relative energy difference (RED) between solvent and lignin according to the theory of Hansen solubility parameter correlated with the synergistic effect of dispersion forces (δ_D), polar interactions (δ_P), and hydrogen bondings (δ_H) (**Table 2.2**).[71,72] The equation entitled 'Hansen's space' uses the solvent single-point coordinates and the space solute sphere as the interaction radius (R_O) to calculate the solubility parameter difference (R_a) (**Equation 1**).[72] The RED is defined as the ratio of R_a/R_o, and a high fractionation yield (solubility in organic solvents) should be achieved when RED between the solvent and lignin is less than 1.0.[73] Positive deviations from 1.0 usually result in a gradual decrease in the lignin solubility for a given solvent.

$$R_a^2=4(\delta_{D1}-\delta_{D2})^2+(\delta_{P1}-\delta_{P2})^2+(\delta_{H1}-\delta_{H2})^2 \quad \textbf{(1)}$$

where

δ_{D1}, δ_{P1}, δ_{H1}: hansen solubility parameters of solvent

δ_{D2}, δ_{P2}, δ_{H2}: hansen solubility parameters of lignin

A sequential solvent extraction strategy using ethyl acetate (EtOAc), ethanol (EtOH), methanol (MeOH), and acetone was reported to be effective in decreasing the heterogeneity of softwood kraft lignin in terms of molar mass and functionalities (**Figure 2.10a**).[71,74] In this way, lignin fractions with narrow $Đ_M$ but sequentially increased molar mass were obtained. The hydrogen bonding interactions between extraction solvent and lignin were demonstrated to play a major role in deciding the chemical composition of lignin, especially for the relative content of hydroxyl, carbonyl, and carboxyl groups.[75] A higher content of hydroxyl groups is expected to be conveyed to the lignin fraction extracted by a solvent with a higher hydrogen bonding

component (*i.e.*, δ_H) of its solubility parameters.[75] The chemical nature of the extraction solvents, such as polar protic solvent, polar aprotic solvent, and non-polar solvent, will also influence the appearance, hygroscopicity, and thermal properties of lignin fractions.[76]

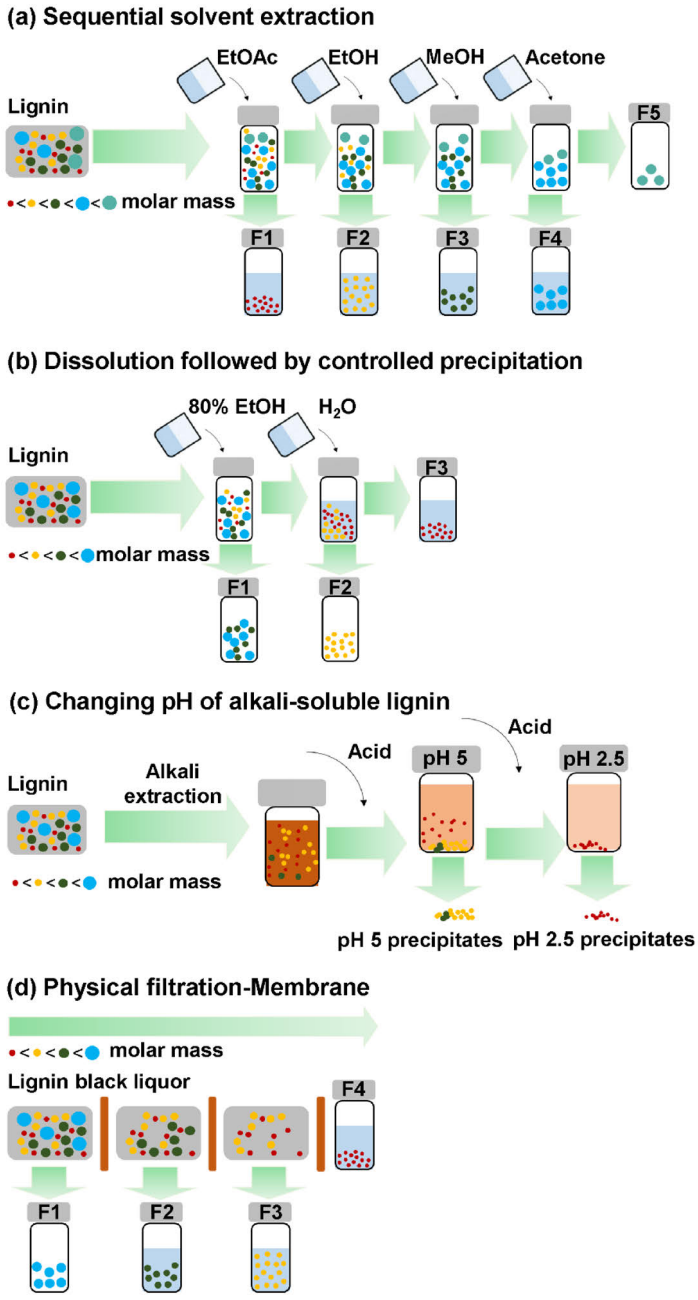

Figure 2.10. *Schematic illustration of the process for lignin fractionation: (a) sequential fractionation in organic solvents, (b) fractionation using organic solvent–water mixture, (c) gradient acid precipitation, and (d) membrane ultrafiltration.*

Table 2.2. Hansen solubility parameters for lignin and solvents.[71,72]

solvents	δ_D (MPa$^{1/2}$)	δ_P (MPa$^{1/2}$)	δ_H (MPa$^{1/2}$)
lignin[a]	21.9	14.1	16.9
acetone	15.5	10.4	7.0
EtOAc	15.8	5.3	7.2
i-PrOH	15.8	6.1	16.4
EtOH	15.8	8.8	19.4
MeOH	15.1	12.3	22.3
water	15.5	16.0	42.3
chloroform	17.8	3.1	5.7

[a]milled wood lignin from spruce (*Picea excelsa*), R_O = 13.7.[72]

Lipophilic wood extractives, mainly composed of free fatty and resin acids, sterols, sterol esters, and triglycerides, can be deposited on lignin during black liquor precipitation, which imposes significant challenges for elucidation of lignin structure and determination of lignin properties, such as thermal properties.[66] Organic solvents, such as methyl *tert*-butyl ether (MTBE) and acetone, are suitable solvents to remove extractives from lignin. To better understand the cause-effect relation between lignin structural characteristics and material properties, lignin purification is therefore considered as important as designing efficient fractionation sequences. The solvent fractionation sequence reported by Liu *et al*. (*i.e.*, 70% MeOH–water, anhydrous acetone, MTBE–EtOAc) focused on the distribution of impurities in softwood kraft lignin fractions, such as extractives, carbohydrates, and elemental sulfur.[65] High-purity lignin fraction with a moderate molar mass was obtained at the end of the sequence.[65] It has been reported that EtOH–water, acetone–water, and *γ*-valerolactone–water systems have been successfully applied to the sequential fractionation of lignin to enhance its antioxidant and antibacterial capacities.[77–79] For instance, solvent-fractionated lignin of low molar mass, containing a higher content of phenolic-OH groups, possessed higher antioxidant and antibacterial activities.[77–79] The positive effect of the side chain structure of lignin (*e.g.*, conjugated double bonds and -OCH_3 groups) also contributed to the antibacterial activities of lignin.[77] In the recent state-of-the-art studies on solvent-tailored lignin fractionation, reactive fractionation was reported to be promising for the facile functionalization of lignin.[80] In terms of the economic feasibility of lignin solvent fractionation, Jiang *et al*. reported a detailed techno-economic analysis on industrial-scale lignin fractionation using organic solvents, such as acetone, EtOH, EtOAc, isopropyl

alcohol (*i*-PrOH), MeOH, and methyl ethyl ketone, where solvent losses and raw lignin costs determined capital expenditures.[81]

2.3.2. Fractionation using pH control

pH-controlled precipitation of lignin fractions from an alkaline solution is another promising approach for lignin fractionation (**Figure 2.10c**). Lignin macromolecules are polyelectrolytes in aqueous solution that dissociate and dissolve at alkaline conditions due to the ionization of phenolic-OH and -COOH groups. The pH-controlled lignin fractionation strategy is essentially based on the dissolution of lignin followed by a gradual decrease in pH value to induce lignin aggregation through the protonation of dissolved lignin with hydrogen ions. It has been reported that the aggregation tendency of lignin in an alkaline solution is mainly determined by the configuration of lignin in the dissolved state and the molecular architecture of lignin and the chemical structure of lignin.[82,83] First, the dependence of lignin solubility in an alkaline aqueous solution on the molar mass of lignin suggested that lignin with a higher molar mass tended to precipitate first due to its lower solubility.[84] Second, the acidity of phenolic structures is important not only for the dissolution of lignin associated with many reactions in wood chemistry (*e.g.*, delignification during pulping, bleaching, and leaching of lignin during pulp washing), but also for the ease of lignin aggregation during pH-controlled fractionation. Typically, lignin contains structures with acid dissociation constants, p*K*a, in the range of about 7.3 to 10.5 (**Table 2.3**). [85,86] Lignin-related chemical moieties with higher p*K*a values tend to precipitate first due to their weaker acidic groups, and their dissociation is susceptible to pH decrease.[85]

Table 2.3. The p*K*a in lignocellulosic materials.[85,86]

functional groups	p*K*a values
R-CH(OR')COOH	3 – 4
phenyl-OH	9.5 – 10.5
guaiacyl-OH	7.4 – 10.3
syringyl-OH	7.3 – 10.0
hemiacetalic	12 – 12.5
alcoholic	13.5 – 17.0

The yield of the lignin fractions was also related to the p*K*a value of the lignin structure, and when the pH value exceeded the p*K*a threshold of phenolic-OH groups, such as pH at 9, more than 50% of the lignin was precipitated (**Table 2.4**).[87] Furthermore, the pH sequence applied in lignin fractionation can affect the purity of lignin in terms of carbohydrates. Hemicellulose fragments

containing -COOH groups are supposed to be enriched in the low molar mass lignin fraction that precipitates at low pH values (*e.g.*, pH-range 3 – 4),[85] whereas the lignin-carbohydrate complexes tend to precipitate at higher pH values.[87]

Table 2.4. The yield of sequentially precipitated lignin at different pH values.[87]

lignin	content (wt%)	pH			
		9	7	5	3
softwood kraft lignin	yield	50	37	11	1
hardwood kraft lignin	yield	52	34	10	3

2.3.3. Fractionation by membrane ultrafiltration

Ultrafiltration is another approach to refine and control the molar mass and reactivity of heterogeneous lignin. In most cases, dissolved lignin is treated under elevated pressure and temperature through a series of membranes with high to low molar mass cut-off values (**Figure 2.10d**). Dead-end and cross-flow filtration modules using ceramic membranes or polymeric membranes (*e.g.*, polyethersulfone and polypropylene) are two common ultrafiltration methods for lignin fractionation.[88] Cross-flow ultrafiltration mode using ceramic membranes with molar mass cut-off values of 15 kDa, 5 kDa, and 1 kDa has been reported to efficiently fractionate softwood and hardwood kraft black liquor in the aspect of molar mass and other physiochemical properties.[89,90] More importantly, it was concluded that low molar mass lignin fractions contained lower contents of aliphatic-OH and -OCH_3 groups as well as lower content of carbohydrates, but higher contents of phenolic-OH groups and β-O-4' structures than the high molar mass fractions.[89,90]

The biorefinery industry has demonstrated the feasibility of lignin ultrafiltration from laboratory to commercial scale. Ecohelix and MetGen biotechnologies are two representative cases in the Nordic biorefinery industry, which combine ultrafiltration and enzymatic processes for the oxidative upgrading of lignin.[43,91] Polymers of lignosulfonate-carbohydrate with an amphiphilic structure are the target product of the Ecohelix process, wherein ultrafiltration endows the possibility to tailor the laccase-polymerized moieties.[43] In contrast, laccase-depolymerized kraft lignin obtained using the MetGen biotechnology was sequentially fractionated by cross-flow ultrafiltration units using polyethersulfone membranes with 70 kDa to 1 kDa molar mass cut-off values, and the retentate fraction above 70 kDa was found to be a good candidate for anti-creep applications in packaging.[91] The combination of solvent extraction and membrane-assisted ultrafiltration has

also been reported for lignin fractionation.[92] However, economic feasibility should be considered in terms of the scalability of upgrading lignin using membrane ultrafiltration in biorefineries.

2.3.4. Lignin nanoparticles

Lignin can form hydrocolloids such as LNPs through self-assembly.[93] The common approaches for preparing LNPs include solvent shifting,[94] controlled evaporation of atomized lignin solution droplets,[95] acid precipitation,[96,97] and emulsion templating.[98] So far, the solvent shifting method is the predominating technique for fabricating spherical LNPs, although the controlled evaporation method is more promising to scale up the production of LNPs. In addition, the solvent shifting method has the advantages of low infrastructure requirements, simple experimental processes, and lower energy consumption than using the controlled evaporation method. Nowadays, aqueous dispersions of colloidal LNPs are more commonly prepared by dissolving lignin in an organic solvent–water mixture, such as tetrahydrofuran (THF)–water, acetone–water, EtOH–water, followed by a rapid shifting of the solvent to water (antisolvent), and finally using evaporation or dialysis method to remove the organic solvent (**Figure 2.11**).[93]

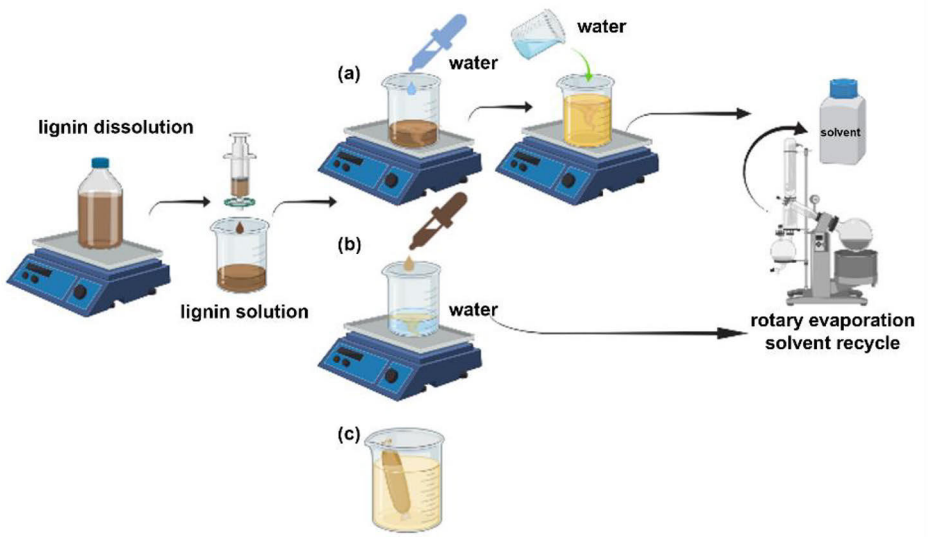

Figure 2.11. *Schematic representation of different solvent shifting methods, including (a)water into lignin-solvent, (b) lignin-solvent into water, and (c) dialysis of lignin solution against water. Created with BioRender.com.*

The solvent-dependent effect of the structural characteristics of lignin on the fabrication process of LNPs has been investigated. It was confirmed that the presence of polar protic solvents (*e.g.*, EtOH and ethylene glycol) deteriorated

the spherical morphology of LNPs compared to the use of polar aprotic solvents (*e.g.*, THF, acetone, and γ-valerolactone).[99] The underlying self-assembly mechanism for lignin nanosphere formation during solvent shifting is nucleation-and-growth.[70] Hydrophobic aromatic interactions dedicate compact micelle nuclei *via* π-π stacking, while random collision and aggregation of the nuclei drive the growth of nanoparticles. Lignin has an amphiphilic structure, and the hydrophilic moieties with more phenolic-OH and -COOH groups adsorb onto the particle surface during self-assembly.[70,100] Consequently, LNPs possess interfacial interactions in nanomaterials. In addition, the resulting high electric surface charge prevents further aggregation of LNPs into irregularly shaped clusters and provides durable dispersibility in water.

The size of LNPs can be tailored by tuning the structural features of lignin in terms of aromatic density and electronic aromatic interactions, which are deemed as the dominant intermolecular force for lignin nanosphere formation.[101] More specifically, high molar mass lignin derived from solvent fractionation favored the formation of small-size LNPs because the aromatic moieties of high molar mass fractions are separated by aliphatic side chains, resulting in a lower aromatic density.[68,102] Similarly, it has been previously reported that the participation of lignin aliphatic-OH groups in intramolecular hydrogen bonds usually limits the formation of non-covalent bonds with other lignin molecules, resulting in smaller particle sizes.[102] Strategies to increase electronic aromatic interactions, such as increasing the phenolic-OH content through lignin phenolation, could result in larger particle sizes.[103] In addition, the physical conditions for preparing LNPs (*e.g.*, concentration, mixing speed, the ratio of water to organic solvent) can also significantly influence the particle size.[104]

2.4. Lignin functionalization

2.4.1. Chemical functionalization

Multiple reactive sites of lignin, such as non-condensed methine carbons (C_{Ar-H}), phenolic-OH, aliphatic-OH, -COOH, and -OCH_3 groups, have been widely used in application-specific functionalization. Chemical functionalization strategies of lignin mainly include phenolation, hydroxymethylation, methylation, demethylation, epoxidation, allylation, amination (Mannich reaction), and carboxyalkylation. Phenolation is one of the most efficient methods to increase the reactivity of lignin by increasing the content of phenolic-OH groups and non-condensed *ortho* positions of the phenol (**Figure 2.12a**).[105] Lignin

phenolation is a versatile reaction that can be performed at acid-catalyzed and base-catalyzed conditions.[105,106] Natural phenolic compounds, such as tannic acid, have been reported to be alternative precursors for phenolation of lignin.[107] The phenolated lignin could improve the efficiency of the Mannich reaction, which allows the attachment of amine-bearing molecules to the aromatic ring of lignin in the presence of formaldehyde (**Figure 2.12b**).[108] To date, the feasibility of using phenolated lignin to prepare high-performance materials has been demonstrated in phenolic resins,[106] polyurethane foams,[109] and phenol-hydroxymethylfurfural resins.[110]

The polymeric nature of lignin makes it one of the prime candidates for aromatic building blocks in macromolecular polymers. In this application scenario, lignin is demanded to possess functional moieties (*e.g.*, oxirane or double bonds) essential for chemical cross-linking and polymerization. Henn *et al.* reported a water-based lignin epoxidation approach based on the principle of interfacial catalysis, in which lignin molecules stabilized the epichlorohydrin droplets in an emulsion-like medium. Simultaneously, lignin molecules were functionalized *in situ* with oxirane groups at the interface between the aqueous alkaline lignin solution and epichlorohydrin droplets (**Figure 2.12c**).[104] High degree of epoxidation was achieved in only a few minutes. Moreover, the epoxidized lignin derivatives with oxirane moieties can be cross-linked with polyether diamine and self-cross-linked *via* phenolic-OH groups (**Figure 2.12d**) at elevated temperatures (*e.g.*, 130 – 160 °C), which provides the possibility to fabricate bio-based composite adhesives with high lignin content.[74,104] Moreover, functionalization affects the solubility of lignin, *e.g.*, epoxidized lignin can be solubilized in water at pH above 8, while unmodified lignin is usually poorly soluble in aqueous solution below pH 10.[104] To functionalize lignin with double bonds, allylation using allyl halides (*e.g.*, allyl chloride and allyl bromide) (**Figure 2.12e**) and allyl glycidyl ether is one of the most effective approaches.[111,112] Lignin with allyl-terminated moieties can be cross-linked *via* thiol-ene click chemistry to fabricate thermosets,[111,112] and can be multifunctionalized through epoxidation,[113] photo-induced crosslinking, and free-radical polymerization.[114]

Strategies to enhance the reactivity of lignin macromolecules towards polymerization include: (i) lignin fractionation to derive fractions with high content of phenolic-OH groups for functionalization and (ii) fabrication of lignin-based macroinitiators and macromolecular chain-transfer (macro-CT) agents.[115,116] Lignin functionalized *via* phenolic-OH with bromopropionyl

group (**Figure 2.12f-g**) and xanthate (**Figure 2.12h-i**) can be utilized as macroinitiators for atom transfer radical polymerization and as macro-CT agents for reversible addition-fragmentation transfer polymerization, respectively.[115,116] Large amount of hydroxyl groups in lignin allows it to be used as a polyol to prepare polyesters through direct polymerization approaches, such as *via* ring-opening polymerization to fabricate lignin-caprolactone copolymer (**Figure 2.12j**) for coating metal surfaces.[117] Cao *et al*. prepared lignin-based polyols through thiol-ene click chemistry (**Figure 2.12k**) to fabricate polyurethane anticorrosive coatings.[118] Nowadays, lignin-based liquid polyols have enormous application potentials, especially in polyurethane foams, wherein cyclic carbonates (*e.g.*, ethylene carbonate) have been reported to efficiently convert lignin phenolic-OH groups to primary aliphatic-OH groups.[119]

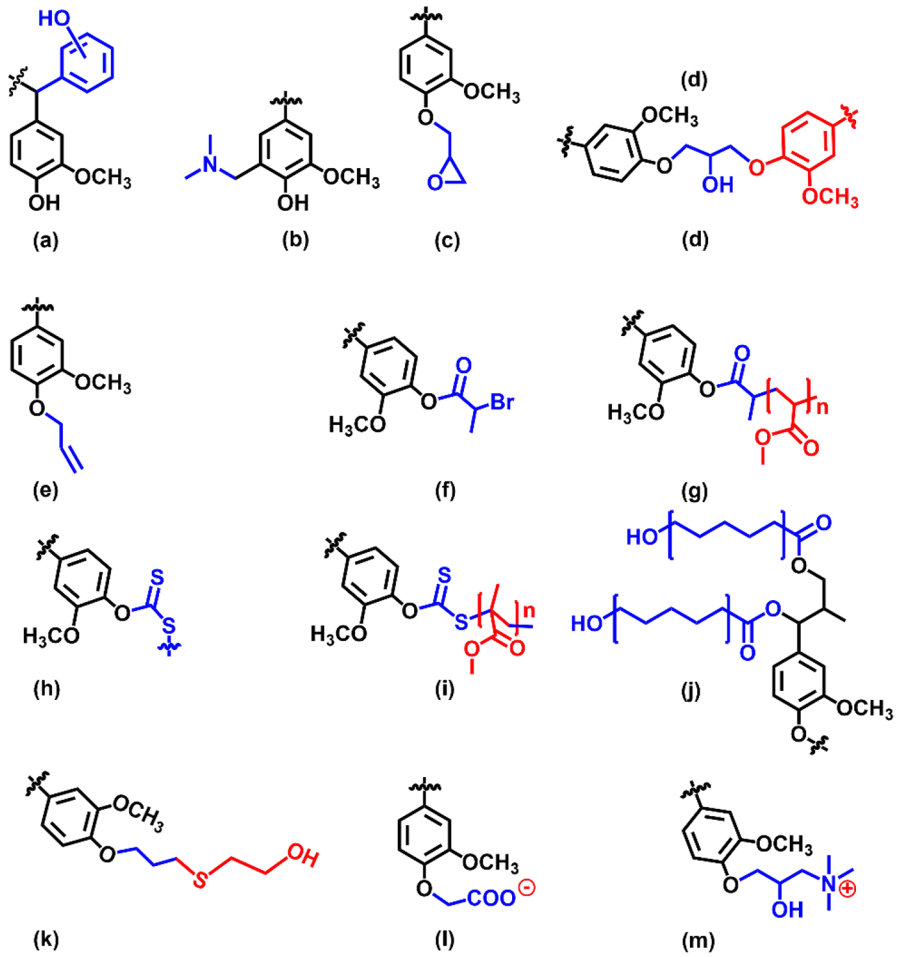

Figure 2.12. *Lignin chemical functionalization strategies.*

The inherent amphiphilicity of lignin has been utilized in stabilizing emulsions and modulating interfacial interactions. The amphiphilic interface of lignin could be tailored *via* alkylation and carboxyalkylation (**Figure 2.12l**) to enhance functionalities for emulsion stabilization.[120,121] Moreover, lignin cationization *via* base-catalyzed etherification of lignin hydroxyl groups with oxirane groups from glycidyltrimetylammonium chloride exhibited the potential to modulate lignin interfacial interactions through tunable surface charges (**Figure 2.12m**).[122,123]

2.4.2. Biochemical functionalization

Laccases are widely studied phenol-oxidizing metalloenzymes, *i.e.*, multi-copper oxidases, which are promising biocatalysts for the oxidation, polymerization, and depolymerization of phenolic macromolecular substrates, such as lignin (**Figure 2.13a**) and tannin.[124] In the laccase-catalyzed oxidation of a phenolic substrate (*e.g.*, lignin with phenolic-OH groups), O_2 is the only co-substrate for laccase to achieve its oxidative capacity. Under aerobic conditions, laccases catalyze the one-electron oxidation of the phenolic substrate with the formation of a resonance-stabilized phenoxy radical and transfer four electrons to the catalytic copper atoms, which are used to reduce O_2 to two water molecules.[125] The substrate range of laccases can be extended with the aid of a laccase redox mediator (*e.g.*, syringaldehyde, acetosyringone, acetovanillone), which can function as intermediate electron shuttles to oxidize the non-phenolic moieties of lignin macromolecules (**Figure 2.13b**).[91,126] The overall reactivity of laccase-lignin oxidation is heavily dependent on the structural feature of lignin. Vignali *et al*. reported that a high ratio of phenolic-OH to aliphatic-OH groups resulted in lignin polymerization, while a decreased ratio of phenolic-OH to aliphatic-OH groups resulted in net depolymerization.[69] Laccase could also functionalize lignin. Morena *et al*. fabricated antibacterial lignin-tannic-acid nanoparticles using a sonoenzymatic approach (*i.e.*, laccase oxidation assisted with high-intensity ultrasound).[107] This process simultaneously polymerized lignin with tannic acid and converted the polymerized lignin-tannic-acid into nanoparticles.

Laccases of bacterial origin have a much lower redox potential (~ 340 mV) than those of fungal origin (~ 790 mV), while bacterial-derived laccases are generally more thermostable and can work over a broader pH range (*e.g.*, pH-range 4 – 9) than fungal-derived laccases (pH-range 3 – 5).[127,128] Recently, a new genetically evolved bacterial laccase (commercialized as MetZyme® product) was reported to efficiently oxidize hardwood mild acidolysis lignin at

highly alkaline conditions (pH 10.5). This alkaliphilic laccase was further applied in the study of Paper III and Paper IV.

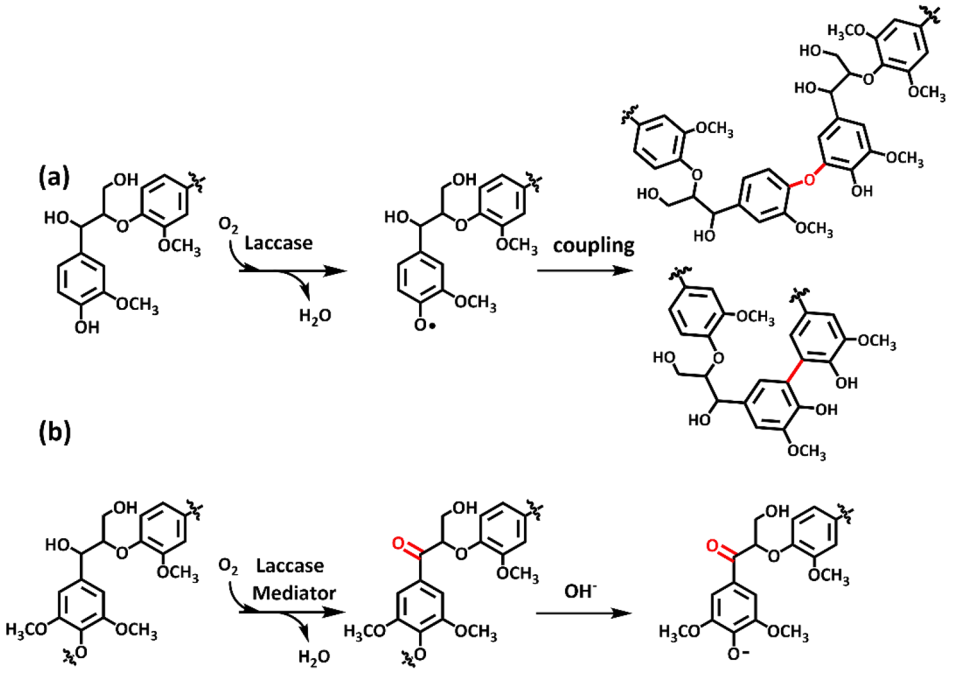

Figure 2.13. *Schematic representation of laccase-driven oxidation of (a) phenolic and (b) nonphenolic lignin units.*[91,124]

2.4.3. Functionalization of LNPs in dispersion state

Currently, lignin nanomaterials with versatile surface functionalities and improved chemical stability at extreme pHs or in certain organic solvents are emerging as bio-based building blocks that are plausibly alternative to fossil-based and inorganic nanoparticles such as polystyrene or silica nanoparticles. To improve the chemical stability of LNPs at harsh alkaline conditions (pH > 9), recalcitrant moieties are commonly demanded to be present in lignin macromolecules. Polymerization and covalent cross-linking of lignin aromatic rings, such as interfacial and intraparticular cross-linking *via* enzyme-catalyzed oxidation,[129] intraparticular cross-linking *via* phenolic resin curing and epoxy resin condensation chemistries, are existing strategies in the literature.[94,130–132] Functionalization of alkali-stable LNPs in a dispersion state has been demonstrated in *in situ* reduction and nucleation of metallic particles (*e.g.*, silver and gold) and covalent surface functionalization of LNPs with cationic moieties (*e.g.*, ammonium groups) at extreme pH conditions, *etc.*[94,130,131,133] Enhancing the hydration barrier effect on the surface of LNPs *via*

tuning their polarity through grafting polymers (*e.g.*, oleic acid and fluorinated oleic acid ester) has been demonstrated to overcome the aggregation of LNPs at acidic conditions (pH < 2.5).[133,134]

2.5. Lignin industrial applications

In general, lignin valorization is explored through two different routes: controlled depolymerization into small molecules and as a building block to construct functional lignin-based polymeric materials. Considering the structural features of technical lignin, it is not always feasible to depolymerize lignin into monomers, especially when lignin contains pronounced condensed structures.[135] However, despite the initial challenges associated with the heterogeneous structure of lignin, the valorization of this intriguing aromatic biopolymer in its polymeric form has come a long way in providing sustainable solutions for industry-demanded applications.[1] Promising value-added applications of lignin are phenols (*e.g.*, phenolic adhesives) and polyols in the short term and thermoplastics and carbon-based materials (*e.g.*, carbon fibers and bio-char) in the long term.[136]

2.5.1 Thermosets

The phenolic macromolecular backbone of lignin is the basis of its use in the manufacture of various thermosetting materials, such as phenolic resins (*i.e.*, LPF adhesives) and epoxy resins. The phenolic resin, currently widely used in various products, such as furniture, floor coverings, thermal insulation, flame-retardant, and sandpaper, can be prepared by either acid-catalyzed or base-catalyzed condensation polymerization of phenol with formaldehyde.[137] If formaldehyde reacts with phenol at acidic conditions and the molar ratio of formaldehyde/phenol is lower than 1, thermoplastic novolacs will be produced (**Figure 2.14a**).[138] In contrast, if the molar ratio of formaldehyde/phenol is higher than 1 and the reaction between phenol and formaldehyde occurs at basic conditions, thermosetting resols will be formed (**Figure 2.14b**).[138] Nowadays, lignin research for innovation has taken significant commercialization steps and created industrial technologies to reduce the share of petrochemical-based feedstocks in phenolic resins. A representative plywood mill using sustainable lignin-based WISA BioBond gluing technology (LPF adhesives in which lignin substitutes 50% of the phenol) for plywood manufacturing is UPM, and WISA™ plywood has been commercialized. The demand for sustainable thermosetting adhesives for plywood and particleboard is expected to rapidly increase as concrete is being replaced by wood for construction to reduce carbon dioxide emissions. Lignin-containing

epoxy resin is another promising wood adhesive based on the lignin epoxidation strategy *via* epichlorohydrin.[74,104]

Formaldehyde-free and phenol-free lignin-based adhesives have been reported, such as lignin-glyoxal, lignin-tannin-glyoxal, and lignin-starch adhesives.[139–141] Compared to thermoset adhesives integrating proteins or polysaccharides, lignin can endow the thermosets with water resistance, high wet bonding strength, thermal stability, and low cost. However, the role of lignin in adhesives remains challenging to undertake since different types of lignin have different compositions and chemical structural features.[139]

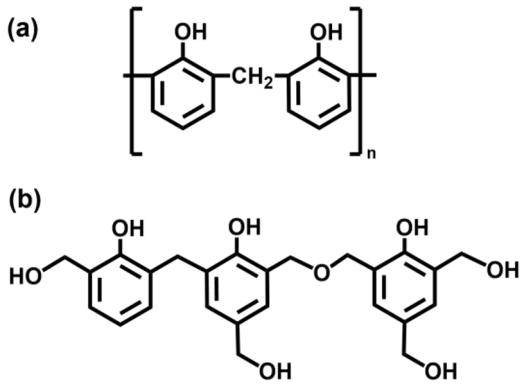

Figure 2.14. *Representative structures of (a) novolac and (b) resol resin.[138]*

2.5.2. Thermoplastics

Producing thermoplastic materials with added functionalities represents another economically beneficial way to utilize lignin. The common approaches for preparing lignin-based thermoplastic materials include plasticizing lignin with small-molecule plasticizers (*e.g.*, ethylene glycol), blending with miscible polymers (*e.g.*, poly(ethylene oxide)),[142] blending with immiscible polymers (*e.g.*, polylactic acid), and chemical modification through polymer grafting and polymerization.[132,143,144] Lignin-based thermoplastic materials have revealed potential in engineering plastics, thermoplastic elastomers, and carbon fiber precursors.[142] One of the most attractive applications of thermoplastic lignin-based composites is latex for functional bio-based adhesives, paints, coatings, and packaging, which are all essential to our daily life. Natural latex is the cytoplasmic content of latex vessels found beneath the bark of mature rubber trees, such as *Hevea brasiliensis*.[145] Synthetic latex is a stable colloidal emulsion in water containing polymeric particles (*e.g.*, acrylics and styrene-butadiene) with a few hundred nanometers in particle size, which are usually fabricated

by emulsion polymerization of water-immiscible monomers. Two techniques, *i.e.*, seeded free-radical emulsion polymerization and controlled radical emulsion polymerization of amphiphilic block copolymers (commonly a macro-CT agent) in aqueous dispersed systems, have proven effective in fabricating hybrid latex colloids and core-shell latex colloids, including bio-latex.[116,146–148] These processes involve emulsion, miniemulsion, dispersion polymerization, and polymerization-induced self-assembly techniques to produce latex colloids with well-defined morphology.[147,149,150]

In the most recent decade, forest biorefinery concepts have been developed to provide woody biopolymers that are renewable and sustainable alternatives to petroleum-based building blocks in latex fabrication. Many cases utilize bio-latex dispersions, such as hemicelluloses and starch, in barrier and pigment binder packaging applications.[146,151,152] GGM, the major hemicellulose derived from softwood, was functionalized with polymerization-active allyl groups *via* base-catalyzed etherification.[146] Free-radical emulsion polymerization of butyl acrylate (BA) monomer with allylated GGM in aqueous media successfully fabricated bio-latex films with highly transparent, hydrophobic, and flexible characteristics. The hemicellulose content of the obtained bio-latex could reach about 50%, which exhibited a tremendous perspective for sustainable packaging.

In contrast, lignin, a natural 'binder' and 'barrier' for the plant cell wall, is seriously underestimated. Only relatively small amounts of lignin have been used in bio-latex (1 – 10 wt%).[116,148] Integrating significant amounts of lignin into latex is challenging due to the poor solubility and dispersibility of lignin in water, which usually reduces the emulsion polymerization performance regarding hydrophobic monomer conversion.[148] The development of lignin-containing latex has great potential to find its revenue in functional coatings and packaging applications. In this application scenario, polymerization-active lignin with good solubility in water, LNPs with surface functionality and durable dispersibility in water, and a low glass transition temperature (Tg) of lignin to ensure the formation of a smooth and flexible latex film might be the fundamental characteristics of lignin-containing latex colloids that can support high lignin content.

2.5.3. Nanocomposites containing LNPs

LNPs have been demonstrated for various attractive applications, such as carrier and delivery of cargos (*e.g.*, therapeutics),[68] hybrid nanoparticles,[94] stabilizers for durable Pickering emulsions,[97] bio-adhesives,[104,131] and polymer

nanocomposites.[32,104,131] Among the demonstrated applications of LNPs, their use to mediate interfacial interactions in nanocomposites to fabricate high-performance materials has gained immense interest. It has previously been shown that the surface of LNPs can modulate the polymerization of water-immiscible monomers in water medium and generate energy-dissipative interactions with entangled polymer chains in toughening of cellulose-polycaprolactone nanocomposites,[153] polystyrenes,[154] poly(vinyl alcohol),[155] pectin-polyacrylic acid hydrogels, *etc*.[156]

LNPs, as one of the most innovative nanostructured materials, have attracted a heightened interest in sustainable packaging applications, where LNPs can impart several beneficial characteristics to bioplastics, such as enhanced mechanical properties,[32,33] antimicrobial properties, antioxidant activity,[157] ultraviolet-shielding properties, water vapor barrier, and oxygen barrier, compared to the native form of lignin.[158] With the continued focus on sustainability, the development of more easily recyclable and sustainable packaging materials, such as paper and board, cellulose-based polymers, and high-barrier as well as multifunctional bioplastics, is in high need to replace traditional plastic packaging materials.

There are nevertheless unsolved challenges in the current valorization approaches of LNPs in nanocellulose, such as uncontrollable interfacial interactions. In this scenario, the development of strategies capable of modulating the morphology and dispersibility of nanoscale lignin in cellulose dispersions is of high industrial relevance, such as formulation for dispersion barrier coating in packaging applications. In addition, the prerequisites for fabricating functional nanocomposites containing large amounts of LNPs may include: (i) well-defined nanostructures of LNPs in nanocomposites, which can be achieved by templating approach, (ii) durable dispersibility in water and certain organic solvents, which confers resistance to harsh reaction conditions (*e.g.*, extreme acid and alkaline pHs),[94] (iii) amphiphilic characteristics as demanded for Pickering emulsion strategy to enhance the interactions with hydrophilic polymeric matrices and hydrophobic polymers,[153] and (iv) active surface sites available for surface functionalization to enhance the interfacial interactions.[104,132]

2.6. Lignin structure-property correlation

Research on the correlation between lignin structural characteristics and material properties has promoted the application of lignin in bulk materials

and nanomaterials. The existing lignin structure-material property correlations in the literature are summarized in **Table 2.5**.

Table 2.5. Lignin structure-property correlations in lignin-containing materials.

lignin-based materials	lignin resources	lignin structural characteristics	material properties
epoxy resins[74,159,160]	kraft lignin from spruce, eucalyptus	high molar mass; more rigid and condensed linkages	thermomechanical properties, *e.g.*, toughness
polyurethanes[161]	organosolv lignin from poplar	low molar mass with more hydroxyl groups	toughness and ductility
lignin-*graft*-poly(methyl methacrylate) (PMMA) coupling agent[115]	alkaline lignin	high molar mass; high S/G ratio; high flexible/rigid linkage ratio	low elastic modulus, while high strain of the PMMA/lignin-*g*-PMMA blends
thermoplastic polymer/lignin blends[162]	lignosulfonate	low molar mass; less aryl ether linkages; more phenolic-OH groups	high miscibility
carbon fibers[163]	organosolv lignin from hardwood, softwood, herbaceous plants	more linear β-O-4' linkages	higher tensile strength and elastic modulus; enhanced electrical conductivity
LNPs prepared by solvent-shifting[164]	kraft lignin from mixed hardwood	high molar mass and narrow $Đ_M$	spherical morphology
biomedical applications[68]	kraft lignin from spruce, eucalyptus	high molar mass; surface distribution of carbohydrates	interaction between LNPs and cancer cells

The properties of thermosets (*e.g.*, epoxy resins and polyurethanes),[74,159–161] thermoplastics (*e.g.*, lignin-based coupling agent and polymer/lignin blends),[115,162] and lignin-based carbon fibers,[163] were enhanced by defining the lignin structure-property relationships using lignin fractionation methodologies or using different biomass feedstocks. In terms of nanomaterial applications, lignin structure-property correlations aided our understanding of the impact of lignin structural features on the morphology of LNPs and the impact of surface functionality on biomedical applications.[68,164] Lignin fractionation provides a methodology to rationally design lignin-based materials with tailored properties at the molecular level. More specifically, high

molar mass lignin fractions with more condensed lignin interunit linkages can promote the mechanical properties of thermosets and fabricate uniform lignin nanospheres, while low molar mass fractions with more hydroxyl groups can enhance the miscibility of lignin with thermoplastic and increase the reactivity as polyols. Furthermore, robust tools have been developed to ease the lignin structural correlation, such as using the $Đ_M$ profile of technical lignin to predict the functional heterogeneity and functional group content.[67] The method mentioned above could simulate the effect of the intended purification process.[67]

3. Materials and methods

This section summarizes all materials and methods related to the thesis studies. Further details and experimental protocols can be found in the attached scientific articles (Paper I–IV).

3.1. Lignin and fractionation methodologies

3.1.1. Softwood and hardwood alkaline lignins

Birch (*Betula pendula*) and Norway Spruce (*Picea abies*) AL isolated in the BLN biorefinery process were used for all studies included in this thesis. Water-soluble ash and sugar impurities were removed from the lignin by washing with acidic water (pH 2.5, HCl). Low molar mass impurities such as lipophilic extractives were removed by thorough MTBE extraction.

3.1.2. Sequential solvent fractionation

The alcohols of *i*-PrOH (99.8%, Sigma-Aldrich), EtOH (96%, VWR Chemicals), and MeOH (99.9%, Sigma-Aldrich) were selected to sequentially extract purified birch and spruce AL based on solubility, potential for commercialization, and environmental impact. The initial volume : mass ratio of *i*-PrOH : lignin was 10 : 1 (v/m). Briefly, 50 g of birch AL was dispersed in 500 mL of *i*-PrOH and stirred for 2 hours. The *i*-PrOH-soluble fraction (*i*-PrOH-s) was collected by filtration using 0.2 μm nylon membrane and dried by rotary evaporation under 90 mbar in a 50 °C water bath. The *i*-PrOH-insoluble fraction was extracted by 500 mL of EtOH, and the solution of EtOH-soluble fraction (EtOH-s) was isolated by rotary evaporation under 110 mbar. Similarly, the MeOH-soluble fraction (MeOH-s) was obtained from the EtOH-insoluble fraction. Lignin that remained at the end of the solvent sequence was denoted as residue. All lignin fractions were dried for 12 hours at 40 °C in a vacuum desiccator to eliminate solvent residues.

3.2. General compositional analysis

Klason lignin (acid-insoluble lignin) content was determined gravimetrically following a standardized protocol in which polysaccharides were hydrolyzed by 72 wt% sulfuric acid (H_2SO_4) followed by 3 wt% H_2SO_4 hydrolysis.[165] The acid-soluble lignin content was determined by UV-vis spectrophotometry (Shimadzu UV-2600, Japan) following the previously described protocol.[166] The absorbance difference at 205 nm between Klason lignin filtrate and 3 wt% H_2SO_4 reference solution in a quartz cuvette with 1 cm light path length and

extinction coefficient of 110 L g^{-1} cm^{-1} for lignin were used to calculate the concentration of acid-soluble lignin according to Beer-Lambert law.

To characterize the chemical composition of hemicelluloses in the samples, acid methanolysis in combination with trimethylsilylation were carried out according to a well-established protocol reported by Sundberg *et al*.[167] Trimethylsilylated derivatives of monosaccharides and uronic acids were determined by gas chromatography (GC) equipped with a flame ionization detector (FID) on an Agilent capillary column coated with crosslinked methyl polysiloxane (HP-1, 25 m × 0.20 mm i.d., 0.11 μm film thickness). Then, the hemicellulose content in the samples was quantified against resorcinol using coefficient factors determined by calibration. The data were analyzed using the PerkinElmer TotalChrom Microsoft Windows software package.

The composition of extractives in the samples (MTBE-soluble fraction) was determined by GC equipped with a mass selective detector (MS, HP 5973 GC-MS system, USA) after trimethylsilylation.[65] The content of the extractives was quantified by GC-FID.

3.3. Characterization of lignin structures

The molar mass of the lignin sample was determined by an advanced absolute molar mass detection method.[168] Structural characteristics of lignin, such as functional groups, constituent aromatic units, interunit linkage patterns, and DC values, were determined by nuclear magnetic resonance (NMR) using a Bruker AVANCE III 500 MHz spectrometer equipped with a 5 mm Z-gradient Broadband Observe CryoProbe.

3.3.1. Analysis of molar mass

Molar mass characterization was performed on a high-performance size exclusion chromatograph (SEC) equipped with a multi-angle light scattering detector and a differential refractive index concentration detector. Freeze-dried lignin was dissolved in dimethyl sulfoxide (DMSO) containing 0.05 M lithium bromide to 10 mg mL^{-1} and filtered over a 0.2 μm nylon syringe filter before SEC analysis. The separation was performed on a Jordi Gel Glucose Mixed-bed guard column (50 m × 10 mm i.d) and a Jordi Gel GBR Mixed-bed column (250 m × 10 mm i.d). The molar mass analysis was performed using the following parameters: 0.5 mL min^{-1} flow rate; 60 °C column temperature; 100 μL injection volume; 0.15 mL g^{-1} dn/dc value. ASTRA software, version 7.3.2, was used to evaluate the data.

3.3.2. Hydroxyl group and methoxyl group distributions

Quantitative ^{31}P NMR (202.46 MHz, 298 K) using a *zgig* pulse sequence was performed on the lignin samples to reveal the distribution of aliphatic-OH, phenolic-OH, and -COOH groups according to well-established protocols.[169-171] The samples were prepared as follows: 20.0 mg of freeze-dried lignin powders were dissolved in the solvent mixture of 0.55 mL of anhydrous pyridine and deuterated chloroform ($CDCl_3$) (1.6:1, v/v) that contained relaxation reagent of chromium(III) acetylacetonate ($Cr(acac)_3$, 1.3 μmol) and internal standard of *endo*-N-hydroxy-5-norbornene-2,3-dicarboximide (12 μmol). The ratio of internal standard to lignin was set to 0.6 mmol g^{-1}. The hydroxyl groups were phosphorylated with 0.1 mL of 2-chloro-4,4,5,5-tetramethyl-1,3,2-dioxaphospholane for 30 min prior to ^{31}P NMR measurement. The concentration of $Cr(acac)_3$ was 0.002 M to ensure the complete relaxation of the phosphorus nuclei before the application of the next radiofrequency pulse. Spectrum acquisition parameters included a 10 s pulse delay and 2.0 s acquisition time, and 64 scans were recorded.

The content of -OCH_3 groups was determined with ^{1}H NMR (500.13 MHz, 298 K) using 4-nitrobenzaldehyde as an internal standard.[172] Samples were prepared as follows: around 15.0 mg of acetylated lignin and ~5.0 mg of 4-nitrobenzaldehyde were dissolved in 0.75 mL deuterated DMSO (DMSO-d_6). The ^{1}H NMR spectrum was acquired with the following parameters: *zg30* pulse sequence, 2.0 s relaxation delay, 1.1 s acquisition time, and 64 scans were recorded.

3.3.3. Constituent aromatic units

The lignin subunits (*e.g.*, S, G, and H subunits) and catechol derivatives were determined by pyrolysis-gas chromatography-mass spectrometry (*Py*/GC-MS). Lignin samples (~ 100 μg) were pyrolyzed at 600 °C using a Pyrola 2000 pyrolyzer. The pyrolyzed products were separated on an Agilent 7890B GC instrument equipped with an HP-5MS column (25 m × 0.2 mm i.d, 0.33 μm film thickness) and identified by an Agilent 5977B mass spectrometer. The S/G ratio was determined from the peak area ratio of the S- and G-subunit fragments in the *Py*/GC-MS spectrum.

3.3.4. Quantification of interunit linkages

The main lignin compositional moieties and interunit linkages per 100 aromatic units (Ar) were quantified according to **Equation 2** by multiplicity-edited heteronuclear single quantum coherence (HSQC) in combination with quantitative ^{13}C NMR experiments following previously reported protocols and criteria.[173,174]

X (per 100 Ar) = $I_x/I_{(90.0–78.0/6.0–2.5)}$ (HSQC) × $I_{(90.0–78.0)}/I_{(163.0–100.0)}$ (^{13}C) **(2)**

where

I_x (HSQC): the integral value of signal originating from side-chain HC_β in *β*-O-4' structures (*i.e.*, *β*-O-4' with S-, G-, and H-subunits); HC_α-OH in *β*-*β*' structure, including resinol and epiresinol moieties; HC_α-OH in *β*-5' structure; HC_α-OH in *β-1'* structure in the region of δ_C/δ_H 90.0 – 78.0/6.0 – 2.5; all of the integrations in the HSQC spectrum were carried out at the same contour level

$I_{(90.0–78.0/6.0–2.5)}$ (HSQC): total integral of signal clusters in this region

$I_{(90.0–78.0)}$ (^{13}C): total integral of this region in quantitative ^{13}C NMR spectrum

$I_{(163.0–100.0)}$ (^{13}C): the integral value of total aromatic carbons in the ^{13}C NMR spectrum of birch ALs was assigned a value of 600, while 612 was assigned to spruce ALs, which includes total aromatic carbons and double bond carbons (*e.g.*, stilbene and enol ether structures)[173]

3.3.4a. HSQC NMR

HSQC NMR spectra were acquired using the *HSQCEDETGPSISP2.3* pulse sequence with a relaxation delay of 2.0 s and an acquisition time of 0.13 s, recording 256 increments of 80 scans per increment. The samples were prepared as follows: around 80.0 mg of freeze-dried lignin powders were dissolved in 0.75 mL DMSO-d_6.

3.3.4b. Quantitative ^{13}C NMR

The samples for quantitative ^{13}C NMR (125.78 MHz, 298 K) analysis were prepared as follows: around 200.0 mg of freeze-dried lignin powders were dissolved in 0.55 mL DMSO-d_6 containing relaxation reagent of $Cr(acac)_3$ at a concentration of 0.016 M.[175] The quantitative ^{13}C NMR spectrum was acquired with the following parameters: *zgig* pulse sequence, a relaxation delay of 2.0 s, an acquisition time of 1.1 s, and a total of 20,000 scans were recorded.[175]

3.3.5. Degree of condensation

The DC value per 100 Ar units that emerged from the aromatic substitution pattern at C_2, C_5, and C_6 positions was estimated by *Py*/GC-MS and the content of $C_{Ar–H}$ integrated from the quantitative ^{13}C NMR spectra, according to **Equation 3**, following the protocol reported by Capanema and Balakshin.[175,176]

(2S%+3G%+2H%) - $I_{(125.0–102.0)}/I_{(163.0–100.0)\text{non-acetylated}}$ (^{13}C) **(3)**

Where

2S%+3G%+2H%: the contribution of noncondensed S-subunits, G-subunits, and H-subunits into the resonance at 125–102 ppm[174]

$I_{(125.0–102.0)}/I_{(163.0–100.0)}$: the integral value of $C_{Ar–H}$ per 100 Ar units when assigning the integral of total aromatic carbons in the region of $I_{(163–100)}$ to 600 (birch ALs) or 612 (spruce ALs)[173]

3.4. Thermosetting phenolic resin

3.4.1. Lignin phenolation

Lignin phenolation was optimized for alkali charge and lignin to phenol (L/P) mass ratio. In brief, 3.0 g of dry lignin powder was first mixed with 15.0 g phenol (L/P = 1/5) preheated to 50 °C during stirring, and then a defined amount of 10 M NaOH solution was added to adjust the pH to 8.5, 9.0, 9.4, and 9.8. The phenolation reaction was carried out at 95 °C for 2 hours. The reaction products were dissolved in 40 mL Milli-Q water and precipitated by 1.0 M HCl until pH reached 2.5. The obtained phenolated lignin was thoroughly washed with MTBE to remove residual phenol, followed by drying in a vacuum desiccator at 40 °C to a constant weight. The L/P mass ratio (*e.g.*, L/P of 1/5, 2/5, 3/5, and 5/5) was optimized, with the optimal alkali charge being corroborated by ^{31}P NMR of the phenolated lignin.

3.4.2. Preparation of LPF adhesives and plywood

Thermosetting LPF adhesives were prepared by one-pot batch polymerization, starting with lignin phenolation under the optimized conditions. The hydroxymethylation and polymerization steps were carried out under base catalysis. The total amount of formaldehyde was tuned to maintain a stoichiometric molar ratio (0.6 : 1.0) between formaldehyde and reactive sites in phenolated lignin and phenol, *i.e.*, nonsubstituted *ortho* and *para* positions of the phenolic-OH groups. The temperature of the lignin phenolation reaction was cooled down to 80 °C from 95 °C before 70 % (v/v) of the total formaldehyde and 10 M NaOH solution (8 wt% of the amount of lignin and phenol) was added. The remaining mixture of the formaldehyde and 10 M NaOH solution was added after 1 hour of reaction. The reaction was continued for 1 hour at 80 °C during stirring.

Three-layer plywood was prepared by applying LPF wood adhesive on each side of a core birch veneer (200 mm × 200 mm × 1.3 mm) with an adhesive coat weight of 250 g m^{-2}. The fiber directions of the adjacent veneer were vertically glued together. Then, the three-layer plywood was fabricated through hot-pressing at 145 °C and 1.0 MPa for 10 min.

3.4.3. Curing behavior

The curing behavior of LPF adhesives was determined by differential scanning calorimetry (DSC) using a Discovery DSC 250 calorimeter (TA Instruments, USA). Substantial quantities of water were liberated during the curing process of LPF adhesives. To suppress the interfering endothermic evaporation peak of water, PerkinElmer high-pressure stainless steel capsules were used for DSC analysis.[177] To calculate the activation energy, the samples were heated from 10 to 270 °C at 2.5, 5.0, and 7.5 °C min^{-1} under a nitrogen (N_2) atmosphere (50 mL min^{-1}), respectively.

3.4.4. Wet bonding strength

The wet bonding strength of the plywood specimens was determined using an Instron instrument with a tensile loading of 625 N min^{-1}. Specimens (100 mm × 25 mm × 5 mm) with a slot width of 3.0 mm and a shear section length of 25 mm were prepared according to the GB/T 1765-2013 standard. The specimens were subjected to 28 h boil-dry-boil treatment before the tensile test.

3.5. Thermoplastic bio-latex

3.5.1. Preparation of A-LNPs

Lignin (250 mg, 4.71 mmol g^{-1} hydroxyl groups) was dissolved in 10 mL of 0.5 M NaOH solution. The allyl glycidyl ether solution (135 mg, 1.18 mmol) was introduced dropwise to the alkaline lignin solution in a two-necked round-bottom flask connected with a reflux condenser under the N_2 atmosphere. The reaction was continued for 10 hours at 60 °C during stirring. The reaction media was dialyzed against Milli-Q water using a 1000 Da dialysis membrane (Spectra/Por®7) to obtain a dispersion of allylated LNPs (A-LNPs) and to remove the unreacted components. The same sample preparation procedure was carried out to obtain the A-LNP-x dispersions, where x denotes the molar ratio of allyl glycidyl ether to lignin hydroxyl groups.

3.5.2. Preparation of bio-latex using A-LNPs as structural templates

A-LNP-pBM latex colloids composed of an A-LNP core (250 mg) and a poly(butyl acrylate-*co*-methyl methacrylate) (pBM) shell were prepared by semi-batch free-radical emulsion polymerization of BA and methyl methacrylate (MMA) monomers in an A-LNPs dispersion (~20 mL). Sodium dodecyl sulfate (SDS) and ammonium persulfate (APS) were used as the surfactant and the thermally-induced free-radical initiator, respectively.

Latex films with a thickness of about 150 μm were prepared by loading A-LNP-pBM latex onto a plastic petri dish with a dry mass loading of 25 – 26 mg m^{-2}, followed by drying and annealing at 50 °C for 18 hours.

3.5.3. Monomer conversion

Monomer conversion kinetics during the emulsion polymerization of BA and MMA with A-LNPs as structural templates were determined using a high-performance liquid chromatograph (HPLC) equipped with a UV diode array detector performed at 210 nm. The BA and MMA residues in latex were extracted with HPLC-grade MeOH. The acrylate monomers were separated on an Agilent Poroshell 120 EC-C18 column. For quantitative determination, the peak areas of the chromatograms obtained from the residual monomers were compared to standard calibration curves obtained by plotting the peak areas against known concentrations of BA and MMA monomer standards.

3.6. Cellulose–lignin nanocomposites

3.6.1. Laccase-catalyzed lignin oxidation and polymerization

Laccase solution (~ 560 μL) with enzyme activity of 357 U mL^{-1} was added to 20 mL lignin solution (~ 10 mg mL^{-1}, pH 10). The mixture was incubated at 39 °C with ambient air circulation during stirring for a predetermined time. The laccase-treated lignin was isolated through acid precipitation at pH 2.5 using 2 M HCl, followed by centrifugation (8000 rpm, 10 min). The precipitates were collected and freeze-dried.

3.6.2. *In situ* laccase-catalyzed lignin polymerization using nanocellulose as a structural template

Microfibrillated cellulose (MFC) dispersion was prepared from bleached birch kraft pulp (UPM, Finland) through mechanical refining using a Valmet ProLab™ laboratory refiner, followed with homogenization with a high-pressure homogenizer. The MFC dispersion (200 mL, 0.4 wt%) was mixed with lignin solution (~ 10 mg mL^{-1}, pH 10) to achieve lignin contents of 15 wt%. The MFC/lignin mixture was equilibrated to 39 °C and pH 10 during stirring with aeration, and thereafter, laccase solution with the activity of 1 U mg^{-1} of lignin was introduced to initiate the *in situ* polymerization reaction. Dispersions of laccase-polymerized MFC/lignin were obtained after inactivating laccase in a 90 °C water bath for 15 min.

3.6.3. Preparation of cellulose–lignin nanocomposite films

The MFC/lignin film was fabricated using a vacuum-filtration method. In short, laccase-polymerized MFC/lignin dispersion was diluted to a solid content of 0.2 wt% with NaOH solution (pH 10) and vacuum-filtrated on a 0.2 μm nylon membrane. The wet film was washed with distilled water until the pH of the filtrate was neutral, and then the film was air-dried under a 5 kg load at room temperature. The film samples were stored in a conditioned room (23 °C, 50% relative humidity) before further characterizations.

3.7. Hemicellulose–lignin nanocomposites

3.7.1. Preparation of L-LNPs

Freeze-dried laccase-polymerized lignin powder (~ 100 mg) was dissolved in 100 mL THF/H_2O (9 : 1, v/v) medium. The mixture was stirred at 500 rpm for 3 hours and then filtrated through a 0.2 μm polytetrafluoroethylene syringe filter to remove the insoluble lignin. 200 mL of distilled water was added dropwise into the lignin solution during rapid stirring (~ 1000 rpm), and thereafter, another 200 mL of water was added to the mixture and stirred continued for 20 min. THF was removed from the water medium by rotary evaporation, and the dispersion of LNPs from laccase-polymerized lignin (L-LNPs) was concentrated using centrifugation.

3.7.2. *In situ* reduction of Ag^+ on the surface of L-LNPs

To prepare L-LNPs with surface-embedded silver nanoparticles (L-LNP@Ag), 2 mL of the L-LNPs (~ 8 mg mL^{-1}) was mixed with 4 mL of silver ammonia solution (10 mg mL^{-1}, pH 11), followed by incubating at 30 °C for 4 hours during shaking. The L-LNP@Ag was purified by repeated steps of centrifugation and redispersion in distilled water by mixing and vortexing. The silver loading in L-LNP@Ag was determined using inductively coupled plasma-optical emission spectroscopy (ICP-OES) combined with a microwave digestion pretreatment.

3.7.3. Preparation of GGMMA/L-LNP@Ag photo-crosslinkable resin and hydrogel

The methacrylated GGM derivative (GGMMA) was synthesized by reacting Norway spruce GGM with a number-average molar mass of 9 kDa with methacrylic anhydride at alkaline conditions (pH 8).[178] The degree of substitution of the methacryloyls was 0.25 per sugar unit as determined by quantitative ^{13}C NMR. The photo-crosslinkable resin was formulated in water with GGMMA, lithium phenyl-2,4,6-trimethylbenzoylphosphinate (LAP) photoinitiator, and varied contents of L-LNP@Ag, ranging from 0.02 to 0.5 wt%. The 10GGMMA/0.1L-LNP@Ag resin was prepared by mixing 125 μL of L-

LNP@Ag dispersion (~ 8 mg mL^{-1}) and 50 µL of LAP aqueous solution (50 mg mL^{-1}) with 825 µL of distilled water and then with 100 mg GGMMA powder.

The honeycomb constructs of GGMMA/L-LNP@Ag hydrogels were fabricated by an M-One Pro 30 digital light processing (DLP) printer (Makex Co., Ltd, China) operating at a wavelength of 405 nm with an x–y nominal printing resolution of 33 µm. The printing parameters were set as follows: 0.5 mL of 10GGMMA/0.1L-LNP@Ag resin, exposure time 80 s, and layer thickness 35 µm.

3.8. Analysis of thermal properties

3.8.1. Thermal degradation temperature

The thermal stability of the lignin samples was determined by thermal gravimetric analysis using a Q500 thermogravimetric analyzer (TA Instrument, USA). The freeze-dried samples (~ 10 mg) were weighed into an alumina disposable crucible (T 210127, China) and heated from 30 to 800 °C at 10 °C min^{-1} under the N_2 atmosphere.

3.8.2. Glass transition temperature

The Tg of the samples was measured with a Discovery DSC 250 calorimeter using a heating-cooling-heating temperature program under continuous N_2 flow. The freeze-dried samples were weighed into a Tzero pan (T 140829, Switzerland) sealed with a Tzero lid (T 140826, Switzerland) and then transferred to the calorimeter containing a reference, *i.e.*, a sealed Tzero pan. The temperature corresponding to the half-height midpoint of the glass transition region in the second heat capacity *vs.* temperature plot is reported as the Tg using TRIOS v5.5.1.5 software.

3.9. Characterization of nanoparticles

3.9.1. Dispersion stability

3.9.1a. Hydrodynamic diameter and size dispersity

The intensity-weighted average hydrodynamic diameter (Z-average) and size dispersity ($Đ$) of nanoparticles were determined by a Zetasizer Nano instrument (Malvern Instruments, UK). The diluted nanoparticle dispersion (~ 0.02 wt%) was measured with the following parameters: a Helium-Neon laser wavelength of 632.8 nm; a scattering angle of 173°; refractive index and viscosity of the dispersant (water) were set to be 1.330 and 0.887×10^{-3} pa.s, respectively; the refractive index and absorption value of the nanoparticles were set to be 1.595 and 0.200, respectively. The Z-average and $Đ$ values were

collected through three consecutive measurements, for which the mean result was reported.

3.9.1b. ζ-potential analysis

The ζ-potential analysis was performed on diluted nanoparticle dispersions (~ 0.02 wt%) using a Zetasizer Nano instrument (Malvern Instruments, UK) with a disposable folded capillary cell (DTS1070).

3.9.2. Nanoparticle morphology

3.9.2a. Transmission electron microscopy

The morphology of nanostructures was characterized using a JEM-1400 PLUS microscope (JEOL Ltd., Japan) in the bright-field mode. The samples were prepared as follows: around 5 μL of the diluted nanoparticle dispersion was dropped onto a carbon film supported copper grid (200 mesh, TED PELLA INC. USA) and incubated at ambient temperature for 3 min followed by blotting of excess liquid with a filter paper before loading into the microscope. In order to enhance the contrast of latex colloids in the bright-field mode, the samples of pBM and A-LNP-pBM latex colloids were prepared by the uranyl acetate negative staining method. The average particle size was measured by imaging 150 – 200 particles from TEM images using ImageJ software.

3.9.3. Surface tension

The surface tension of allylated lignin solutions (1.0 mg mL^{-1}, pH 13.3) against air was measured with a Krüss force tensiometer-K100 using a Wihelmy plate at 25 °C.

3.9.4. Surface chemistry

3.9.4a. ^{1}H NMR

The ^{1}H NMR method reported by Pylypchuk *et al*., *i.e.*, NMR pulse sequence combining pre-saturation and excitation sculpting water suppression, was applied to evaluate the surface functionality of A-LNPs in aqueous dispersion.[179] In short, the surface-distributed allyl groups of A-LNPs were quantified by ^{1}H NMR (500.13 MHz, 298 K) using 3-(trimethylsilyl) propionic-2,2,3,3-d_4 acid, sodium salt as internal standard in deuterated water. *zgesgp* pulse sequence with a relaxation delay time of 1.0 s and an acquisition time of 2.0 s was used to record the ^{1}H NMR spectra for a total of 64 scans.

3.9.4b. X–ray photoelectron spectroscopy

The allyl-terminated chains distributed in the near-surface layer of A-LNPs and the valence state of Ag on the surface of L-LNPs were determined by X-ray

photoelectron spectroscopy (XPS). The Gaussian (70%) – Lorentzian (30%) function was used to approximate the line shape for the core-level region deconvolution. The C 1s signal at 284.8 eV was used as an internal standard for binding energy calibration. The full width at half maximum was constrained during the deconvolution of all core-level regions.

3.9.4c. Ultraviolet–visible spectroscopy

The characteristic surface plasmon resonance absorption peak of metallic silver was measured by ultraviolet–visible spectroscopy (Shimadzu UV-2600, Japan).

3.9.5. Surface wettability

The surface wettability of A-LNPs was evaluated in the form of their thin films, which were prepared by absorbing anionic A-LNPs onto the poly-L-lysine-coated silicon wafer according to a previously reported protocol.[180] The static water contact angle (WCA) measurements were performed using a sessile drop method on a KSV CAM200 instrument.

3.9.6. Crystal structure

The crystalline structure of L-LNP@Ag was determined by X-ray diffraction (XRD) using a Bruker D8 ADVANCE diffractometer (Bruker-AXS, Germany) with CuKα radiation (λ = 1.54184 Å).

3.10. Characterization of nanocomposite films

3.10.1. Analysis of nanostructured surface

3.10.1a. Atomic force microscopy

All the atomic force microscopy (AFM) measurements were carried out with a MultiMode 8 AFM (Bruker, Santa Barbara, CA) equipped with a Nanoscope V controller in ambient air at room temperature (22.3 ± 2 °C, 60 ± 5% relative humidity). The used scan size was 5 × 5 μm^2 with a resolution of 1024 × 1024 pixels. The scanning speed was 1 Hz. Nanoscope Analysis (version 1.5, Bruker) was used for data analysis.

The topographical characteristics and surface mechanical properties of the A-LNP-pBM films were determined in the PeakForce quantitative nanomechanical mapping (PF-QNM) mode. SCANASYST-AIR probe (Bruker, k: 0.4 N/m, f_0: 70 kHz) was used for the PF-QNM AFM measurements. The spring constant was calibrated at 33 – 35 N m^{-1} by using the Sader method. A clean fused silica substrate (Bruker, Santa Barbara, CA) was used to calibrate the deflection sensitivity (32 – 34 nm V^{-1}) and a reference polystyrene film (Bruker,

Santa Barbara, CA) with a Young's modulus of 2.7 GPa was used to calibrate the tip radius at a certain indentation depths, typically 2 – 3 nm. Derjaguin-Muller-Toporov model was used to calculate the stiffness distribution.

3.10.1b. Small–angle X–ray scattering

The small-angle X-ray scattering (SAXS) analysis of the neat pBM and A-LNP-pBM films was performed under vacuum at 25 °C using synchrotron X-rays (λ = 1.542 Å) from Spring-8 beamline BL03XU. The q-range was calibrated by measuring lanthanum hexaboride standard sample with known diffraction peak positions.

3.10.2. Analysis of mechanical properties

3.10.2a. Dynamic mechanical analyzer

Temperature-dependent profiles of films on extensional moduli were determined by a MCR 702 multidrive dynamic mechanical analyzer (DMA, Anton Paar, Austria) equipped with a convection temperature device (CTD 180, Anton Paar, Austria). The DMA temperature ramp test for the MFC/lignin films was performed on specimens (30 mm × 4 mm × 35 μm) with the following parameters: heat from 35 to 170 °C at 5 °C min^{-1} under 1 Hz oscillation frequency and 0.01% tensile strain. The DMA temperature ramp test for neat pBM and A-LNP-pBM latex films was performed on specimens (10 mm × 3 mm × 200 μm) with the following parameters: heat from 0 to 50 °C at 5 °C min^{-1} under 1 Hz oscillation frequency and 0.1% tensile strain.

3.10.2b. Tensile strength test

The tensile strength of the MFC/lignin films (30 mm × 4 mm × 35 μm, gauge length of 4 – 5 mm) was determined with an Instron instrument at a strain rate of 1 mm min^{-1} according to the ASTM D638 standard. The mechanical properties of the latex films (40 mm × 0.5 mm × 200 μm) were evaluated using a Lloyd Ir30 universal testing machine equipped with a 250 N loaded cell at a strain rate of 20 mm min^{-1}. The toughness of the latex films was determined by the area under the stress-strain curve up to the fracture point. The results are reported as mean values ± standard deviation of four samples.

3.10.3. Analysis of water barrier properties

The water vapor transmission rate (WVTR) of the film samples was measured according to the ASTM E96/E96M-10 standard.

3.11. Characterization of photo-crosslinked hydrogels

3.11.1. Printing fidelity

The printing fidelity of the DLP-printed honeycomb hydrogel was determined with a Nikon ECLIPSE E200 digital microscope equipped with a Nikon digital sight DS-US camera.

3.11.2. Antimicrobial activities

The bactericidal ratios of the GGMMA/L-LNP@Ag hydrogel against *Escherichia coli* (*E. coli, K12 DSM498*) and *Staphylococcus aureus* (*S. aureus, ATCC 25923*) were quantified using broth-microdilution method.

4. Results and discussion

4.1. Fractionation of alkaline lignin using solvent (Paper I & III)

To establish the correlations between lignin structural characteristics and the properties of the resulting materials and further to enhance the integration of lignin into functional materials, technical lignin was carefully fractionated and analyzed. Industrial birch and spruce ALs were fractionated through a sequential solvent fractionation approach using *i*-PrOH, EtOH, and MeOH. The rationale of the selection of the raw material is that these two wood species are expected to produce structurally distinct ALs based on their monolignol compositions. In addition, compared to kraft lignin and organosolv lignin, AL does not contain sulfur and is not benzyl derivatized, which can warrant the reactivity of lignin in chemical integration to materials. The solvent solubility power within the proposed fractionation sequence was increased, which realized the sequential fractionation of lignin and provided two series of solvent-soluble lignin fractions with a total extraction yield of around 80 wt% from birch AL and 60 wt% from spruce AL (**Table 4.1**). The high fractionation yield of the EtOH-s fraction was due to the lower energy difference between EtOH and lignin (RED = 0.98) than that of *i*-PrOH (RED = 1.06). The higher polarity and hydrogen bonding capacity of MeOH (δ_P = 12.3, δ_H = 22.3) than EtOH (δ_P = 8.8, δ_H = 19.4) facilitated the dissolution of lignin in MeOH, although its RED value (1.07) was higher than that of EtOH.

Table 4.1. The calculated RED values for lignin solubility in extraction solvents and the extraction yield of solvent-soluble fractions.

solvents	RED	yield (wt%)	
		birch AL	spruce AL
i-PrOH	1.06	18	20
EtOH	0.98	50	19
MeOH	1.07	13	17

4.1.1. Purity of lignin fractions

Lignin with high purity is one of the most important prerequisites for the research of lignin structure-property correlations. The purity of the lignin samples after extensive purifications were examined in terms of the content of structural components (*e.g.*, lignin and hemicelluloses), extractives, and ash (**Table 4.2**). It was found that carbohydrates and ash impurities were gradually enriched along the fractionation sequence of *i*-PrOH, EtOH, and MeOH, especially in residue lignin. The main hemicelluloses in birch ALs were xylans,

while the hemicelluloses in spruce ALs composed of xylans and GGMs. The lignin content as well increased along the fractionation sequence. The extractive content of birch (0.24 wt%) and spruce (0.10 wt%) AL was low, which indicated that MTBE could effectively remove extractives from lignin samples. It should be noted that all three sequential lignin fractions had low contents of impurities (*i.e.*, extractives, carbohydrates, and ash) below 1.0 wt%, which is negligible in inducing variations of lignin properties.

Table 4.2. Compositions (wt%) in birch and spruce ALs.

lignin samples	Klason lignin	acid-soluble lignin	carbohydrates	extractives	ash
birch AL	90.6	0.03	1.48	0.24	0.09
B-*i*-PrOH-s	84.3	0.10	0.24	0.44	0.03
B-EtOH-s	89.7	0.04	0.46	0.07	0.03
B-MeOH-s	91.1	0.02	1.08	---[a]	0.04
B-residue	85.5	0.02	8.36	---[a]	0.15
spruce AL	91.4	0.06	0.70	0.10	0.05
S-*i*-PrOH-s	84.8	0.20	0.57	0.31	---[a]
S-EtOH-s	90.1	0.06	0.78	0.11	---[a]
S-MeOH-s	92.3	0.03	0.97	---[a]	---[a]
S-residue	92.5	---[a]	1.11	---[a]	0.06

[a]denotes not detected.

4.1.2. Molar mass and thermal properties

The molar mass and $Đ_M$ are crucial metrics for assessing the applications of lignin, especially as phenolic precursors for polymer synthesis. In a general scenario, lignin is demanded to have a homogeneous feature in terms of $Đ_M$. The birch and spruce ALs investigated in this thesis had a weight-average molar mass (M_W) of 7200 and 17,600 g mol^{-1} and a $Đ_M$ of 2.8 and 2.1, respectively. The molar mass of lignin fractions increased along the sequence of solvent fractionation (**Figure 4.1a-b** and **Table 4.3**). Compared to the molar mass characteristics of the initial technical lignin, lignin fractions with more narrow $Đ_M$ values (1.2 – 1.6) were obtained after solvent fractionation, which proved that solvent fractionation is an effective approach for refining technical lignin. It is worth noting that the B-*i*-PrOH and S-*i*-PrOH fractions had a similar M_W of 3200 ~ 3700 g mol^{-1}, while the EtOH-s fractions from birch and spruce AL also had a similar M_W of 5000 g mol^{-1}. It further demonstrates that solvent selection is a tool for tailoring lignin characteristics.

Table 4.3. Molar mass characteristics of lignin samples.

lignin samples	birch AL		spruce AL	
	M_W (g mol^{-1})	$Đ_M$	M_W (g mol^{-1})	$Đ_M$
AL	7200	2.2	17600	2.1
i-PrOH-s	3700	1.3	3200	1.2
EtOH-s	5000	1.5	5100	1.2
MeOH-s	8400	1.6	9600	1.2
residue	27800	3.1	49210	1.9

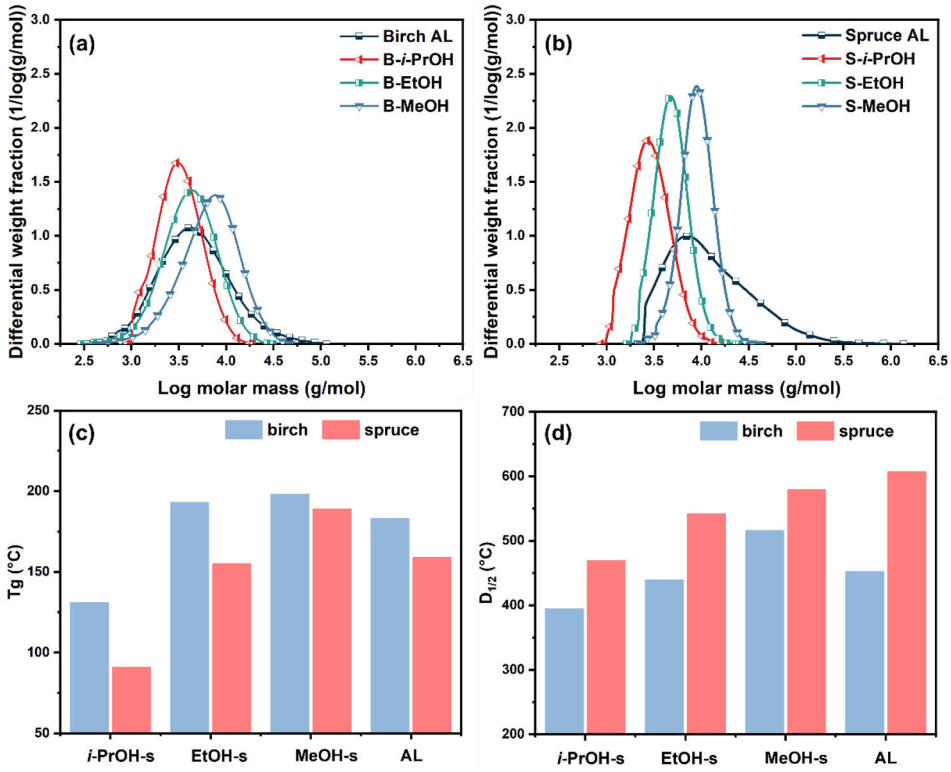

Figure 4.1. *The molar mass of (a) birch and (b) spruce ALs fractions, including initial ALs. (c) Tg and (d) $D_{1/2}$ of birch and spruce AL fractions, including initial ALs. Figure 4.1a-b is adapted from its original version in Paper III.*

The key thermal parameters of birch and spruce ALs, such as Tg and decomposition temperature ($D_{1/2}$) at 50% weight loss of the initial mass, were compared in **Figure 4.1c-d**. It was found that the Tg and $D_{1/2}$ values increased along the fractionation sequence. This indicates that the mobility of lignin molecules was restrained by an increased lignin molar mass, which in turn resulted in enhanced thermal stability. The behavior of lignin during heat treatment is important for the manufacture of thermosets and thermoplastics.

Lignin macromolecules must be flexible enough (*i.e.*, low Tg values) to be covalently integrated into a thermally-induced polymer system. Noteworthy, the spruce AL fractions had higher $D_{1/2}$ but lower Tg values than their birch AL counterparts, suggesting unwanted structural changes such as temperature-induced lignin polymerization may have occurred on birch AL fractions during DSC analysis with an annealing temperature of 200 °C.

4.2. Lignin structural characteristics (Paper I & III)

It is known that effective solvent fractionation strategies can control the molar mass and $Đ_M$ of lignin and modulate its compositional pattern and functional group distribution. In a general scenario, all these lignin characteristics are strictly interdependent. Therefore, a comprehensive structural elucidation of the obtained lignin fractions was performed using *Py*/GC-MS and NMR techniques to achieve reliable lignin structure-property correlations. The effect of solvent fractionation on the structural characteristics of AL fractions in terms of constituent aromatic pattern, interunit linkages, the content of functional groups, and condensation degree was determined.

4.2.1. Constituent aromatic units and interunit linkages

The aromatic constituent pattern of birch ALs, as delineated by *Py*/GC-MS chromatograms and HSQC spectra, consisted of S- and G-subunits, while those of spruce were exclusively G-subunits. The *i*-PrOH-s fraction from birch AL had the highest S/G subunit ratio (3.3), which decreased with increasing molar mass of lignin (original data in Paper III). This indicates that S-subunits with two *ortho*-methoxy groups tend to be enriched in low molar mass fraction of birch ALs. The abundance (Ar%) of interunit linkages that construct lignin macromolecules was determined by the combination of HSQC and quantitative ^{13}C NMR (**Figure 4.2**). It should be noted that carbohydrates did not interfere with the quantification of lignin substructures using ^{13}C NMR due to their negligible content.

Native interunit linkages of lignin, such as β-O-4′, β-5′, and β-1′ were basically cleaved during the alkaline pulping, in which only the resinol structure (β-β′) and its derivatives (*e.g.*, secoisolariciresinol) were retained, especially for birch ALs (**Figure 4.2a**). Meanwhile, terminal moieties (*e.g.*, aryl glycerol and dihydro cinnamyl alcohol) and aryl-vinyl structures, including stilbene (*e.g.*, stilbene from β-1′ and β-5′ structures) and aryl enol ether moieties (*e.g.*, *cis*-enol ether and *trans*-enol ether), were formed concomitantly, especially in spruce ALs (**Figure 4.2b**). It was found that spruce AL low molar mass fraction

presented more aryl-vinyl structures than the high molar mass ones. These structures are of primary importance in understanding the reactivity of laccase-catalyzed lignin oxidation/polymerization since they are very reactive toward oxygen.

It is also clear that all fractions of the same wood species have the same interunit linkage pattern, albeit at different abundances. Recent research pertaining to lignin fractionation has proposed a molar-mass-dependent profile of interunit linkages that the low molar mass fractions presented less abundant linkages with respect to the high molar mass ones.[38,74] For instance, *β*-O-4′, *β*-*β*′, *β*-5′ interunit linkages were enriched in high molar mass fractions of softwood kraft lignin as semi-quantified by HSQC spectra.[74] However, no clear trend of interunit linkage abundance was delineated in birch and spruce ALs by the combination of HSQC and quantitative ^{13}C NMR.

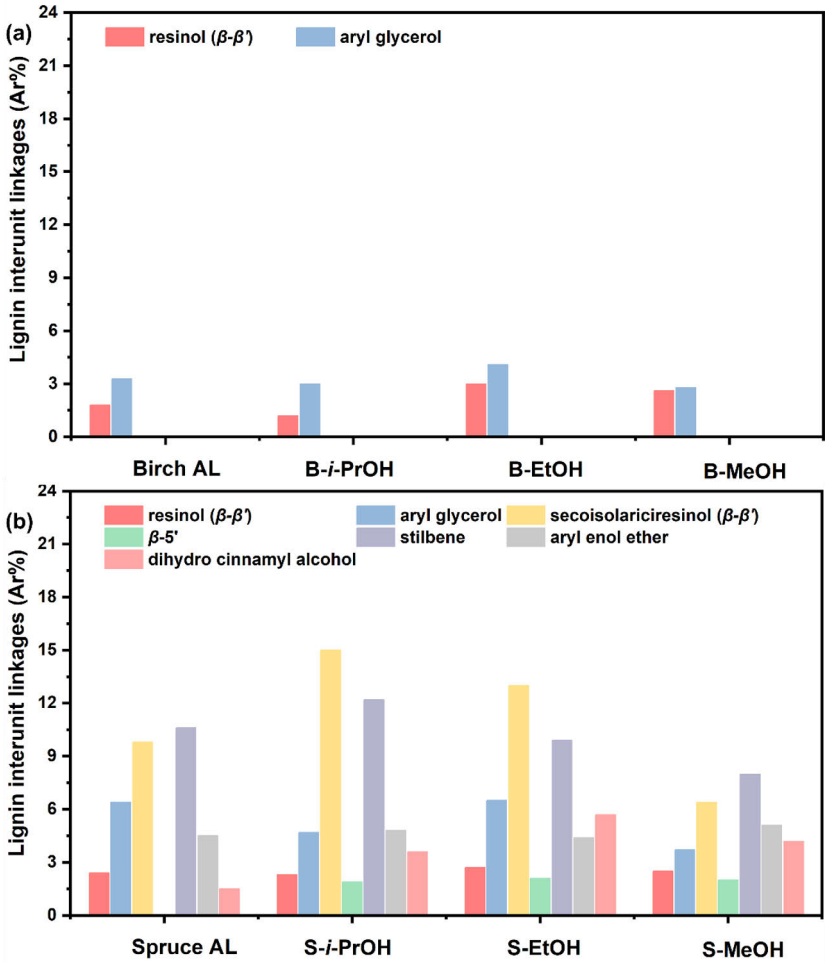

Figure 4.2. *Quantification of interunit linkages of (a) birch and (b) spruce ALs.*

4.2.2. Functionality and degree of condensation

In a general scenario, phenolic-OH and -OCH_3 groups serve as reactive sites for lignin chemical and biochemical functionalization. As shown in **Figure 4.3**, the functional group content in ALs was refined by solvent fractionation. The total amount of phenolic-OH (for both C_5-substituted and non-condensed phenolic-OH form) and -OCH_3 in birch and spruce AL fractions sequentially decreased along the fractionation sequence and correlated with increasing molar mass of the lignin fractions (**Figure 4.3a-b**). In addition, birch ALs had a higher content of C_5-substituted phenolic-OH groups, whereas spruce ALs had rather more non-condensed phenolic-OH groups (**Figure 4.3c-d**). Nevertheless, it should be noted that the C_5-substituted phenolic-OH groups in birch ALs included both phenolic S-subunits and C_5-condensed phenolic-OH forms. In contrast, the C_5-substituted phenolic-OH groups in spruce ALs consisted only of C_5-condensed phenolic-OH, which was also corroborated by constituent aromatic unit analysis.

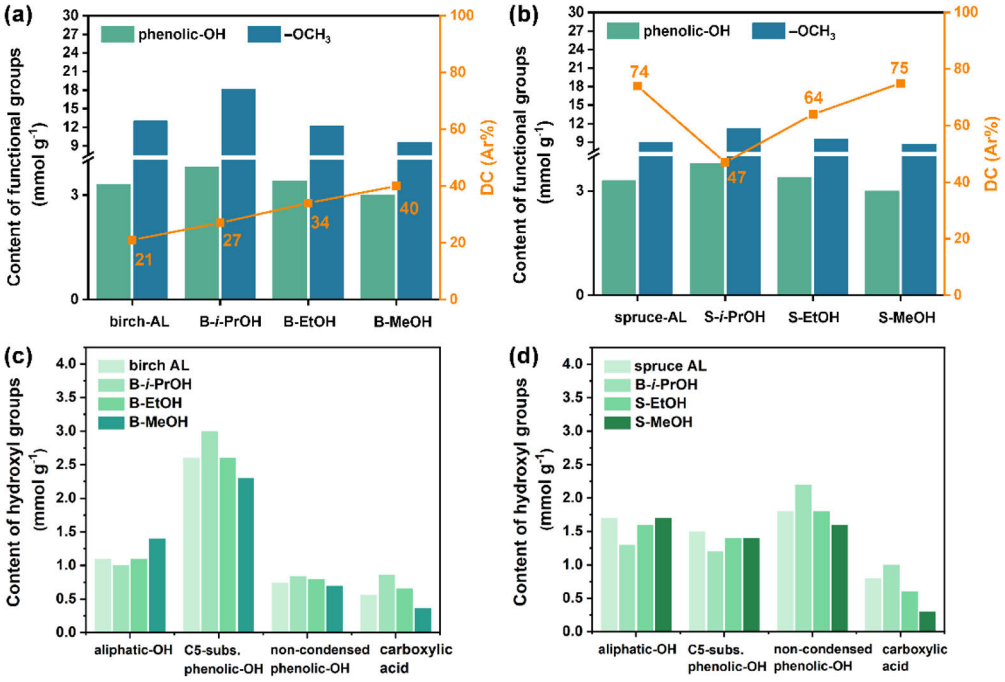

Figure 4.3. *Functional group content, DC values, and hydroxyl group distributions in (a) birch and (b) spruce lignin fractions, including initial ALs.*

The tuning of the functional groups by solvent fractionation was also reflected in the phenolic-OH/aliphatic-OH ratio. It was found that the ratio of phenolic-OH to aliphatic-OH groups was higher in birch ALs (*e.g.*, B-*i*-PrOH-s (3.8) > B-

EtOH-s (3.1) > B-MeOH-s (2.1)) than in spruce ALs (*e.g.*, S-*i*-PrOH-s (2.6) > S-EtOH-s (2.0) > S-MeOH-s (1.8)). In addition, low molar mass lignin fraction possessed a high ratio of phenolic-OH to aliphatic-OH groups, and the ratio decreased with increasing lignin molar mass. More importantly, qualitative descriptions of birch and spruce ALs can be derived from the aforementioned structural elucidation. Birch AL fractions have fewer aliphatic side chains than the spruce AL fractions. This was concluded from the lower abundance of interunit linkages and the lower content of aliphatic-OH groups in the side chains of birch ALs than their spruce AL counterparts.

Functionality not only means the content of reactive sites but also means steric accessibility. The DC value of lignin is an important parameter to indicate its reactivity, especially for later functionalization efforts. The calculated DC values of birch AL fractions, *i.e.*, B-*i*-PrOH-s (27 Ar%) < B-EtOH-s (34 Ar%) < B-MeOH-s (40 Ar%), showed increased accumulation of condensed structures at C_2, C_5, and C_6 positions along the fractionation sequence (**Figure 4.3a**). Similarly, low molar mass lignin fractions from spruce AL possessed low condensation degree values, *i.e.*, S-*i*-PrOH-s (47 Ar%) < S-EtOH-s (64 Ar%) < S-MeOH-s (75 Ar%) (**Figure 4.3b**). It is worth noting that spruce ALs had relatively higher DC values than their birch AL counterparts. In a general scenario, in chemical reactions involving reactive sites of lignin, condensed lignin is associated with higher steric hindrance, lower chemical accessibility, and decreased reactivity compared to less condensed counterparts. These molar-mass-dependent differences in lignin functionality and reactivity turned out to be highly relevant for later chemical and biochemical functionalization of lignin, where the accessibility of reactive sites for initiating the reaction is important.

4.3. Fundamental understanding of lignin molecular structure – property correlations

This section investigates the effect of lignin molecular structure on the reactivity of lignin towards chemical and biochemical functionalization. The correlation between the surface functionality of A-LNPs and their physiochemical properties was determined to further exploit lignin as a structural template in bio-based nanostructured materials.

4.3.1. Effect of chemical accessibility on lignin phenolation (Paper I)

Understanding the reactivity of lignin towards chemical functionalization at the molecular level (*e.g.*, chemical reactivity and steric accessibility of the

reactive sites) is vital for designing high-performance lignin-based materials. In this thesis, the reactivity of lignin fractions in base-catalyzed phenolation under optimized conditions (pH 9.4 and L/P 0.4) was investigated, targeting thermosetting phenolic resins (resoles) with lignin covalently integrated *via* a one-pot polymerization approach.

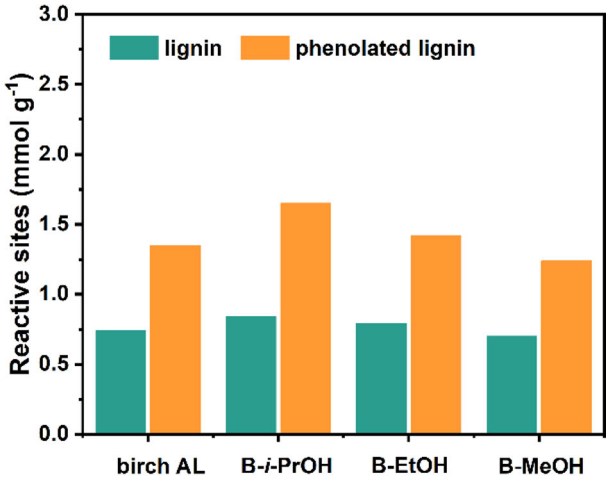

Figure 4.4. *Reactive sites of lignin and phenolated lignin for resole synthesis.*

In lignin, the non-substituted *ortho* and *para* positions of the phenolic-OH groups are considered as the reactive sites for resole synthesis, where formaldehyde can react and cause hydroxymethylation, also as reactive sites for subsequent polymerization and thermal curing. The differences in the degree of phenolation between birch ALs are shown in **Figure 4.4**. It was found that the content of reactive sites in the phenolated lignin increased as the molar mass of the non-phenolated counterpart decreased. The content of reactive sites for resole synthesis was the highest in the phenolated B-*i*-PrOH-s lignin (1.65 mmol g^{-1}, increased by 96%) and the lowest in the phenolated B-MeOH-s lignin (1.25 mmol g^{-1}, increased by 77%). Nevertheless, considering the underlying phenolation mechanism, *i.e.*, cleavage of lignin side chains and phenolation at CH-α positions,[105] the B-EtOH-s fraction retaining the most abundance of alkyl-O-alkyl interunit linkages and aryl glycerol moieties (**Figure 4.2a**) should be more reactive towards phenolation than the B-*i*-PrOH-s fraction. From this perspective, it is believed that molar-mass-dependent differences in the lignin condensation degree dominate the chemical accessibility of lignin. More specifically, the low molar mass lignin fraction (*e.g.*, B-*i*-PrOH-s fraction) with a low DC value had better steric accessibility, facilitating the diffusion of phenols into the lignin macromolecular structure.

In contrast, the high molar mass lignin fractions, such as the B-MeOH-s fraction, showed recalcitrance toward chemical functionalization due to high steric hindrance.

4.3.2. Effect of surface functionalities on the physiochemical properties of A-LNPs (Paper II)

For valorizing lignin in bio-based nanostructured materials, it is crucial to develop a simple method to functionalize the surface of nano-sized lignin (*e.g.*, colloidal LNPs) and further control its physiochemical properties. This thesis presented a facile method to prepare surface-active LNPs. In this approach, functionalization of lignin macromolecules with allyl groups through anionic ring-opening of oxirane groups at alkaline conditions was followed by dialysis purification against water, where the pH changes *in situ* facilitated the formation of a dispersion of A-LNPs (**Figure 4.5a-b**). Lignin self-assembly as nanospheres was evident from the TEM imaging, and the contrast differences seen on individual A-LNPs support the hypothesis that the allyl-terminated polymer chains can assemble on the particle surface, as indicated by red arrows in **Figure 4.5c**. The main mechanism for the formation of A-LNPs is the protonation of ionized hydroxyl groups of lignin macromolecules to trigger self-assembly with their surrounding molecules.

Tailoring the particle size of colloidal LNPs offers the possibility to tune interfacial interactions in terms of surface area and abundance of surface functionalities. It was found that tailoring the confined surface functionality (*i.e.*, allyl groups), ranging from 0.31 to 1.23 mmol g^{-1} (**Table 4.4**), indeed tuned the particle size of A-LNPs (**Figure 4.5c**). The A-LNPs size decreased with increasing surface functionality in the order A-LNP-1.0 (225 nm) > A-LNP-1.5 (195 nm) > A-LNP-2.5 (150 nm) > A-LNP-4.0 (140 nm). This might be associated with the susceptibility of ionized hydroxy groups to be protonated, which in turn was related to the cohesion of molecules during nucleation and growth. In the sample series of A-LNP-1.0 to A-LNP-4.0, the ratio of aliphatic-OH to phenolic-OH groups increased with increasing allylation degree of lignin, *e.g.*, A-LNP-1.0 (1.9) < A-LNP-1.5 (4.2) < A-LNP-2.5 (5.6) < A-LNP-4.0 (9.6) (original data in Paper II). The allylated lignin macromolecule with a higher aliphatic-OH to phenolic-OH ratio was more prone to nucleation than with lower ones since ionized aliphatic-OH groups are susceptible to pH decrease due to their higher p*K*a values than phenolic-OH groups.[85] This rationalized the decreasing size of A-LNPs as the increase of allylation degree of lignin. Moreover, surface tension values of the allylated lignin alkaline solutions

decreased as the total allyl content increased (original data in Paper II), *e.g.*, A-LNP-1.0 (47.0 mN m^{-1}) > A-LNP-1.5 (44.8 mN m^{-1}) > A-LNP-2.5 (44.0 mN m^{-1}) > A-LNP-4.0 (42.4 mN m^{-1}), indicating reduced cohesion between neighboring lignin molecules, which further dedicated to the formation of smaller-sized A-LNPs.

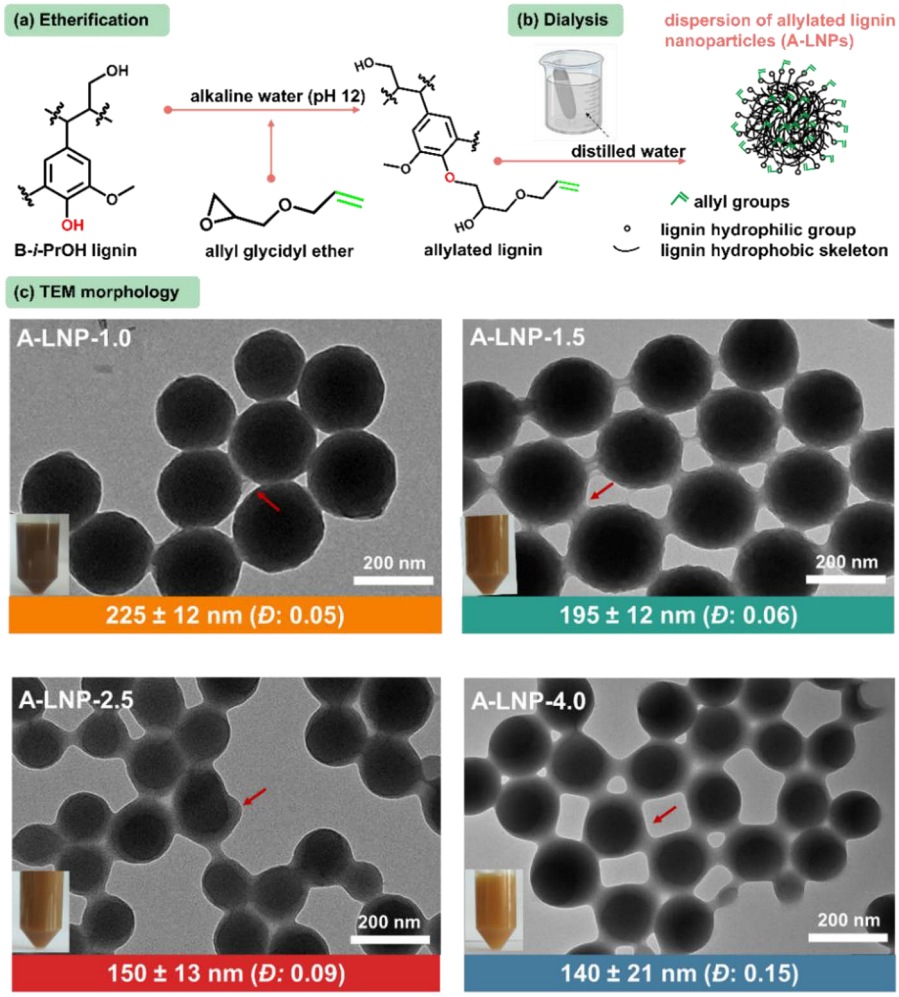

Figure 4.5. *(a-b) Design strategy for A-LNPs. (c) TEM images of A-LNPs. The insets in (c) are photographs of the A-LNPs dispersions. This figure is adapted from its original version in Paper II.*

Table 4.4. Distribution of allyl groups and physiochemical properties of A-LNPs.

samples	total allyl groups (mmol g^{-1})	allyl groups on A-LNPs (mmol g^{-1})	Tg (°C)	WCA (°)
B-*i*-PrOH-s	---[a]	---[a]	125	39
A-LNP-1.0	2.15	0.31	80	27
A-LNP-1.5	2.35	0.57	57	32
A-LNP-2.5	2.61	1.04	48	44
A-LNP-4.0	2.80	1.23	77	34

[a]denotes not detected

In addition to surface functionality, the accessibility of the active domains of A-LNPs plays an even more crucial role, especially when using it as a structural template for constructing nanostructures, *e.g.*, by core-shell emulsion polymerization. Therefore, the effect of the surface functionality of A-LNPs on their domain flexibility (Tg values) and surface wettability (WCA values) was determined. The Tg values of A-LNPs decreased from 125 °C of B-*i*-PrOH-s to 48 °C of A-LNP-2.5 (**Table 4.4**). The changes in Tg values are proposed to be the result of the allyl-terminated chains acting as flexible segments, increasing the domain flexibility and molecular mobility of the lignin macromolecule. In addition, the surface hydrophobicity of A-LNPs increased from 27° to 44° as the surface functionality increased (**Table 4.4**), which can facilitate its application as a structural template for interaction with hydrophobic monomers. Nevertheless, when the surface-distributed allyl groups were increased to 1.23 mmol g^{-1}, the A-LNP-4.0 colloids exhibited a higher Tg transition at 77 °C and a lower WCA value at 34.3° than A-LNP-2.5. This observed recalcitrance of lignin macromolecules is most likely due to excessive entanglement of the allyl-terminated chains, exposing the newly formed aliphatic-OH groups outward.

Despite recent research efforts on lignin allylation, the function of allyl groups has only been validated in organic solvent-assisted thermosetting resin applications.[112] This thesis contributed to a green and holistic processing approach for lignin allylation and extended the application of allylated lignin to nanostructured aqueous dispersion. In addition, this approach can mitigate the need for petrochemical-based crosslinkers to provide robust LNPs, which are required for surface functionalization to occur at harsh conditions, such as alkaline conditions. Compared with other existing strategies for the surface functionalization of LNPs, the synthesis of A-LNPs overcomes the demanding reaction conditions required for direct surface functionalization, such as mild reaction pH and moderate medium, to retain LNPs as uniform nanostructures.

4.3.3. Fractionation-dependent laccase-catalyzed lignin oxidation and polymerization kinetics (Paper III)

In this section, the lignin functionalization strategies were extended from chemical to biochemical perspectives to further understand the lignin molecular structure-property correlations. Laccase-catalyzed lignin oxidation experiments were carried out using MetZyme® alkaliphilic laccase to investigate the correlation between structural characteristics of lignin and lignin reactivity towards enzymatic oxidation. It should be noted that the bacterial-derived MetZyme® laccase is known for its extended pH working range and high thermostability. It allows the lignin-laccase reaction to proceed at an alkaline pH that favors lignin solubilization and phenolic oxidation of lignin molecules (**Figure 4.6a**).

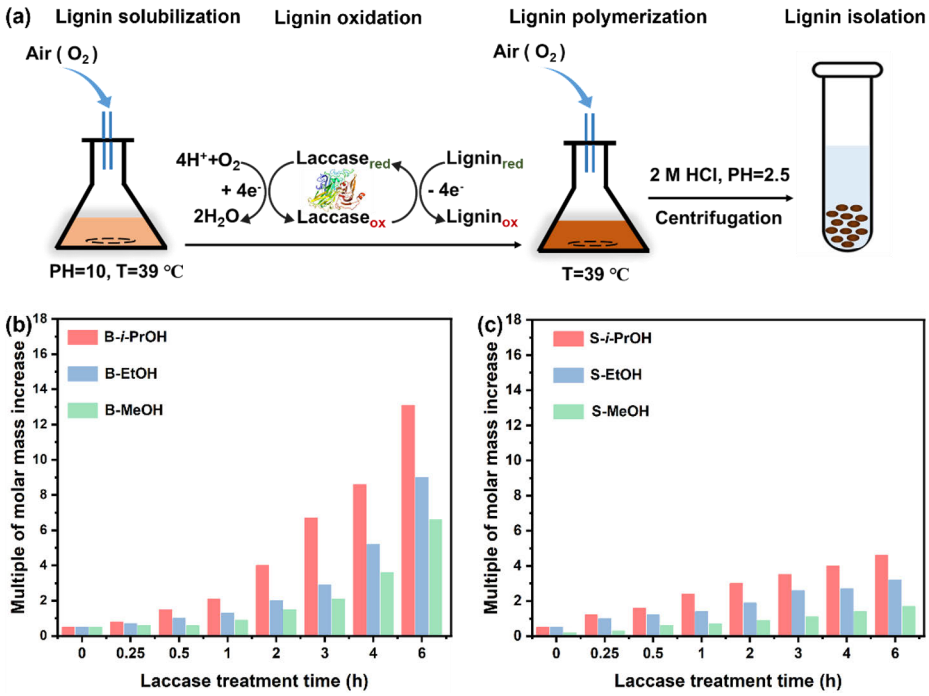

Figure 4.6. *(a) Representative scheme for the laccase-catalyzed oxidation and polymerization of lignin fractions at an alkaline aqueous solution. Molar mass evolution throughout laccase treatment on (b) birch and (c) spruce AL fractions. This figure is adapted from its original version in Paper III.*

The oxidation efficiency of laccase on different lignin fractions was monitored by molar mass determination. The results demonstrated that laccase treatment induced lignin polymerization resulting in higher molar mass values (**Figure 4.6b-c**). In addition, fractionation-dependent lignin polymerization kinetics

were observed for birch and spruce ALs. More specifically, the *i*-PrOH-s fraction with low molar mass, high content of phenolic-OH groups, and low DC values reached a higher molar mass polymerization degree than EtOH-s and MeOH-s fractions. Presumably, the phenolic substrates of low molar mass lignin fractions had higher chemical accessibility and lower steric hindrance to the laccase molecules than the high molar mass ones. However, spruce AL fractions were less reactive towards laccase-catalyzed polymerization in terms of molar mass increase than birch AL fractions, even for the fractions that had a comparable initial molar mass and content of phenolic-OH groups, such as B-*i*-PrOH and S-*i*-PrOH fractions. The inert profile of the spruce AL fractions towards laccase-catalyzed polymerization can be attributed to three other factors in addition to the higher initial DC values compared to the birch ALs. First, the HSQC spectra of air-treated and laccase/air-treated B-*i*-PrOH-s and S-*i*-PrOH-s revealed that even in the absence of laccase, spruce AL fractions were rather prominent in air-induced oxidation of aryl-vinyl moieties (original data in Paper III). However, the spruce AL fractions were less pronounced than the birch AL fractions in terms of oxidative condensation and polymerization at the aromatic rings. Second, spruce AL fraction had a lower ratio of phenolic-OH to aliphatic-OH groups than that of birch AL fraction, *e.g.*, S-*i*-PrOH-s (2.6) < B-*i*-PrOH-s (3.8), which may cause the spruce lignin macromolecules to depolymerize, although the overall reactivity was the polymerization of lignin.[69] Third, birch AL fractions had more -OCH_3 groups than their spruce AL counterparts (**Figure 4.3a-b**). The resonance effect of the electron pair on the -OCH_3 moieties is believed to activate lignin aromatic rings toward electrophilic substitution and stabilize phenoxy radicals toward oxidation and radical coupling reaction.[115]

Table 4.5. Catechol derivatives in the laccase-polymerized birch AL fractions.

samples	birch ALs (%)[a]	
	initial	polymerized[b]
i-PrOH-s	4.5	22.4
EtOH-s	6.7	20.4
MeOH-s	8.0	8.0

[a]the ratio of catechol derivatives to lignin units was determined by *Py*/GC-MS. [b]6 hours laccase treatment.

Noteworthy, the content of catechol and catechol derivatives (*e.g.*, 3-methoxylcatechol, 3-methylcatechol, and 4-methylcatechol) significantly increased in the laccase-treated birch AL fractions (**Table 4.5**). This indicates that in addition to laccase-mediated oxidation of lignin phenolic-OH groups,

oxidative demethylation of lignin also occurred upon laccase treatment, concomitantly with the formation of catechol groups. The content of catechol derivatives increased in the order of MeOH-s, EtOH-s, and *i*-PrOH-s, which was aligned well with the degree of lignin polymerization in **Figure 4.6b**.

4.4. Enzymatic tailoring of lignin-based nanostructures

Fractionation-dependent lignin polymerization kinetics not only provide fundamental insights into the correlation between lignin structural characteristics and laccase-catalyzed polymerization properties, but also present new perspectives on valorizing lignin in bio-based nanostructured materials. In this thesis, two templating approaches were validated for the efficient valorization of laccase-polymerized lignin to functional nanomaterials. First, the development of durable cellulose dispersions containing nano-sized lignin was achieved *via in situ* polymerization of lignin with dispersed MFC present as a structural template. Second, the alkali resistance of laccase-polymerized lignin allowed the development of multi-functional lignin nanospheres, which can serve as surface-active templates for *in situ* reduction of Ag^{+} at highly alkaline conditions. In this section, birch AL fractions were selected for the study due to their higher reactivity to laccase-induced polymerization than their spruce AL counterparts.

4.4.1. *In situ* polymerization of lignin in fiber suspension at controlled conditions (Paper III)

Due to the inherent affinity of lignin and cellulose, it was hypothesized that laccase-catalyzed lignin polymerization in the aqueous phase would allow a nanoscale control of the spatial confinement of polymerized lignin on nanocellulose surface (**Figure 4.7**). The main reasons for selecting MFC as the structural template were the ease of obtaining MFC through mechanical refining and homogenization and the low negative surface charges of MFC that could inhibit the repulsion of lignin molecules from nucleation.

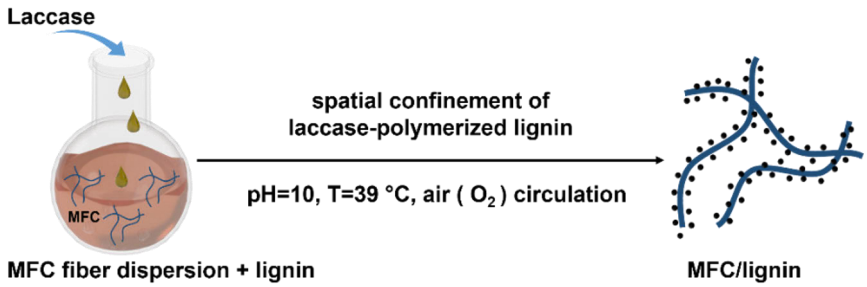

Figure 4.7. *Representative scheme for the in situ alignment of laccase-polymerized lignin on MFC.*

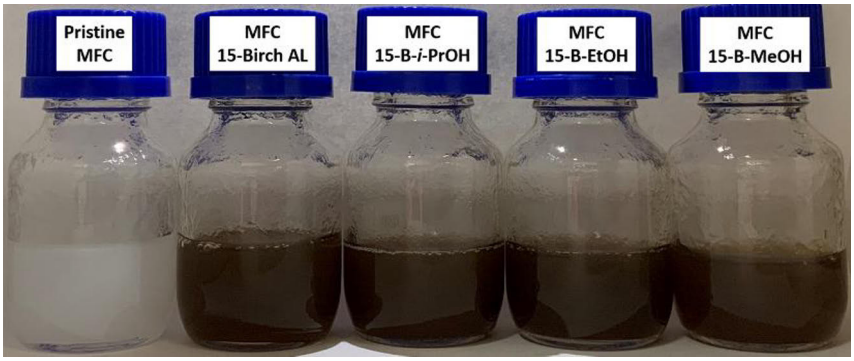

Figure 4.8. *Photographs of MFC and MFC/lignin reaction mixtures upon 2 hours of laccase treatment at 15 wt % lignin loading. This figure is adapted from its original version in Paper III.*

The MFC/lignin dispersions obtained from the one-pot *in situ* lignin polymerization (15 wt%) in the presence of MFC showed good dispersibility (**Figure 4.8**). The surface characteristics of MFC/lignin fibers were determined by TEM measurements (**Figure 4.9**). It was found that when B-*i*-PrOH-s and B-EtOH-s fractions were used as the phenolic substrates, the dissolved lignin in the medium was polymerized into a nanostructured platelet-like morphology and was evenly coated in alignment along the orientation of fibers. However, for the unfractionated birch AL and B-MeOH-s fraction, the polymerized lignin tended to form larger aggregates and appear as a thick coating on the fiber joints. It is speculated that different interfacial interactions between lignin and fiber surfaces (residual lignin compounds) lead to differences in the nucleation and growth of lignin molecules on the fiber surface when laccases initiate the radical oxidative coupling reaction. Lignin fractions with high phenolic-OH content (*e.g.*, *i*-PrOH-s and EtOH-s fractions) could nucleate on the surface of MFC fibers, which was driven by more reactive sites in lignin molecules available for radical reactions. In contrast, lignin fractions with low phenolic-OH content (*e.g.*, MeOH-s fraction) tended to polymerize at fiber joints because residual lignin compounds were enriched there. Other factors considering the dispersibility of nano-sized lignins on the fiber surface may include different aliphatic-OH to phenolic-OH content ratios of the corresponding laccase-polymerized lignin, which was also related to different laccase-catalyzed polymerization kinetics. The biochemical conversion of phenolic-OH groups decreased in the order of B-*i*-PrOH-s (60%) > B-EtOH-s (38%) > B-MeOH-s (21%) upon laccase treatment, resulting in the former fraction having a higher aliphatic-OH to phenolic-OH ratio than the latter ones (original data in Paper III). The participation of lignin aliphatic-OH groups in intramolecular hydrogen

bonding might limit the formation of non-covalent bonds with other lignin molecules, resulting in a uniform and smaller particle size.[102]

Overall, it is confirmed that fractionation-dependent lignin polymerization kinetics can facilely modulate the nanoscale spatial localization of laccase-polymerized lignin in the nanocellulose fiber network. Therefore, the templating approach of *in situ* polymerization of lignin in fiber suspension at controlled conditions is validated to be strategically feasible in deriving LNPs-containing cellulose composites with uniform nanostructures.

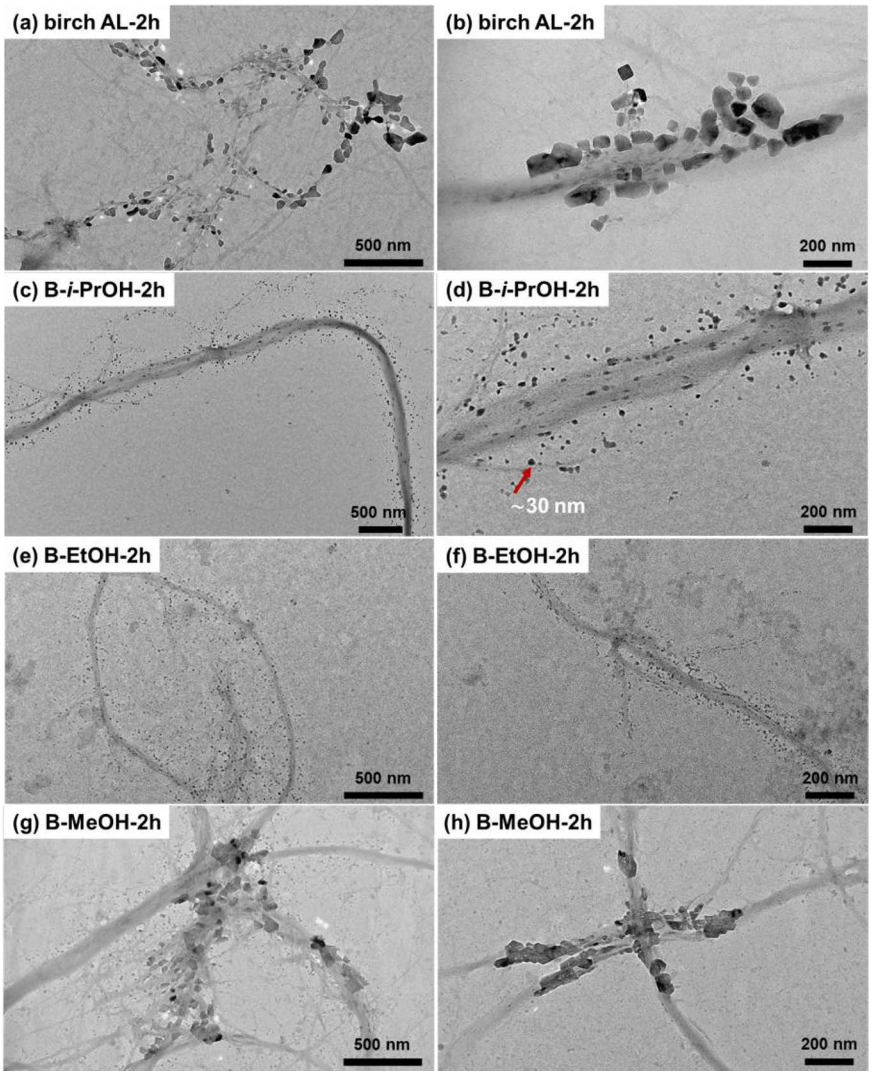

Figure 4.9. *TEM images of spatial confinement of the laccase-polymerized birch ALs (15 wt % loading, 2 hours laccase treatment) on the surface of MFC fibers. This figure is adapted from its original version in Paper III.*

4.4.1a. Demonstration of the potential of cellulose-lignin dispersions in packaging applications

The application potential of the laccase-polymerized MFC/lignin dispersion for packaging materials was evaluated by the water barrier properties and the mechanical properties of the corresponding films prepared by vacuum filtration.

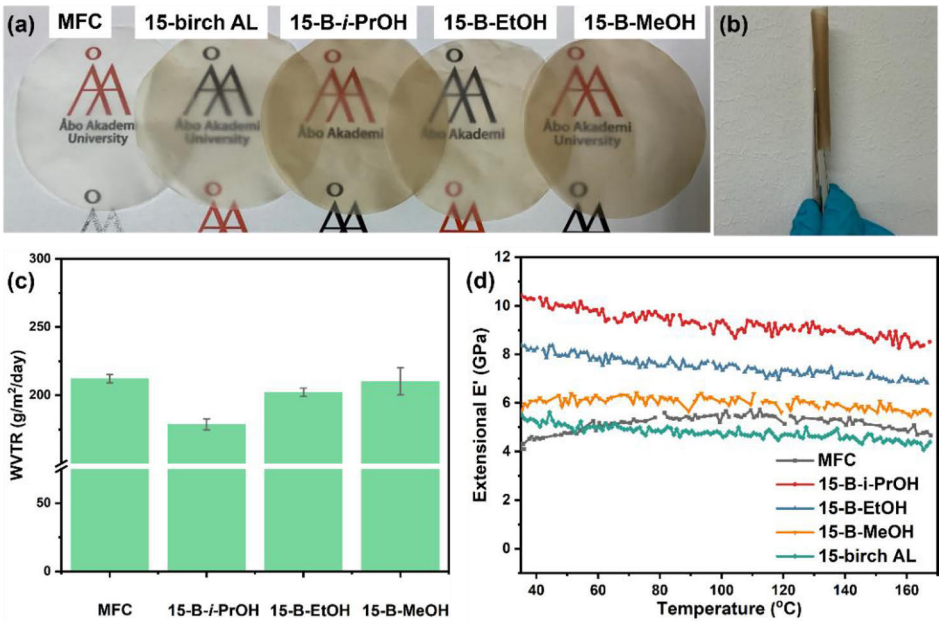

Figure 4.10. *(a) Images of laccase-polymerized MFC/lignin films with a nominal lignin content of 15 wt%. (b) The 15-B-i-PrOH film was rolled to demonstrate flexibility. (c) WVTR values of the MFC/lignin films. (d) Extensional E' vs. temperature curves for neat MFC and MFC/lignin films. This figure is adapted from its original version in Paper III.*

The nanocomposite films prepared from all three birch AL fractions exhibited high transparency and were mechanically flexible at a film thickness of 30 – 40 µm, as illustrated in **Figure 4.10a-b.** In the WVTR tests, the nanocomposite films of 15-B-*i*-PrOH and 15-B-EtOH showed slightly lower WVTR values of 179 and 202 g/m^2/day, respectively, compared to 212 g/m^2/day for the neat MFC films (**Figure 4.10c**). However, the films of 15-B-MeOH did not show any improvement on the water vapor barrier properties due to the inhomogeneous morphology of the MFC/lignin fibers (**Figure 4.9g-h**). Subsequently, the mechanical properties of the MFC/lignin nanocomposite films were determined by the temperature sweep experiment (**Figure 4.10d**). Compared to the neat MFC films, the MFC/lignin films exhibited higher extensional storage modulus (E'), except for the 15-birch AL sample containing

unfractionated lignin. The nanocomposite film of 15-*i*-PrOH showed the highest E' of around 10 GPa, which corresponded to a significant enhancement of E' for the neat MFC film at around 5 GPa, but was still foldable (**Figure 4.10b**). In addition, the E' of the MFC/lignin films decreased as the polymerization degree of the lignin fractions decreased, which correlated well with the dispersibility of the polymerized lignin in the MFC dispersion. As a conclusive remark, this study developed a new templating approach to introduce nano-sized lignin nucleation and growth on renewable cellulose, offering an effective route towards *in situ* synthesis of functional fibrils and related cohesive films that provide the possibility for barrier coating in packaging applications.

4.4.2. Direct surface functionalization of LNPs at alkaline conditions (Paper III & IV)

The prerequisite for direct surface functionalization of colloidal LNPs under robust conditions (*e.g.*, highly alkaline pHs) is the restraint transition of well-dispersed nano-sized lignin into functional nanostructures or hybrids. Chemically cross-linking lignin using phenol-formaldehyde and epoxy resin curing chemistries is the main approach in the existing literature to prepare robust and functional LNPs. From the perspective of 'green' and sustainability, environmentally friendly alternatives are highly demanded to eliminate petroleum-based cross-linkers in this type of application.

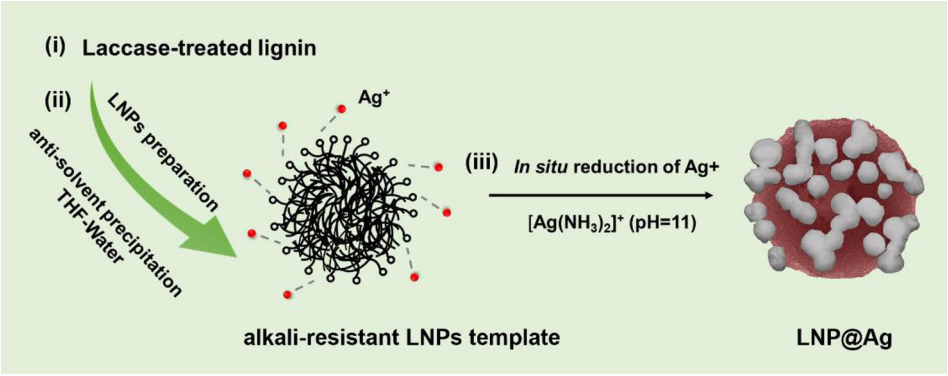

Figure 4.11. *Design strategy for LNP@Ag hybrid.*

This thesis hypothesized that the insufficient alkali resistance of conventional LNPs could be addressed by applying a laccase-catalyzed lignin polymerization strategy (**Figure 4.11**). The applicability of this innovative functional strategy was demonstrated through the *in situ* reduction of Ag^+ in silver ammonia solution (pH 11) on the surface of L-LNPs. The complexation between

$[Ag(NH_3)_2]^+$ ions and anionic carboxyl groups arranged on the surface of L-LNPs served as the initial sites for Ag^+ reduction by the phenolic-OH and -OCH_3 groups in lignin molecules.[183]

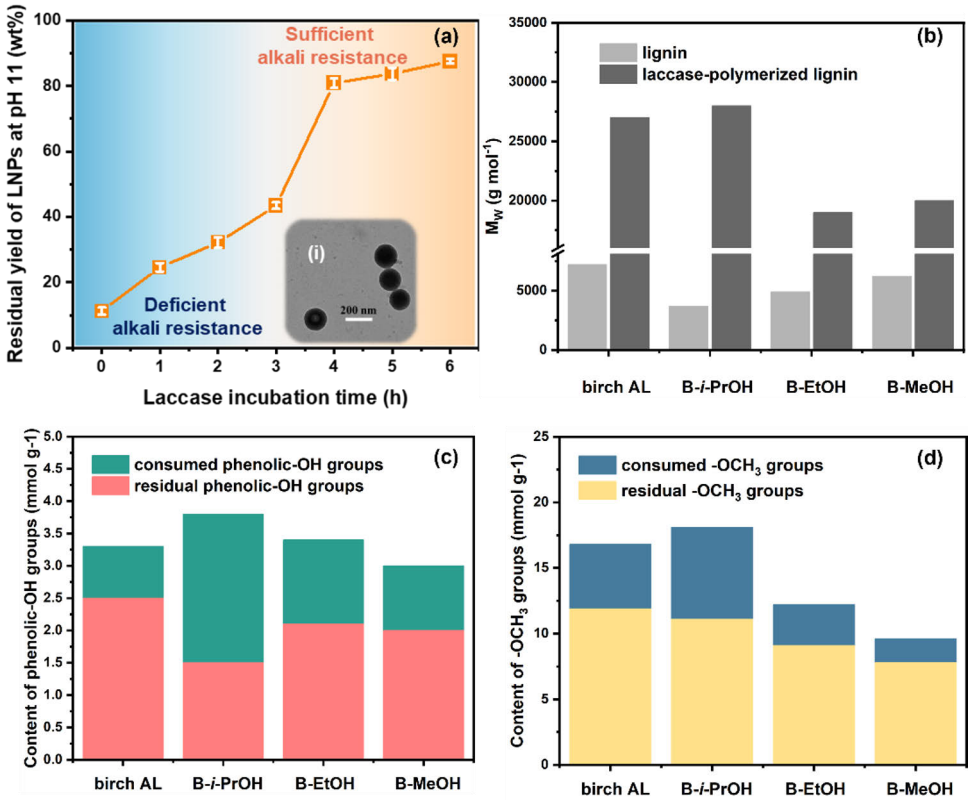

Figure 4.12. *(a) Alkali resistance of L-LNPs obtained from laccase-polymerized B-MeOH-s fraction in pH 11 solution. The inset (i) in (a) was the TEM image of L-MeOH-4-NPs sample. (b) Molar mass, (c) phenolic-OH and (d) -OCH_3 groups of birch lignin fractions upon 4 hours of laccase treatment. This figure is reproduced from Paper IV with permission from the Royal Society of Chemistry.*

It should be noted that an over 4 hours enzymatic treatment was necessary for the polymerization of the B-MeOH-s fraction to ensure the alkali resistance of the L-LNPs in pH 11 ammonia solution (**Figure 4.12a**). The dissolution of LNPs was mainly caused by the deprotonation of phenolic-OH groups, which have p*K*a values in the range of about 7.3 to 10.5 (**Table 2.3**).[85,86] In contrast to the low alkali resistance of conventional LNPs, over 80 wt% of L-LNPs fabricated from laccase-polymerized lignin could be retained as uniformly nano-sized lignin at pH 11 condition (**Figure 4.12a** insert TEM image). Presumably, laccase-induced oxidative coupling of phenoxy radicals raised the lignin condensation and the formation of robust interunit carbon-carbon linkages, resulting in increased molar mass as well as decreased phenolic-OH content

(**Figure 4.12b-c**), which further limited the dissolution of laccase-polymerized lignin at high pH conditions. The applicability of L-LNPs as surface-active structural templates for the *in situ* Ag^+ reduction was investigated from the aspects of hierarchical nanostructure of the L-LNPs@Ag, colloidal stability, and crystalline characteristics as well as valence state of Ag. In addition, the resource efficiency and environmental impact of the L-LNP@Ag manufacturing process were evaluated.

4.4.2a. Lignin fractionation to realize the suitable surface functionalities of L-LNPs

The functionalities of laccase-polymerized lignin for Ag^+ reduction, *e.g.*, phenolic-OH (including catechol groups) and -OCH_3 groups, were evaluated in **Figure 4.12c-d**. It should be noted that the L-LNPs fabricated from B-MeOH-s fraction showed deficient alkali resistance but possessed the capacity to reduce Ag^+ (**Figure 4.13a**), even though it had the highest molar mass among birch AL fractions. Indeed, there is a 'competition' for the lignin functional groups, especially the phenolic-OH groups, in terms of gaining alkali resistance through oxidative polymerization and facilitating Ag^+ reduction. The higher the laccase-catalyzed lignin polymerization degree, *i.e.*, L-*i*-PrOH-s (6.6-fold) > L-EtOH-s (2.9-fold) > L-birch AL (2.8-fold) > L-MeOH-s (2.2-fold), the more phenolic-OH and -OCH_3 groups were consumed, and the less were left for Ag^+ reduction (**Figure 4.12c-d**). In an extreme case, the intensive oxidation of phenolic-OH groups in laccase-polymerized B-*i*-PrOH-s fraction compromised its surface functionalities towards reducing Ag^+, although the pronounced lignin-lignin condensation promoted its alkali stability (**Figure 4.13b**). In addition to the degree of polymerization, it was found that the lignin reactivity with respect to residual functional groups could also be modulated by using solvent fractionation in combination with the laccase-catalyzed polymerization approach (**Figure 4.12c-d**). The L-MeOH-s lignin favored the balance between alkali resistance and preserving the amount of residual phenolic-OH and -OCH_3 groups for Ag^+ reduction. This resulted in a uniform surface-embedded hierarchical nanostructure of L-LNP@Ag (**Figure 4.13e**), where the L-LNPs presented as highly dispersible and nanoscale polymeric templates for *in situ* reduction of AgNPs ($\backsim$21 nm) in an aqueous medium.

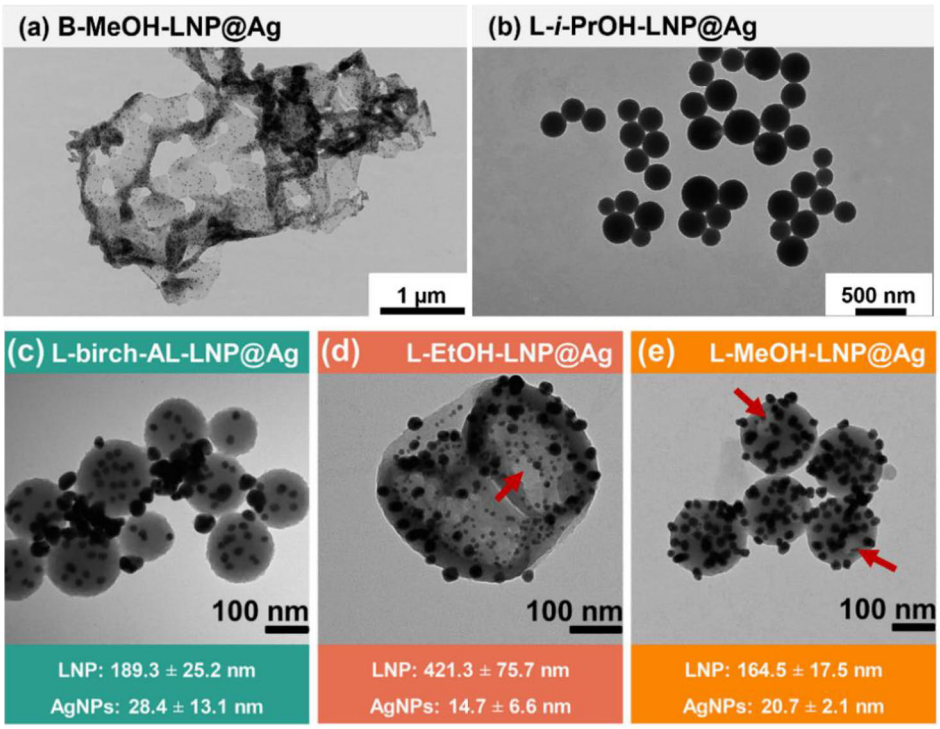

Figure 4.13. *TEM images of LNP@Ag from B-MeOH-s fraction and polymerized birch AL fractions (4 hours laccase treatment). The L-LNP@Ags were prepared in 10 mg mL^{-1} of $[Ag(NH_3)_2]^+$ solution. This figure is reproduced from Paper IV with permission from the Royal Society of Chemistry.*

Furthermore, the molecular difference of laccase-polymerized lignin also affected the hierarchical morphology of the *in situ* reduced AgNPs on L-LNPs. When using L-birch-AL-LNPs as the template, AgNPs tended to form large aggregates (28.4 ± 13.1 nm) in the vicinity of the nanospheres instead of being surface embedded. This is believed to be associated with the heterogeneity of the L-birch-AL ($Đ_M$ of 8.9). This further confirms the significance of lignin fractionation in obtaining high-performance lignin hybrid nanomaterials. Meanwhile, the L-EtOH-LNPs and AgNPs embedded on the surface were less homogenized than those of L-MeOH-LNP@Ag as comparing the dispersity values of L-LNPs and AgNPs in **Figure 4.13d-e**. Small and compact nanospheres and some particles with hollow circular regions were obtained from L-MeOH-s lignin, whereas large and incomplete particles were derived from L-EtOH-s lignin, as indicated by red arrows in **Figure 4.13d-e**. This suggests that two distinct formation mechanisms may have been involved during solvent shifting when preparing L-LNPs from these laccase-polymerized lignin fractions. The high molar mass L-MeOH-s lignin molecules were prone to precipitate as solid nanospheres by aggregating the pronounced

hydrophobic regions in lignin *via* the nucleation-and-growth mechanism. The formation of hollow structures of L-EtOH-LNPs and L-MeOH-LNPs during solvent-shifting is possibly associated with a nanoemulsion formation before the self-assembly due to the presence of amphiphilic lignin structures. Nevertheless, the hollow structure of L-EtOH-LNPs with penetrating holes and cracks was different from the solid particles prepared from L-MeOH-LNPs. This is indicative of the presence of more amphiphilic lignin molecules in the L-EtOH-s during nanoemulsion formation, as a similar phenomenon has been reported previously.[181,182]

4.4.2b. Physiochemical properties of L-MeOH-LNP@Ag

The colloidal stability of L-LNP@Ag was investigated by dynamic light scattering measurement, which revealed a stable and insensitive feature of the L-LNP@Ag to variations in pH range from 2.5 to 12, with no significant change in the average particle size (**Figure 4.14a**). The negative surface charge of L-LNP@Ag, deriving from deprotonated phenolic-OH groups and -COOH moieties generated from the redox reaction between the $[Ag(NH_3)_2]^+$ complex and L-LNPs, dictated its colloidal stability in dispersions. The relatively high surface charge of L-LNP@Ag (ζ-potential-range – 40 to – 55 mV) can induce sufficient electrostatic repulsion to hinder particle aggregation, although the absolute value of the ζ-potential dramatically decreased when the pH value was lower than 4 and higher than 12 (**Figure 4.14b**).

The loading amount of AgNPs on the L-LNP@Ag was determined as 47.2 wt% by ICP-OES measurement, which confirmed a high efficacy of laccase-polymerized lignin for reducing Ag^+. The XRD pattern elucidated the metallic form of Ag in L-LNP@Ag. Diffraction peaks at 2θ = 38.1°, 44.1°, 64.4°, 74.4°, and 81.5°, were assigned to the typical face-centered-cubic crystalline structure of metallic Ag (**Figure 4.14c**). Furthermore, the calculated lattice constant (α_0) of Ag (α_0 = 4.0900 Å) deviated only 0.10% from the standard α_0 (4.0857 Å), confirming a well-defined crystalline structure. It should be noted that the individual crystallite size of Ag calculated from the XRD pattern using the Scherrer equation was around 4.0 nm, which was smaller than the particle size of AgNPs (~ 21 nm) estimated from TEM measurement (**Figure 4.13e**). This indicates that AgNPs were formed as distinct clusters of about 5 individual Ag particles. The valence state of Ag on the surface of L-LNPs was determined by XPS analysis (**Figure 4.14d**). The bands observed at binding energies of 368.8 and 374.9 eV in the Ag 3d high-resolution spectrum were attributed to Ag $3d_{5/2}$ and Ag $3d_{3/2}$ of Ag^0, respectively. In addition, no diffraction peaks of silver

oxides (*e.g.*, Ag_2O and AgO) were found in the XRD pattern of L-LNP@Ag. This indicates that the functional groups on the surface of L-LNPs can effectively reduce and stabilize nascent AgNPs with a well-defined crystalline structure.

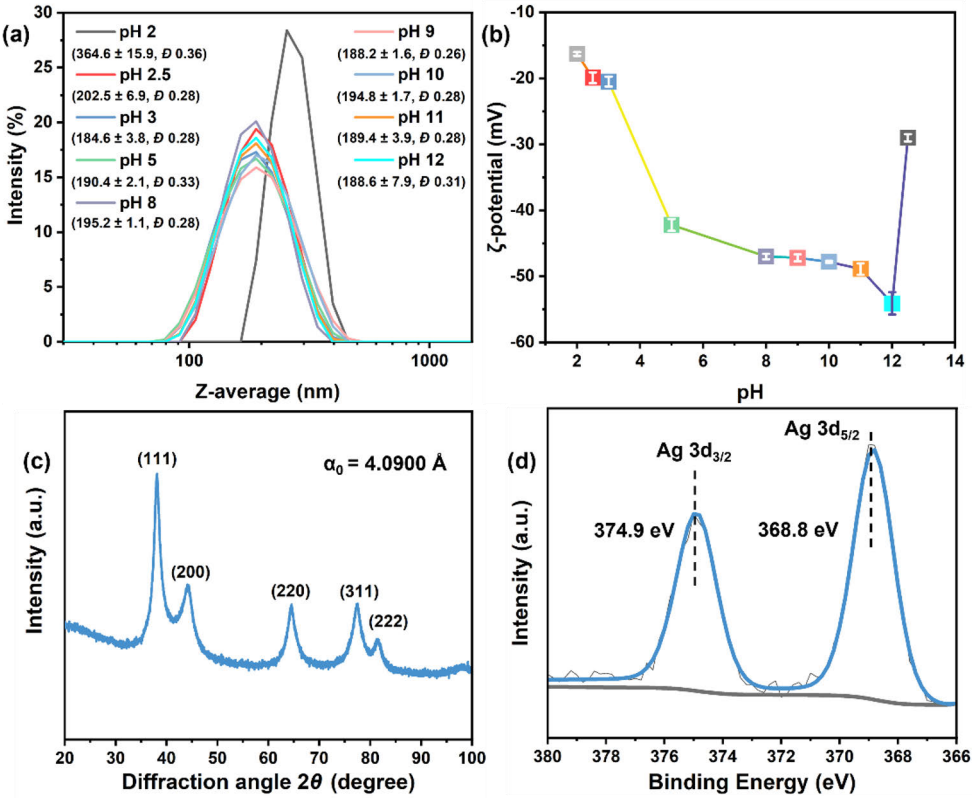

Figure 4.14. *Physiochemical properties of L-MeOH-LNP@Ag: Effect of pH on (a) Z-average and (b) ζ-potential. (c) XRD pattern. (d) Ag 3d high-resolution XPS spectrum. This figure is reproduced from Paper IV with permission from the Royal Society of Chemistry.*

4.4.2c. Resource efficiency and environmental impact of the L-LNP@Ag manufacturing process

Two metrics for evaluating the resource efficiency (*i.e.*, reaction mass efficiency – mass of product/mass of total input) and environmental impact (*i.e.*, *E* factor – mass of waste/mass of product) of the L-LNP@Ag manufacturing process were compared in **Table 4.6** based on different concentrations of silver precursor solution and reaction times. It was found that the reaction mass efficiency and *E* factor were improved when decreasing the concentration of $[Ag(NH_3)_2]^+$ solution from 10 (sample 1#) to 5 (sample 2#) and 3 mg mL^{-1} (sample 3#), although the particle size and loading of AgNPs decreased, the crystalline structure did not change significantly in terms of crystallite size and

α_0 (**Table 4.7**). It can be assumed that a higher concentration of L-LNPs (lower concentration of $[Ag(NH_3)_2]^+$) could result in a faster reduction of Ag^+ and capping of the formed AgNPs, which favored the formation of small-sized AgNPs. It should be noted that further extending the reaction time from 4 to 6 hours (sample 4#), impaired both resource efficiency and environmental impact (**Table 4.6**). Therefore, it is recommended to fabricate L-LNP@Ag in $Ag(NH_3)_2NO_3$ solution with intermediate concentration and moderate reaction time to maximize the resource efficiency and minimize the waste.

Overall, the advantages of synthesized hybrid L-LNP@Ag include: (i) high efficacy of L-LNPs as structural templates to reduce Ag^+ as metallic Ag^0 with a well-defined crystalline structure; (ii) using only natural polymer lignin as nano-carrier and stabilizer of AgNPs; (iii) durable dispersibility in aqueous phase and certain organic solvents, such as alcohols.

Table 4.6. Mass-based metrics of the L-MeOH-LNP@Ag manufacturing process.

samples	mass input (mg)		reaction time (h)	L-LNP@Ag (mg)	waste (mg)	mass-based metrics	
	L-LNP	$[Ag(NH_3)_2]^+$				mass efficiency (%)	*E* factor
1 #	16	40	4	24.2	28.6	43	1.18
2 #	16	20	4	23.0	9.8	64	0.43
3 #	16	12	4	17.4	7.4	62	0.42
4 #	16	40	6	23.0	29.8	41	1.29

Table 4.7. Property comparison of the AgNPs synthesized based on different concentrations of silver precursor solutions.

samples	AgNPs size (nm)[a]	crystallite size (nm)[b]	α_0 (nm)[b]	AgNPs loading (wt%)[c]
1 #	20.7 ± 2.1	4.0	4.090	47.2
2 #	16.1 ± 1.9	3.7	4.092	46.8
3 #	8.1 ± 1.2	3.5	4.091	30.6

[a]estimated from TEM measurement; [b]calculated from XRD measurement; [c]calculated from ICP-OES measurement.

4.4.2d. Demonstration of the utilization potential of L-LNP@Ag in lignin–hemicellulose photo-crosslinkable resins

One of the attractive approaches to promoting sustainable and multipurpose use of woody biopolymers for high-value biomaterials is the utilization of nanocellulose, modified hemicelluloses, and lignin/LNPs for hydrogels in biomedical applications, especially through 3D printing.

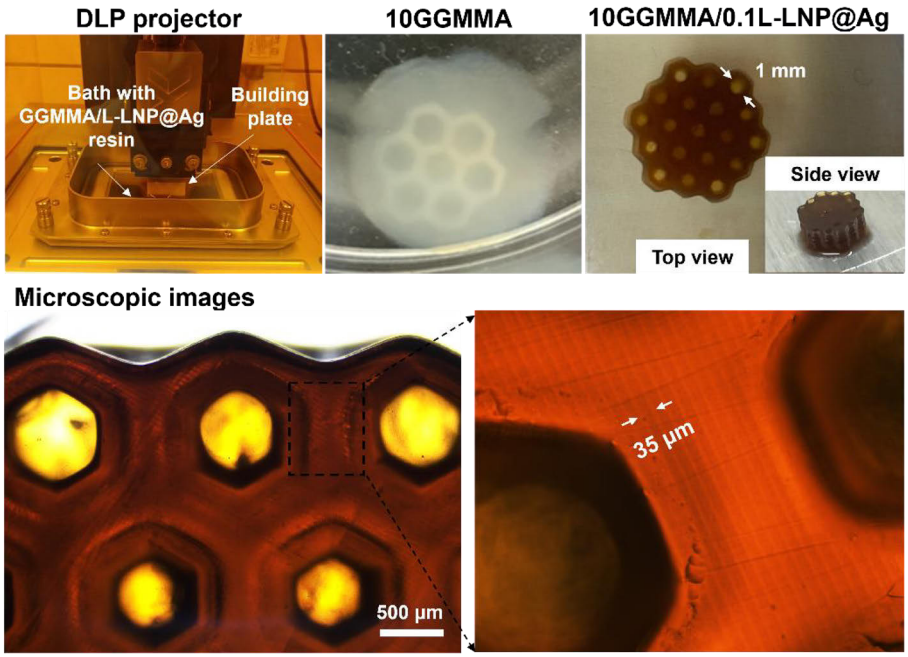

Figure 4.15. *DLP projector, DLP-printed honeycomb scaffolds of the 10GGMMA and 10GGMMA/0.1L-LNP@Ag hydrogels with a height of 3 mm, optical microscopic image of the 10GGMMA/0.1L-LNP@Ag hydrogel, and its zoom image demonstrating high resolution. This figure is reproduced from Paper IV with permission from the Royal Society of Chemistry.*

The utilization potential of L-LNP@Ag was demonstrated in developing woody-polymer-based resins and constructing a customer-designed hydrogel *via* lithography-based DLP printing. In this application scenario, GGM was chemically modified with methacryloyls to synthesize a photo-crosslinkable polymeric matrix (GGMMA). Then, a novel resin containing 10 wt% GGMMA and 0.1 wt% L-LNP@Ag was prepared and used for DLP printing operating at 405 nm (**Figure 4.15**). The pure GGMMA hydrogel exhibited poor printing resolution due to weak light absorption and resulted in excessive crosslinking in the honeycomb. Noteworthy, the doping of GGMMA with 0.1 wt% L-LNP@Ag significantly improved the lateral and axial printing fidelity of the GGMMA matrix and mirrored the designed geometry with a 1 mm pore size and 35 μm layer thickness. This indicates that L-LNP@Ag can function as an effective photo-absorber to mitigate excess light penetration into the printing objects since the surface plasmon resonance absorption peak of metallic silver (380 – 420 nm) covers the DLP UV light source (405 nm) (original data in Paper IV). In addition, the GGMMA/L-LNP@Ag hydrogel possessed strong antimicrobial properties against both *E. coli* and *S. aureus*. Upon 1-hour incubation, the

bactericidal ratio of 10GGMMA/0.1L-LNP@Ag hydrogel reached 53% and 75% against *E. coli* and *S. aureus*, respectively, and almost all bacteria were inactivated after a 2-hour incubation (original data in Paper IV). The high printing fidelity and strong antimicrobial activity of the developed photo-crosslinkable resin of woody polysaccharides and hybrid silver-lignin nanospheres make it a promising material suitable for biomedical applications.

4.5. Lignin characteristic – material property correlations

4.5.1. Thermosetting resoles with tailored wet bonding strength (Paper I)

LPF adhesives are one of the prime applications of lignin in the form of polymer. Sequential lignin fractionation methodology was applied to unravel fundamental insights on the correlation between lignin structural characteristics and wet bonding strength of resoles, which were prepared by substituting 30 to 70 wt% of phenol with lignin under alkaline catalysis (**Figure 4.16a**). All the resoles were synthesized by one-pot batch polymerization, starting with lignin phenolation to introduce more reactive sites to lignin macromolecules for resole synthesis.

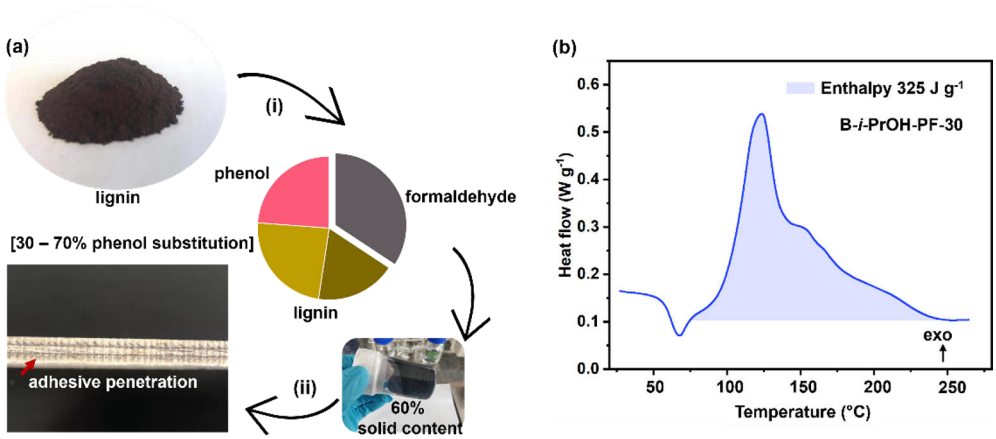

Figure 4.16. *(a) Representative scheme for the (i) synthesis of LPF adhesives by one-pot batch polymerization and (ii) preparing plywood by hot-pressing. (b) DSC thermogram of B-i-PrOH-PF-30 at a heating rate of 5 °C min-1. This figure is adapted from its original version in Paper I.*

DSC analysis was used to obtain key thermal parameters of resole curing, including activation energy and enthalpy. The DSC thermogram of B-*i*-PrOH-PF-30 adhesive (30% of phenol was substituted by lignin) showed two distinctive exothermic peaks typical of resole curing, as illustrated in **Figure 4.16b**. The first exothermic peak (126 – 128 °C) resulted from the addition reaction between the free reactive sites for hydroxymethylation in the

aromatic ring and residual formaldehyde in the resoles. The second exothermic peak (150 – 160 °C) was attributed to the polymerization reaction *via* the formation of methylene linkages during thermal curing.[184] It was found that resoles containing lignin fractions of the same origin with low molar mass and high phenolation degree (*e.g.*, B-*i*-PrOH-s and B-EtOH-s fractions) had lower activation energy and higher enthalpy (*i.e.*, exothermic heat) than those containing high molar mass lignin fractions (**Table 4.8**). This indicates that lignin fractions that had higher reactivity for phenolation also had higher chemical accessibility (*i.e.*, more reactive sites) and lower steric hindrance in the resole curing reaction.

Consequently, the wet bonding strength of the glued plywood increased with the decreasing molar mass of birch AL fractions (**Figure 4.17a**). In the tensile strength test, wood failure was seen to account for the fracture of plywood bonded with B-*i*-PrOH-PF-30 (2.16 MPa) and B-EtOH-PF-30 (1.95 MPa), which was due to a high wet bonding strength (**Figure 4.17b**). In contrast, low wet bonding strength due to cohesive failure of adhesive was observed for plywood bonded with unfractionated birch AL-PF-30 (1.28 MPa), B-MeOH-PF-30 (1.00 MPa), and residue-PF-30 (0.56 MPa) adhesives, as illustrated in **Figure 4.17b**. Poor water resistance of the residue-PF-30 adhesive was observed during the boil-dry-boil pretreatment, possibly due to the high content of hemicelluloses (8.4%) in the birch AL residue lignin. In addition to the aspects of lignin structural characteristics that determine the curing properties of resoles, B-*i*-PrOH-PF and B-EtOH-PF adhesives may penetrate better into the porous wood structure, resulting in a strong wood bonding.

Table 4.8. DSC analysis of LPF adhesives (lignin substituted 30 wt% of phenol).

samples	T_P (°C)			curing enthalpy[a]	activation energy[b]
	2.5 °C min^{-1}	5.0 °C min^{-1}	7.5 °C min^{-1}	J g^{-1}	kJ mol^{-1}
birch AL-PF-30	119.74	129.15	133.62	311	94.4
B-i-PrOH-PF-30	116.87	126.40	132.65	325	86.0
B-EtOH-PF-30	117.55	126.76	131.74	316	93.4
B-MeOH-PF-30	118.25	126.98	131.60	252	95.2
residue-PF-30	118.48	127.00	133.28	215	95.7

[a]integration of the exothermic peak with respect to the linear baseline of the DSC curve obtained at a heating rate of 5 °C min^{-1}. [b]activation energy was calculated according to the Kissinger method.[185]

Nevertheless, it was found that the larger the amount of phenol was attempted to replace with B-*i*-PrOH-s fraction, the more difficult it was, as evident from

the decrease in wet bonding strength as lignin content increased from 30 to 70 wt% (**Figure 4.17c**). The *i*-PrOH-s fraction from spruce AL had comparable molar mass and $Đ_M$ to its birch AL counterpart and theoretically had more reactive sites for resole synthesis. However, the S-*i*-PrOH-PF adhesives had slightly lower wet bonding strength than B-*i*-PrOH-PF (**Figure 4.17c**), indicating that the theoretical reactive sites in spruce AL fractions might not be fully available. Moreover, this indeed confirmed that the molar-mass-dependent differences in lignin, such as the condensation degree associated with the steric accessibility of lignin reactive sites, may play a more critical role than molar mass and the number of reactive sites in the covalent integration of lignin to high-performance resoles.

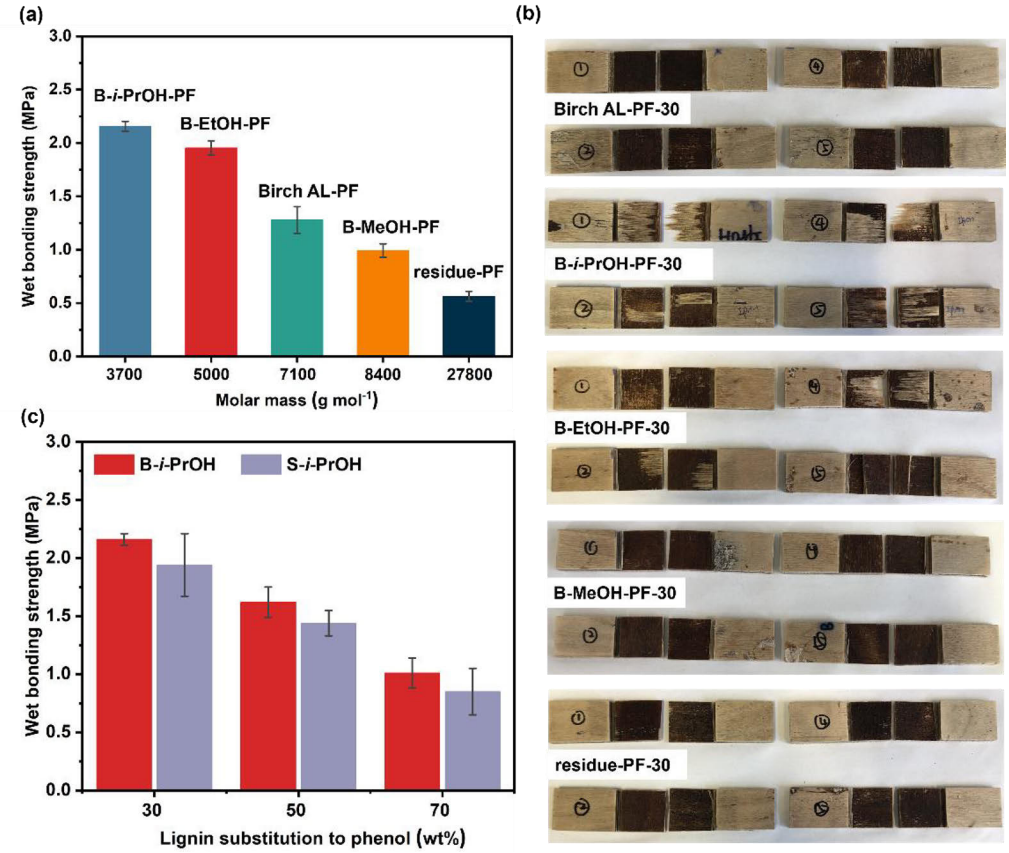

Figure 4.17. *(a) The wet bonding strength of plywood as a function of M_W of birch ALs. (b) Wood failure performance of the LPF adhesives. (c) Comparison of wet bonding strength of the plywood glued by B-i-PrOH-PF and S-i-PrOH-PF adhesives. This figure is adapted from its original version in Paper I.*

Overall, this thesis demonstrated that tailored wet bonding strength of thermosetting LPF wood adhesives could be achieved by refining heterogeneous technical lignin into well-defined fractions *via* sequential solvent fractionation. Moreover, 80% of birch AL (*i.e.*, B-*i*-PrOH-s and B-EtOH-s) fractions derived from solvent fractionation can be used to replace phenol in resole resins with a substitution degree of up to 70%, and the wet bonding strength can still meet the requirements for exterior-grade panels (I grade, 0.7 MPa). This suggests that the covalent integration of lignin macromolecules into resole could be enhanced by solvent fractionation. This study further supports the opportunity to valorize hardwood lignin in LPF manufacturing as they present no disadvantages over the softwood counterparts, although hardwood lignin has often been considered less preferential due to their high content of allegedly less reactive S-subunits in the resole applications.

4.5.2. Thermoplastic bio-latex with tunable mechanical properties (Paper II)

Surface-active nano-sized lignin (*e.g.*, A-LNPs discussed in 4.3.2) is rising as a class of sustainable nanomaterials that can be integrated into latex colloids. However, fundamental knowledge of the correlation between the surface functionality of LNPs and the integration efficiency in latex colloids and from it thermally processed latex films is scarce. This thesis presented a facile but high-performance approach to integrate A-LNPs as the surface-active hard cores in the core-shell free-radical emulsion polymerization of BA and MMA acrylate monomers (**Figure 4.18**). In addition, the research on the effect of surface functionalities on the physiochemical properties of A-LNPs was extended, and the impact of varied content of surface functionalities on the emulsion polymerization performance was further correlated.

The extent of interfacial compatibility between A-LNPs and acrylate monomers was estimated by determining the monomer conversion kinetic during core-shell emulsion polymerization. The monomer conversion of MMA was much more pronounced than that observed for BA, and only residual BA was identified in both pBM and A-LNP-pBM latex emulsions (original data in Paper II). It is worth noting that the monomer conversion rate increased in the order of A-LNP-1.0-pBM (56.5%) < A-LNP-1.5-pBM (90.7%) < A-LNP-4.0-pBM (97.3%) < A-LNP-2.5-pBM (100%), as shown in **Table 4.9**. The A-LNP-1.0-pBM and A-LNP-1.5-pBM latex emulsions had much more BA residues than the neat pBM. It is concluded that A-LNPs with a low content of surface-distributed allyl groups do not significantly promote the emulsion polymerization process of BA

and MMA in terms of monomer diffusion and polymerization rate, which will drive the shell polymer composition of pBM towards the reactive monomer as the degree of conversion increases.

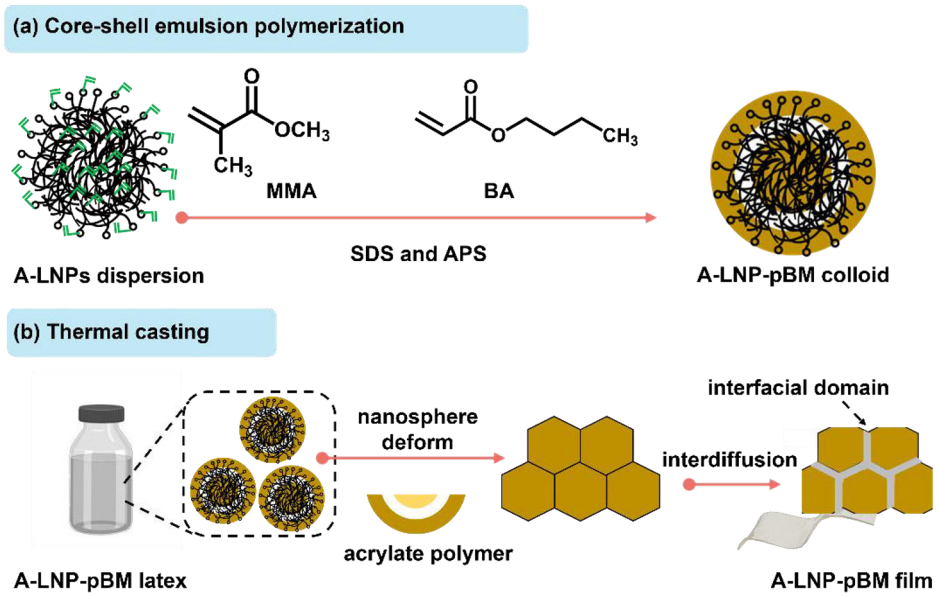

Figure 4.18. *(a) Fabrication of A-LNP-pBM latex colloids through emulsion polymerization of BA and MMA using A-LNPs as a structural template in aqueous media followed by (b) film formation using thermal casting. This figure is adapted from its original version in Paper II.*

Table 4.9. Physiochemical properties of the neat pBM and A-LNP-pBM latex.

samples	A-LNPs	latex emulsion		latex film	
	allyl groups (mmol g^{-1})[a]	monomer conversion (%)[b]	monomer content (mg mL^{-1})[b]	Tg (°C)[c]	d_{inter} (nm)[d]
pBM	---[e]	100	0.02	13	0.80 ± 0.02
A-LNP-1.0-pBM	0.31	56.5	13.8	112	---[f]
A-LNP-1.5-pBM	0.57	90.7	2.6	-12	0.52 ± 0.01
A-LNP-2.5-pBM	1.04	100	0.03	8	0.85 ± 0.01
A-LNP-4.0-pBM	1.23	97.3	0.8	13	1.01 ± 0.01

[a]allyl groups distributed on the surface of A-LNPs. [b]BA monomer was the only residue as determined by HPLC measurement. [c]determined by DSC analysis. [d]estimated from SAXS analysis by Porod's law fitting.[186] [e]denotes not detected. [f]not able to create a film.

It should be noted that while A-LNP-4.0 nanospheres, when compared to A-LNP-2.5-pBM, had a higher surface allyl group content than A-LNP-2.5, the higher Tg and lower WCA values still resulted in a latex emulsion with a higher BA residue content. These results support the hypothesis that BA and MMA

monomers can recognize the molecular-scale differences on A-LNPs. This depends not only on the abundance of the allyl-terminated anchors but also on their sufficient domain flexibility and surface hydrophobicity to enhance the accessibility of the core in the core-shell emulsion polymerization.

The application potential of A-LNP-pBM bio-latex in coating and packaging applications was evaluated in terms of the morphology and thermal properties of the bio-latex colloids and the nanostructure and mechanical properties of the bio-latex films. Compared with the brown color of A-LNP-2.5 and the milky white color of neat pBM, the color of A-LNP-2.5-pBM latex was milky yellowish (**Figure 4.19a**), indicating the high coverage of pBM shell on A-LNPs core. The spherical nanostructures of the pBM and A-LNP-pBM latex colloids were evident from the TEM images, as shown in **Figure 4.19b-f**.

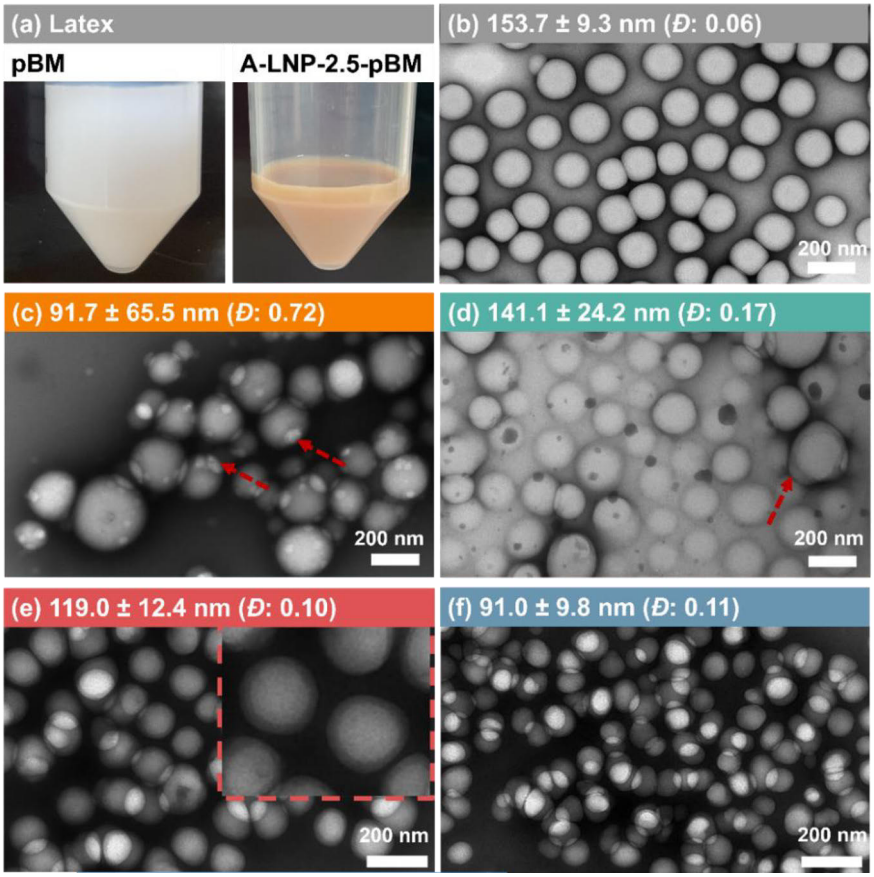

Figure 4.19. *(a) Representative photographs of pBM and A-LNP-pBM latex emulsions. TEM images of (b) pBM, (c) A-LNP-1.0-pBM, (d) A-LNP-1.5-pBM, (e) A-LNP-2.5-pBM, (f) A-LNP-4.0-pBM colloids and their particle size distribution. The inset in (e) is the zoom of the corresponding TEM image showing the stained sulfonate ions from pBM polymer shell.*[187] *This figure is adapted from its original version in Paper II.*

It is noteworthy that the content of surface functionality of A-LNPs had a significant impact on the nanomorphology of A-LNP-pBM. Small domains of pBM homopolymer were present on A-LNP-1.0-pBM latex colloids, indicating surface-initiated polymerization (**Figure 4.19c**). When the A-LNPs with more surface-distributed allyl groups, higher surface hydrophobicity, and lower Tg values than A-LNP-1.0 were used as the polymerization templates, A-LNP-pBM latex colloids presented a concentric core-shell morphology (see inset in **Figure 4.19e**). The *Đ* values of latex colloids derived from TEM image analysis confirmed that A-LNP-2.5-pBM (*Đ* = 0.10) and A-LNP-4.0-pBM (*Đ* = 0.11) colloids had comparably uniform particle size distribution as neat pBM (*Đ* = 0.06). The particle size of A-LNP-pBM colloids was observed to be dependent on the surface functionality of A-LNPs, with an increase in the content of surface-distributed allyl groups from 0.57 to 1.23 mmol g^{-1}, resulting in a significant decrease in the average size of the A-LNP-pBM colloids from 141 to 91 nm (**Figure 4.19d-f**). The A-LNPs core size decreased with increasing surface functionality in the order A-LNP-1.0 (225 nm) > A-LNP-1.5 (195 nm) > A-LNP-2.5 (150 nm) > A-LNP-4.0 (140 nm), which could partially explain the size difference of A-LNP-pBM. More importantly, the A-LNPs core with higher content of polymerization-active anchors and higher domain flexibility (*i.e.*, low Tg values) can facilitate the covalent bonding and interpenetration with the shell of acrylate polymer during emulsion polymerization, which may result in smaller A-LNP-pBM latex colloids.

Self-standing, dense, crack-free, and stretchable pBM and A-LNP-pBM films were obtained by evaporating water from the latex emulsions and annealing at 50 °C (**Figure 4.20**), with the exception of the A-LNP-1.0-pBM latex colloids. The low content of polymerization-active allyl groups in A-LNP-1.0 resulted in a high Tg value (112 °C), confirming that the dominant component of its acrylate polymer shell was PMMA since the PMMA can restrict chain rotation and flexibility during film formation. This further indicates that A-LNP-pBM colloids without core-shell nanostructures are present as nanofillers and interfere with film formation.

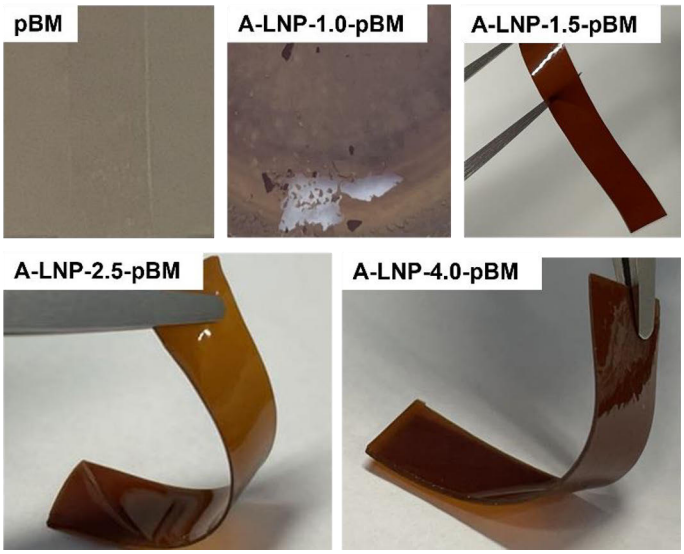

Figure 4.20. *Photographs of pBM and A-LNP-pBM latex films. This figure is adapted from its original version in Paper II.*

The nanostructure of pBM and A-LNP-pBM latex films was investigated by PF-QNM AFM (**Figure 4.21**). Compared with the stiffness modulus distribution in neat pBM latex film, the A-LNP-1.5-pBM latex film exhibited a slight phase separation (**Figure 4.21a-b**). The core-shell boundary of the A-LNP-2.5-pBM latex colloids seemed to deform during film formation and to form a honeycomb-like percolating structure comprising a stiff-elastic phase and a soft-dispersed phase throughout the polymer matrix, as indicated by red arrows in **Figure 4.21c** inset. The stiff core-shell boundary was ascribed to the core-initiated covalent polymerization and the polymer chain coalescence. In addition, the coalescence on core-shell boundaries was more pronounced in the A-LNP-4.0-pBM film (**Figure 4.21d**), with the surface stiffness modulus increasing in the order A-LNP-1.5-pBM (0.48 GPa) < pBM (1.72 GPa) < A-LNP-2.5-pBM (2.96 GPa) < A-LNP-4.0-pBM (6.83 GPa). The low surface stiffness of A-LNP-1.5-pBM latex film may be due to the high concentration of BA residues in its latex emulsion, which also resulted in the extremely low Tg value (-12 °C) of its latex film (**Table 4.9**). It is worth noting that the Tg of A-LNP-2.5-pBM film (8 °C) was lower than the Tg of neat pBM (13 °C), although they had the same acrylate polymer composition (*i.e.*, approximately 100% monomer conversion). This indicates once more the presence of an interpenetrating polymer network in the A-LNP-pBM latex, which is important for tough bio-latex film applications. A-LNP-4.0-pBM latex colloids had a higher Tg value than A-LNP-2.5-pBM. It is expected that the polymer chains of pBM were covalently polymerized with A-

LNP-4.0 nanospheres and were confined on the core surface due to the largest content of surface allyl groups (1.23 mmol g^{-1}). Subsequently, the latex films were quantitatively evaluated in terms of the interpenetration degree of near-surface polymer chains on latex colloids (*i.e.*, sulfate-terminated pBM) using SAXS analysis. In latex films, the average interfacial domain boundary size (d_{inter}) decreased in the order A-LNP-4.0-pBM (1.01 nm) > A-LNP-2.5-pBM (0.85 nm) > pBM (0.80 nm) > A-LNP-1.5-pBM (0.52 nm) (**Table 4.9**). This suggests that the A-LNP-pBM latex colloids with uniform core-shell morphology can exhibit better polymer chain interpenetration than that of the neat pBM. In addition, the degree of interpenetration between pBM polymer shells increased with increasing the surface functionality of A-LNPs, especially when the A-LNP-2.5-pBM and A-LNP-4.0-pBM latex films were compared.

DMA analysis determined the thermal-mechanical properties of the latex films (**Figure 4.21e**). The temperature-dependent function of the extensional E' and loss modulus (E'') for the latex films exhibited the glass-rubber transition process of the pBM phase in the temperature range of 0 − 15 °C, as indicated by the stepwise decrease of extensional E' and the peak in extensional E''. Noteworthy, the Tg identified from the peak of E'', was almost identical to that determined by the DSC analysis. Further heating resulted in a sharp drop in E' for neat pBM film until reaching a rubbery plateau starting from 35 °C, whereas the rubbery plateau of A-LNP-pBM was not obvious up to 50 °C. Compared to neat pBM films, the viscoelastic behavior (the difference between E' and E'') of the A-LNP-pBM films was less dependent on temperature over a wide temperature range (20 − 35 °C). The A-LNP-2.5-pBM and A-LNP-4.0-pBM films also exhibited higher E' values than neat pBM films at room temperature. The thermal-mechanical results of the latex films indicate that the mechanical stiffness of the pBM polymer matrix was increased when A-LNPs were involved in the emulsion polymerization, which is consistent with the PF-QNM AFM results.

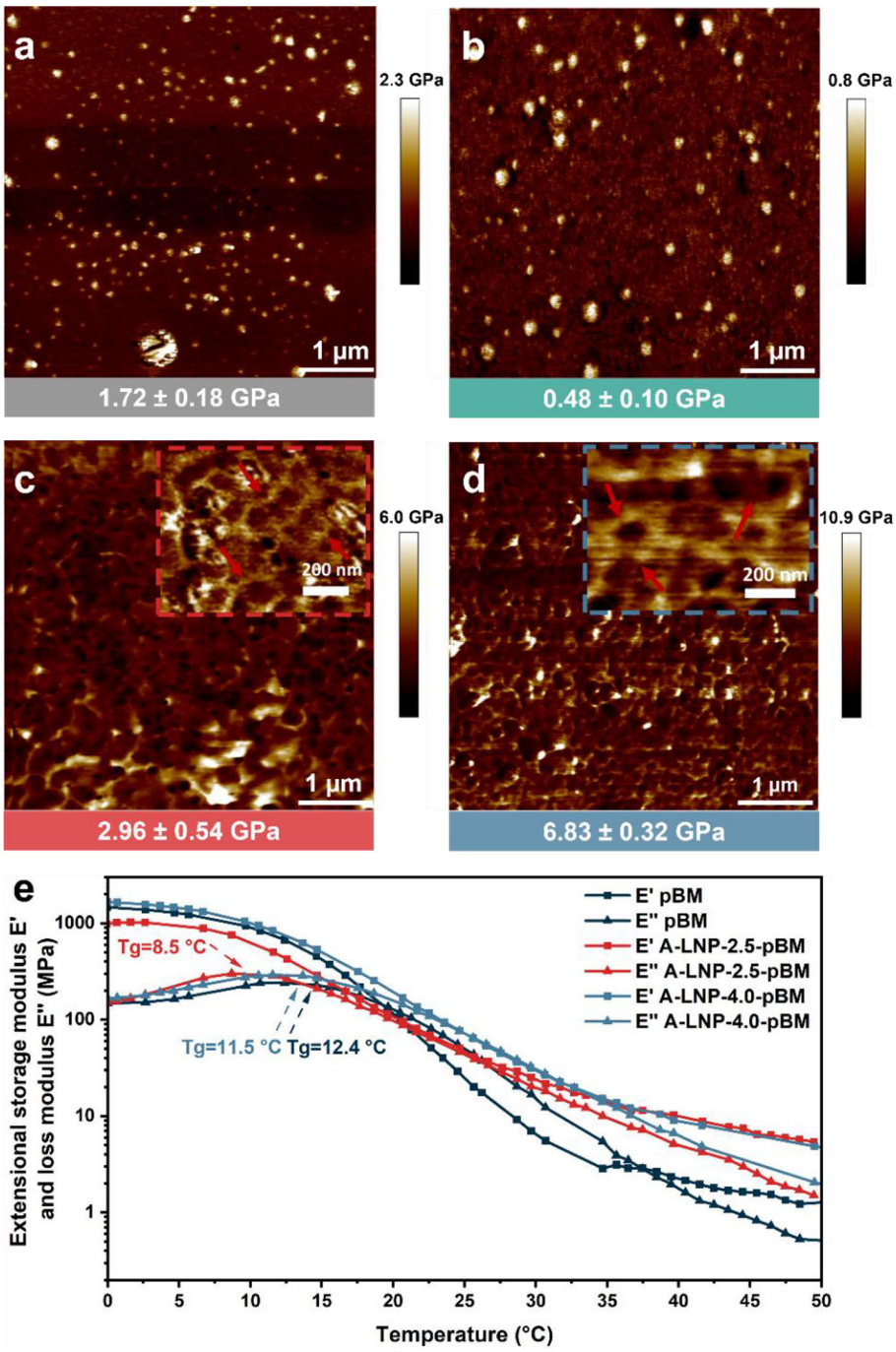

Figure 4.21. *Stiffness modulus distribution in (a) neat pBM, (b) A-LNP-1.5-pBM, (c) A-LNP-2.5-pBM, and (d) A-LNP-4.0-pBM latex films. The insets in (c) and (d) are the zoom of the corresponding AFM image demonstrating the honeycomb-like percolating structure. (e) Extensional E' and E'' vs. temperature curves for latex films. This figure is adapted from its original version in Paper II.*

Tensile strength tests described the tunable mechanical properties of A-LNP-pBM bio-latex films (**Figure 4.22**). Compared with neat pBM film, the A-LNP-pBM film containing the same amount of A-LNPs (20% relative to the total weight of acrylate monomers) showed tunable mechanical properties, from stiff (A-LNP-4.0-pBM) to high toughness thermoplastics (A-LNP-2.5-pBM) to ultrastretchable elastomers (A-LNP-1.5-pBM) through tuning the abundance of polymerization-active allyl groups on A-LNPs. The A-LNP-2.5-pBM achieved a remarkable toughness value above 57.7 MJ m^{-3}, which is 2.9 times higher than that for the neat pBM polymer. The high toughness of A-LNP-2.5-pBM latex film was believed to be associated with the polymerization fashion that the pBM polymer interpenetrates with A-LNPs and spatially surrounds the A-LNPs through polymerization-active anchors. Subsequently, the honeycomb-like percolating nanostructures in the A-LNP-pBM bio-latex films dissipate energy during large deformations.

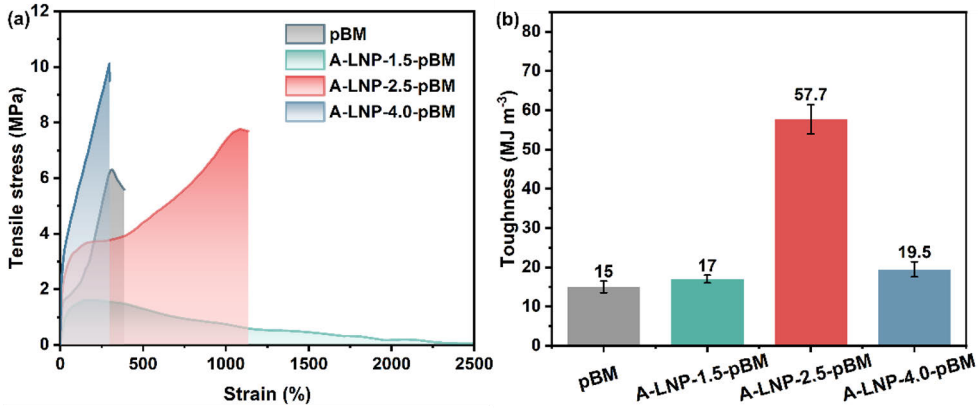

Figure 4.22. *(a) Typical stress-strain curve of the latex film during tensile testing. (b) The toughness of the A-LNP-pBM latex films. This figure is adapted from its original version in Paper II.*

Overall, this thesis presented a facile method to prepare LNPs with tunable surface chemistry metrics, the LNPs being an interfacial-modulating template for directing the core-shell emulsion polymerization of acrylate monomers upon it. The accessibility of the A-LNPs core tailored by the degree of surface functionalization played the most crucial role in determining the emulsion polymerization efficiency and composition of the acrylate polymer shell, which influences the polymer chain coalescence and interpenetrating during film formation. Therefore, the mechanical properties of the A-LNP-pBM latex films can be tailored by balancing the contributions from the aspects mentioned above.

5. Conclusions and future perspectives

5.1. Highlights of this thesis

The proposed sequential lignin solvent fractionation approach (*i*-PrOH, EtOH, and MeOH) can obtain lignin fractions with well-defined properties in terms of purity and structural characteristics. More importantly, extensive lignin purification and comprehensive structural elucidation of the obtained lignin fractions warranted the reliability of lignin structure-property correlation for different applications.

The correlation between lignin structural characteristics and wet bonding strength of thermosetting LPF adhesives was established using lignin fractions from the same origin. Lignin fractions with low molar mass (*e.g.*, *i*-PrOH-s) had more reactive sites and better steric accessibility for resole synthesis than the high molar mass ones (*e.g.*, MeOH-s). When comparing AL fractions from birch and spruce, the molar-mass-dependent differences in lignin, such as the degree of condensation associated with the steric accessibility of reactive sites, were confirmed to be more critical than the reactive sites content in the covalent integration of lignin with resoles.

In terms of bioplastic, this thesis developed a new class of bio-latex by adapting the nanotechnology of lignin macromolecules. The innovation highlights a holistic approach to functionalize lignin macromolecules with allyl-terminated polymer chains through ring-opening of epoxides at alkaline conditions, followed by dialysis purification against water, where the pH changes *in situ* triggered the uniform arrangement of polymerization-active anchors on the nanosphere surface *via* self-assembly. The application of A-LNPs as a polymerization-modulating template in seeded emulsion polymerization of acrylates successfully yielded core-shell-nanostructured latex colloids (A-LNP-pBM). The A-LNP-pBM colloids can further be processed as bio-latex films with extraordinary mechanical properties in terms of toughness and elongation of the A-LNP-integrated polymeric materials. A wide spectrum of mechanical characteristics, ranging from stiff to ductile thermoplastics and further to ultrastretchable elastomers, was achieved by tuning the confined surface functionality of A-LNPs, which had a delicate control over the core-shell emulsion polymerization efficiency and structural evolution of bio-latex colloids. In addition, this new class of aqueous bio-latex colloids had a lignin content as high as 20% in relative to the total weight of acrylate monomers,

which can potentially find industrial applicability as sustainable solutions for coating and packaging applications.

The bacterial-derived alkaliphilic laccase extensively catalyzed the oxidation and polymerization of AL fractions in an aqueous alkaline solution (pH 10). In comparison, AL fractions from spruce were found to be less reactive toward the laccase-catalyzed polymerization than those from birch, which was attributed to the high initial degree of condensation and the much more pronounced aryl-vinyl moieties' oxidation. The structural characteristics of lignin (*e.g.*, functional groups and recalcitrant carbon-carbon linkages) could be tailored by fractionation-dependent lignin polymerization kinetics, and high-performance lignin nanomaterials can be fabricated through the use of the nanostructured templating approach. This biochemical approach was successfully applied to obtain nanocellulose fibers uniformly decorated with *in situ* polymerized nanoscale lignin (~ 30 nm), which has potential in the development of functional bio-based packaging materials. Moreover, the alkali resistance of LNPs, as demanded for direct surface functionalization at chemically demanding conditions, was achieved by tailoring the laccase-catalyzed lignin polymerization degree *via* selecting lignin fractions. This nanoscale polymeric support (L-LNPs) was utilized as a template for *in situ* reduction of Ag^{+} from silver precursor solution (pH 11), while with AgNPs uniformly surface embedded. This enzymatic valorization approach mitigates the need for petroleum-based crosslinkers in this type of application. Subsequently, wood-biopolymer-based hydrogels (GGMMA/L-LNP@Ag) with excellent antimicrobial activity were fabricated by DLP printing, which provided a new frontier in DLP printing research focusing on sustainable resins with good printing fidelity.

As a conclusive remark, we have established facile but high-performance synthesis approaches to integrate lignin, a waste-stream biopolymer, in thermosets, bioplastics, lignin-cellulose nanocomposites, and lignin-hemicellulose photo-crosslinkable resins, which can potentially provide new possibilities for achieving a profitable value chain for biorefinery processes.

5.2. Future perspectives

In terms of lignin fractionation, it is an effective strategy to decrease the molar-mass-dependent heterogeneity of lignin. In this aspect, lignin refining or fractionation efforts are essential and need to be considered before devising strategies for the industrial utilization of lignin. Furthermore, lignin

purification and the design of effective lignin fractionation sequences to produce uniform lignin specifications with well-defined molar mass, functional group content, and degree of condensation are essential to gain more knowledge on the structure-property correlations for different applications. In this case, there is an urgent need to promote standardized lignin characterization methods for establishing reliable lignin structure-property correlations. The economic feasibility of lignin fractionation (*e.g.*, cost of solvents and scalability) should also be considered to realize a profitable value chain for lignin valorization. It should be noted that lignin is application-specific, *i.e.*, lignin from different sources, such as hardwood, softwood, and straw, may not be suitable for the same application due to their different chemical structures. Therefore, lignin structure-property correlation should be established based on experimental scope only and should not be extrapolated to other lignin types. In addition, the properties of lignin fractions derived from solvent fractionation are strictly interdependent. Hence, correlating the lignin-specific functionalities (*e.g.*, aliphatic-OH, phenolic-OH, -COOH, and carbonyl groups) and lignin properties, such as thermal properties, is difficult. The development of new methodological approaches to selectively block other lignin functionalities in order to correlate one structural variable at a time may be applicable.

In terms of lignin-based phenolic resins, there is an inevitable need to develop phenol-free and formaldehyde-free resins to achieve high carbon efficiency in terms of carbon immobilization. However, the lignin development work has not always been straightforward as the current objective of industries is not to make lignin for further utilization but to make paper, bio-ethanol, or other products. It encourages the lignin manufacturers to put more effort into optimizing the lignin extraction processes to produce 'homogeneous' lignin with an even lower molar mass in the future.

In the fabrication of bio-based nanomaterials using surface-active LNPs as a structural template to achieve high lignin content, it is necessary to open up new lignin self-assembly mechanisms and develop methods to prepare nanoscale lignin with diverse morphologies, such as lignin nanofibers, not limited to nanospheres. Lignin nanofibers may provide dispersibility and dispersion viscosity different from lignin nanosphere dispersion, which can offer the potential to fabricate all lignin-based formulations, such as surface coatings and photo-crosslinkable resins.

In constructing nanoscale lignin confined on nanocellulose fibers using a laccase-catalyzed *in situ* polymerization approach, the use of lignin-containing nanocellulose (*e.g.*, unbleached pulp) as a structural template may facilitate the economic viability of the entire process for the preparation of dispersion coating formulations. In the future, it is also essential to investigate the financial viability and biodegradability of the as-produced lignin-containing materials and conduct life cycle assessments to minimize the environmental impact.

6. Acknowledgements

The work in this doctoral thesis was carried out during the time 11.2018-10.2022 in the Laboratory of Natural Materials Technology (NMT) at the Faculty of Science and Engineering of Åbo Akademi University. This work received the main funding from China Scholarship Council (201804910639) and Business Finland Project (43674/31/2020). The research grants from Fortum Foundation, Finnish Forest Products Engineers' Association and the Walter Ahlström Foundation are acknowledged.

My deepest gratitude goes to Dr. Xiaoju Wang, for your enlightening supervision and support. I admire your focus and sharp ideas in research and appreciate your trust and encouragement in training me to become a professional and independent researcher. To improve the work quality, we have shared so many intense, but it turned out to be great moments throughout these years. Xiaoju, you shaped this invaluable journey like no other. Thank you!

I also want to thank all my co-supervisors, Professor Chunlin Xu, Professor Patrik Eklund, Professor Thomas Rosenau, and Professor Stefan Willför. Thank you for being so helpful in putting my research work in motion and giving it perspective. Chunlin, you started the journey of my doctoral thesis on lignin fractionation. You have always provided valuable opportunities for your students and facilitated us to establish research network. I appreciate you letting me in the LigninReSurf project, where I strengthened my research skills on lignin and gained ideas on how to take products from laboratory scale to industrial production. Patrik, thank you for your guidance on lignin chemistry and your curiosity always encouraged me to keep on thinking. Rosi and Stefan, thank you for all the constructive feedback you gave during my research. I would like to thank Professor Orlando J. Rojas for taking on the role as my opponent and Assistant Professor Olena Sevastyanova for reviewing my thesis.

Everyone whom I have worked with at NMT, thank you for the togetherness we have made. Professor Martti Toivakka, Professor Chunlin Xu, Anna Sundberg, Mari Nurmi, Jan Gustafsson, thank you for leading a warm environment for us to grow in and explore. I would like to thank Andrey Pranovich for your help with lab work. You keep showing me science from so many points of view. Jarl Hemming, thank you for your efforts to ensure all the machines running. You two have turned over a lot of stones for us and made so many things easier. You are the hero behind the article. Thank you! All other colleagues, thank you for

always being around and supporting me. It is my great pleasure to meet and work with you.

Finally, I would like to thank my parents for accepting everything about me and loving me deeply. My biggest thanks go to my husband, Qingbo, thank you for all the understanding, motivation, and support.

Luyao Wang

Åbo, July 2023

7. References

(1) Balakshin, M. *et al*. New Opportunities in the Valorization of Technical Lignins. *ChemSusChem* **2021**, *14* (4), 1016–1036.

(2) Menon, V. *et al*. Trends in Bioconversion of Lignocellulose: Biofuels, Platform Chemicals & Biorefinery Concept. *Prog Energy Combust Sci* **2012**, 38 (4), 522–550.

(3) Mariana, M. *et al*. A Current Advancement on the Role of Lignin as Sustainable Reinforcement Material in Biopolymeric Blends. *Journal of Materials Research and Technology* **2021**, 15, 2287–2316.

(4) Muktham, R. *et al*. A Review on 1st and 2nd Generation Bioethanol Production-Recent Progress. *Journal of Sustainable Bioenergy Systems* **2016**, 6, 72–92.

(5) Kumar, P. *et al*. Methods for Pretreatment of Lignocellulosic Biomass of Efficient Hydrolysis and Biofuel Production. *Ind. Eng. Chem. Res.* **2009**, *48* (8), 3713–3729.

(6) Mckendry, P. Energy Production from Biomass (Part 1): Overview of Biomass. *Bioresour Technol* **2002,** 83 (1), 37–46.

(7) Menon, V. *et al*. Trends in Bioconversion of Lignocellulose: Biofuels, Platform Chemicals & Biorefinery Concept. *Progress in energy and combustion science* **2012**, *38* (4), 522–550.

(8) Klemm, D. *et al*. Cellulose: Fascinating Biopolymer and Sustainable Raw Material. *Angewandte Chemie International Edition* **2005**, *44* (22), 3358–3393.

(9) Wohlert, M. *et al*. Cellulose and the Role of Hydrogen Bonds: Not in Charge of Everything. *Cellulose* **2022**, *29* (1), 1–23.

(10) Paajanen, A. *et al*. Chirality and Bound Water in the Hierarchical Cellulose Structure. *Cellulose* **2019**, *26* (10), 5877–5892.

(11) Scheller, H. V. *et al*. Hemicelluloses. Annual Review of Plant Biology **2010**, *61*, 263–289.

(12) Ralph, J. *et al*. Lignins: Natural Polymers from Oxidative Coupling of 4-Hydroxyphenyl-Propanoids. *Phytochemistry Reviews* **2004**, *3*, 29–60.

(13) Wang, J. P. *et al*. Improving Wood Properties for Wood Utilization through Multi-Omics Integration in Lignin Biosynthesis. *Nature Communications* **2018**, *9*, 1–16.

(14) Bond, J. *et al*. Safranine Fluorescent Staining of Wood Cell Walls. *Biotechnic & Histochemistry* **2008**, *83*, 161–171.

(15) Vanholme, B. *et al*. Towards a Carbon-Negative Sustainable Bio-Based Economy. *Front Plant Sci* **2013**, *4*, 174.

(16) Ralph, J. *et al*. Lignins: Natural Polymers from Oxidative Coupling of 4-Hydroxyphenyl-Propanoids. *Phytochem. Rev.* **2004**, *3*, 29–60.

(17) Lancefield, C. S. *et al*. Identification of a Diagnostic Structural Motif Reveals a New Reaction Intermediate and Condensation Pathway in Kraft Lignin Formation. *Chem Sci* **2018**, *9* (30), 6348–6360.

(18) Sangha, A. K. *et al*. Radical Coupling Reactions in Lignin Synthesis: A Density Functional Theory Study. *Journal of Physical Chemistry B* **2012**, *116* (16), 4760–4768.

(19) Anderson, E. M. *et al*. Differences in S/G Ratio in Natural Poplar Variants Do Not Predict Catalytic Depolymerization Monomer Yields. *Nature Communications* **2019** *10*, 1–10.

(20) Li, C. *et al*. Catalytic Transformation of Lignin for the Production of Chemicals and Fuels. *Chem Rev* **2015**, *115* (21), 11559–11624.

(21) Balakshin, M. *et al*. Spruce Milled Wood Lignin: Linear, Branched or Cross-Linked? *Green Chemistry* **2020**, *22*, 3985–4001.

(22) Wang, S. *et al*. The Temptation from Homogeneous Linear Catechyl Lignin. *Trends Chem* **2022**, *4* (10), 948–961.

(23) Liu, C. *et al*. Catalytic Hydrogenolysis of Castor Seeds C-Lignin in Deep Eutectic Solvents. *Ind Crops Prod* **2021**, *169*, 113666.

(24) Li, Y. *et al*. An Ideal Lignin Facilitates Full Biomass Utilization. *Sci Adv* **2018**, *4* (9), eaau2968.

(25) Barros, J. *et al*. The Cell Biology of Lignification in Higher Plants. *Ann Bot* **2015**, *115* (7), 1053–1074.

(26) Santiago, R. *et al*. Impact of Cell Wall Composition on Maize Resistance to Pests and Diseases. *Int J Mol Sci.* **2013**, 14 (4), 6960–6980.

(27) de Oliveira, D. M. *et al*. Ferulic Acid: A Key Component in Grass Lignocellulose Recalcitrance to Hydrolysis. *Plant Biotechnol J* **2015**, *13* (9), 1224–1232.

(28) Terrett, O. M. and Dupree, P. Covalent Interactions between Lignin and Hemicelluloses in Plant Secondary Cell Walls. *Curr Opin Biotechnol* **2019**, *58*, 97–104.

(29) Tarasov, D. *et al*. AqSO Biorefinery: A Green and Parameter-Controlled Process for the Production of Lignin–Carbohydrate Hybrid Materials. *Green Chemistry* **2022**, *24* (17), 6639–6656.

(30) Jiang, Y. *et al*. Effects of Residual Lignin on Mechanical Defibrillation Process of Cellulosic Fiber for Producing Lignocellulose Nanofibrils. *Cellulose* **2018**, *25* (11), 6479–6494.

(31) Wang, Q. *et al*. Flexible Cellulose Nanopaper with High Wet Tensile Strength, High Toughness and Tunable Ultraviolet Blocking Ability Fabricated from Tobacco Stalk *via* a Sustainable Method. *J Mater Chem A Mater* **2018**, *6* (27), 13021–13030.

(32) Farooq, M. *et al*. Strong, Ductile, and Waterproof Cellulose Nanofibril Composite Films with Colloidal Lignin Particles. *Biomacromolecules* **2019**, 20 (2), 693–704.

(33) Liu, Y. *et al*. Strong and Flexible Nanocomposites of Carboxylated Cellulose Nanofibril Dispersed by Industrial Lignin. *ACS Sustain Chem Eng* **2018**, *6* (4), 5524–5532.

(34) Pasquier, E. *et al*. Lignin Nanoparticle Nucleation and Growth on Cellulose and Chitin Nanofibers. *Biomacromolecules* **2021**, *22* (2), 880–889.

(35) Kozlova, L. V. *et al*. Elongating Maize Root: Zone-Specific Combinations of Polysaccharides from Type I and Type II Primary Cell Walls. *Scientific Reports* **2020**, *10*, 10956.

(36) Schutyser, W. *et al*. Chemicals from Lignin: An Interplay of Lignocellulose Fractionation, Depolymerisation, and Upgrading. *Chem Soc Rev* **2018**, *47* (3), 852–908.

(37) Gierer, J. Chemical Aspects of Kraft Pulping. *Wood Science and Technology* **1980**, *14* (4), 241–266.

(38) Crestini, C. *et al*. On the Structure of Softwood Kraft Lignin. *Green Chemistry* **2017**, *19* (17), 4104–4121.

(39) Chakar, F. S. *et al*. Review of Current and Future Softwood Kraft Lignin Process Chemistry. *Ind Crops Prod* **2004**, *20* (2), 131–141.

(40) Dessbesell, L. *et al*. Global Lignin Supply Overview and Kraft Lignin Potential as an Alternative for Petroleum-Based Polymers. *Renewable and Sustainable Energy Reviews* **2020**, *123*, 109768.

(41) Lauten, R. A. *et al*. New Developments in the Commercial Utilization of Lignosulfonates. *Surfactants from Renewable Resources* **2010**, 269–283.

(42) Fiskari, J. *et al*. Acid Sulfite Pulping of Acacia Mangium and Eucalyptus Pellita as a Pretreatment Method for Multiproduct Biorefineries. *Asia-Pacific Journal of Chemical Engineering* **2021**, *16* (6), e2707.

(43) Asikanius, B. *et al*. Durable Biopolymer Films From Lignin-Carbohydrate Complex Derived From a Pulp Mill Side Stream. *Frontiers in Energy Research* **2021**, *9*, 782545.

(44) Glasser, W. G. Lignin-Based Polymers. *Encyclopedia of Materials: Science and Technology* **2001**, 1–4.

(45) Wang, K. *et al*. Organosolv Fractionation Process with Various Catalysts for Improving Bioconversion of Triploid Poplar. *Process Biochemistry* **2012**, *47* (10), 1503–1509.

(46) Zhang, Y. *et al*. Structural Changes of Bamboo-Derived Lignin in an Integrated Process of Autohydrolysis and Formic Acid Inducing Rapid Delignification. *Ind Crops Prod* **2018**, *115*, 194–201.

(47) Kärkäs, M. D. *et al*. Transition-Metal Catalyzed Valorization of Lignin: The Key to a Sustainable Carbon-Neutral Future. *Org Biomol Chem* **2016**, *14* (6), 1853–1914.

(48) Singh, J. K. *et al*. Assessment of Different Pretreatment Technologies for Efficient Bioconversion of Lignocellulose to Ethanol. *Front Biosci (Schol Ed)* **2018**, *10* (2), 350–371.

(49) Rosales-Calderon, O. *et al*. A Review on Commercial-Scale High-Value Products That Can Be Produced alongside Cellulosic Ethanol. *Biotechnol Biofuels* **2019**, *12* (1), 1–58.

(50) Yang, W. *et al*. Synergic Effect of Cellulose and Lignin Nanostructures in PLA Based Systems for Food Antibacterial Packaging. *Eur Polym J* **2016**, *79*, 1–12.

(51) Yang, J. *et al*. Applications of Lignocellulosic Fibers and Lignin in Bioplastics: A Review. *Polymers* **2019**, *11* (5), 751.

(52) Kalliola, A. *et al*. Oxidation Process Concept to Produce Lignin Dispersants at a Kraft Pulp Mill. *Nord. Pulp Pap. Res. J.* **2022**, 37 (2), 394–404.

(53) Yamamoto, M. *et al*. LigniOx Process Concept for Hydrolysis Lignin–Converting Lignin Into Dispersants and Carbohydrate-Rich Residue to Ethanol. Available online at https://ligniox.eu/wp-content/uploads/2019/10/St1_VTT_LigniOx-presentation-1st-ILS-2019.pdf, **2019**. Retrieved 2023–05–23.

(54) Abu-Omar, M. M. *et al*. Guidelines for Performing Lignin-First Biorefining. *Energy Environ Sci* **2021**, *14* (1), 262–292.

(55) Anderson, E. M. *et al*. Reductive Catalytic Fractionation of Corn Stover Lignin. *ACS Sustain Chem Eng* **2016**, *4* (12), 6940–6950.

(56) Xu, J. *et al*. Striding the Threshold of Photocatalytic Lignin-First Biorefining *via* a Bottom-up Approach: From Model Compounds to Realistic Lignin. *Green Chemistry* **2022**, *24* (14), 5351–5378.

(57) Pan, Z. *et al*. Fractionation of Light-Colored Lignin *via* Lignin-First Strategy and Enhancement of Cellulose Saccharification towards Biomass Valorization. *Ind Crops Prod* **2022**, *186*, 115173.

(58) Cao, Z. *et al*. A Convergent Approach for a Deep Converting Lignin-First Biorefinery Rendering High-Energy-Density Drop-in Fuels. *Joule* **2018**, *2* (6), 1118–1133.

(59) von Schoultz, S. Method for Extracting Biomass, WO 2014/ 009604 A1, **2014**.

(60) von Schoultz, S. Method for Extracting Lignin, WO 2015/104460 A1, **2015**.

(61) Pan, X. *et al*. Enhanced Enzymatic Hydrolysis of Steam-Exploded Douglas Fir Wood by Alkali-Oxygen Post-Treatment. *Biotechnology for Fuels and Chemicals* **2003**, 1103–1114.

(62) Gigli, M. *et al*. Fractionation of Industrial Lignins: Opportunities and Challenges. *Green Chemistry* **2020**, *22* (15), 4722–4746.

(63) Giummarella, N. *et al*. Fractional Profiling of Kraft Lignin Structure: Unravelling Insights on Lignin Reaction Mechanisms. *ACS Sustain Chem Eng* **2020**, *8* (2), 1112–1120.

(64) Zinovyev, G. *et al*. Molar Mass-Dependent Profiles of Functional Groups and Carbohydrates in Kraft Lignin. *Journal of Wood Chemistry and Technology* **2016**, *37* (3), 171–183.

(65) Liu, R. *et al*. Fractionation of Lignin with Decreased Heterogeneity: Based on a Detailed Characteristics Study of Sequentially Extracted Softwood Kraft Lignin. *ACS Sustain Chem Eng* **2021**, *9* (41), 13862–13873.

(66) Liu, R. *et al*. Influence of Carbohydrates Covalently Bonded with Lignin on Solvent Fractionation, Thermal Properties, and Nanoparticle Formation of Lignin. *ACS Sustain Chem Eng* **2022**, *10* (44), 14588–14599.

(67) Musl, O. *et al*. High-Resolution Profiling of the Functional Heterogeneity of Technical Lignins. *Biomacromolecules* **2022**, *23* (3), 1413–1422.

(68) Pylypchuk, I. V. *et al*. High-Molecular-Weight Fractions of Spruce and Eucalyptus Lignin as a Perspective Nanoparticle-Based Platform for a Therapy Delivery in Liver Cancer. *Front Bioeng Biotechnol* **2022**, *9*, 1467.

(69) Vignali, E. *et al*. The Laccase-Lig Multienzymatic Multistep System in Lignin Valorization. *ChemSusChem* **2022**, *15* (20), e202201147.

(70) Zwilling, J. D. *et al*. Understanding Lignin Micro- and Nanoparticle Nucleation and Growth in Aqueous Suspensions by Solvent Fractionation. *Green Chemistry* **2021**, *23* (2), 1001–10012.

(71) Duval, A. *et al*. Solvent Screening for the Fractionation of Industrial Kraft Lignin. *Holzforschung* **2016**, *70* (1), 11–20.

(72) Hansen, C. M. and Björkman. A. The Ultrastructure of Wood from a Solubility Parameter Point of View. *Holzforschung* **1998**, *52* (4), 335–344.

(73) Sadeghifar, H. *et al*. Perspective on Technical Lignin Fractionation. *ACS Sustain Chem Eng* **2020**, *8* (22), 8086–8101.

(74) Gioia, C. *et al*. Tunable Thermosetting Epoxies Based on Fractionated and Well-Characterized Lignins. *J Am Chem Soc* **2018**, *140* (11), 4054–4061.

(75) Passoni, V. *et al*. Fractionation of Industrial Softwood Kraft Lignin: Solvent Selection as a Tool for Tailored Material Properties. *ACS Sustain Chem Eng* **2016**, *4* (4), 2232–2242.

(76) Gordobil, O. *et al*. One-Step Lignin Refining Process: The Influence of the Solvent Nature on the Properties and Quality of Fractions. *Polymers* **2022**, *14* (12), 2363.

(77) Xu, Y. *et al*. γ-Valerolactone/Water System for Lignin Fractionation to Enhance Antibacterial and Antioxidant Capacities. *Sep Purif Technol* **2021**, *279*, 119780.

(78) Sadeghifar, H. *et al*. Fractionation of Organosolv Lignin Using Acetone:Water and Properties of the Obtained Fractions. *ACS Sustain Chem Eng* **2017**, *5* (1), 580–587.

(79) Wang, G. *et al*. Successive Ethanol–Water Fractionation of Enzymatic Hydrolysis Lignin to Concentrate Its Antimicrobial Activity. *Journal of Chemical Technology & Biotechnology* **2018**, *93* (10), 2977–2987.

(80) Balakshin, M. *et al*, Upgrading Lignin from Lignin-Containing Residues through Reactive Extraction, US10240006B2, **2015**.

(81) Jiang, X. *et al*. Lignin Fractionation from Laboratory to Commercialization: Chemistry, Scalability and Techno-Economic Analysis. *Green Chemistry* **2020**, *22* (21), 7448–7459.

(82) Zhao, W. *et al*. From Lignin Association to Nano-/Micro-Particle Preparation: Extracting Higher Value of Lignin. *Green Chemistry* **2016**, *18*, 5693–5700.

(83) Wang, G. *et al*. Fractionation of Alkali-Extracted Lignin from Steam-Exploded Stalk by Gradient Acid Precipitation. *Sep Purif Technol* **2013**, *105*, 98–105.

(84) Evstigneev, E. I. Factors Affecting Lignin Solubility. *Russian Journal of Applied Chemistry* **2011**, *84* (6), 1040–1045.

(85) Hubbe, M. *et al*. Lignin Recovery from Spent Alkaline Pulping Liquors Using Acidification, Membrane Separation, and Related Processing Steps: A Review. *BioRes.* **2014**, *14* (1), 2300–2351.

(86) Ragnar, M. *et al*. PKa-Values of Guaiacyl and Syringyl Phenols Related to Lignin. *Journal of wood chemistry and technology* **2000**, *20* (3), 277–305.

(87) Lourençon, T. V. *et al*. Hardwood and Softwood Kraft Lignins Fractionation by Simple Sequential Acid Precipitation. *Sep Purif Technol* **2015**, *154*, 82–88.

(88) Toledano, A. *et al*. Lignin Separation and Fractionation by Ultrafiltration. *Sep Purif Technol* **2010**, *71* (1), 38–43.

(89) Zhu, W. *et al*. Lignin Separation from Kraft Black Liquor by Combined Ultrafiltration and Precipitation: A Study of Solubility of Lignin with Different Molecular Properties. *Nord Pulp Paper Res J* **2016**, *31* (2), 270–278.

(90) Costa, C. A. E. *et al*. Lignin Fractionation from E. Globulus Kraft Liquor by Ultrafiltration in a Three Stage Membrane Sequence. *Sep Purif Technol* **2018**, *192*, 140–151.

(91) Hämäläinen, V. *et al*. Enzymatic Processes to Unlock the Lignin Value. *Front Bioeng Biotechnol* **2018**, *6*.

(92) Allegretti, C. *et al*. Two-Step Fractionation of a Model Technical Lignin by Combined Organic Solvent Extraction and Membrane Ultrafiltration. *ACS Omega* **2019**, *4* (3), 4615–4626.

(93) Figueiredo, P. *et al*. Green Fabrication Approaches of Lignin Nanoparticles from Different Technical Lignins: A Comparison Study. *ChemSusChem* **2021**, *14* (21), 4718–4730.

(94) Morsali, M. *et al*. Stabilized Lignin Nanoparticles for Versatile Hybrid and Functional Nanomaterials. *Biomacromolecules* **2022**, *23* (11), 4597–4606.

(95) Ago, M. *et al*. High-Throughput Synthesis of Lignin Particles (∼30 nm to ∼2 μm) *via* Aerosol Flow Reactor: Size Fractionation and Utilization in Pickering Emulsions. *ACS Appl. Mater. Interfaces* **2016**, *8* (35), 23302–23310.

(96) Alipoormazandarani, N. *et al*. Functional Lignin Nanoparticles with Tunable Size and Surface Properties: Fabrication, Characterization, and Use in Layer-by-Layer Assembly. *ACS Appl Mater Interfaces* **2021**, *13* (22), 26308–26317.

(97) Shomali, Z. et al. Carboxyalkylated Lignin Nanoparticles with Enhanced Functionality for Oil–Water Pickering Emulsion Systems. *ACS Sustain Chem Eng* **2022**, *10* (50), 16563–16577.

(98) Nypelö, T. E. *et al*. Lignin Supracolloids Synthesized from (W/O) Microemulsions: Use in the Interfacial Stabilization of Pickering Systems and Organic Carriers for Silver Metal. *Soft Matter* **2015**, *11* (10), 2046–2054.

(99) Ma, Y. *et al*. Solvent Effect on the Production of Spherical Lignin Nanoparticles. *Green Chemistry* **2023**, *25* (3), 993–1003.

(100) Österberg, M. *et al*. Biobased Nanomaterials─The Role of Interfacial Interactions for Advanced Materials. *Chem Rev* **2023**, 1*23* (5), 2200–2241.

(101) Andeme Ela, R. C. *et al*. Lignin Nanoparticle Morphology Depends on Polymer Properties and Solvent Composition: An Experimental and Computational Study. *ACS Appl Polym Mater* **2022**, *4* (10), 6925–6935.

(102) Pylypchuk, I. V. *et al*. Structural and Molecular-Weight-Dependency in the Formation of Lignin Nanoparticles from Fractionated Soft- and Hardwood Lignins. *Green Chemistry* **2021**, *23* (8), 3061–3072.

(103) Ou, J. *et al*. Revealing the Structural Influence on Lignin Phenolation and Its Nanoparticle Fabrication with Tunable Sizes. *ACS Sustain Chem Eng* **2022**, *10* (45), 14845–14854.

(104) Henn, A. *et al*. Interfacial Catalysis and Lignin Nanoparticles for Strong Fire- and Water-Resistant Composite Adhesives. *Green Chemistry* **2022**, *24*, 6487–6500.

(105) Jiang, X. *et al*. Phenolation to Improve Lignin Reactivity toward Thermosets Application. *ACS Sustain Chem Eng* **2018**, *6* (4), 5504–5512.

(106) Yang, S. *et al*. Characterization and Phenolation of Biorefinery Technical Lignins for Lignin–Phenol–Formaldehyde Resin Adhesive Synthesis. *RSC Adv* **2014**, *4* (101), 57996–58004.

(107) Morena, A. G. *et al*. Antibacterial Properties and Mechanisms of Action of Sonoenzymatically Synthesized Lignin-Based Nanoparticles. *ACS Appl Mater Interfaces* **2022**, *14* (33), 37270–37279.

(108) Du, X. *et al*. Modification of Industrial Softwood Kraft Lignin Using Mannich Reaction with and without Phenolation Pretreatment. *Ind Crops Prod* **2014**, *52*, 729–735.

(109) Yang, L. *et al*. Modification of Renewable Resources—Lignin—by Three Chemical Methods and Its Applications to Polyurethane Foams. *Polym Adv Technol* **2014**, *25* (10), 1089–1098.

(110) Zhang, Y. *et al*. Sustainable Bio-Phenol-Hydroxymethylfurfural Resins Using Phenolated de-Polymerized Hydrolysis Lignin and Their Application in Bio-Composites. *Ind Crops Prod* **2016**, *79*, 84–90.

(111) Jawerth, M. *et al*. Renewable Thiol-Ene Thermosets Based on Refined and Selectively Allylated Industrial Lignin. *ACS Sustain Chem Eng* **2017**, *5* (11), 10918–10925.

(112) Ribca, I. *et al*. Exploring the Effects of Different Cross-Linkers on Lignin-Based Thermoset Properties and Morphologies. *ACS Sustain Chem Eng* **2021**, *9* (4), 1692–1702.

(113) Miao, J. T. *et al*. Biobased Heat Resistant Epoxy Resin with Extremely High Biomass Content from 2,5-Furandicarboxylic Acid and Eugenol. *ACS Sustain Chem Eng* **2017**, *5* (8), 7003–7011.

(114) Rahman, M. *et al*. Significance of Polymers with Allyl Functionality in Biomedicine: An Emerging Class of Functional Polymers. *Pharmaceutics* **2022**, *14* (4), 798.

(115) Cao, Q. *et al*. A Well-Defined Lignin-Based Filler for Tuning the Mechanical Properties of Polymethyl Methacrylate. *Green Chemistry* **2021**, *23* (6), 2329–2335.

(116) Xu, Y. *et al*. Synthesis of Lignin-Based MMA-co-BA Hybrid Resins from Cornstalk Residue *via* RAFT Miniemulsion Polymerization and Their Characteristics. *Polymers* **2021**, *13* (6), 968.

(117) Najarro, M. C. *et al*. Tuning the Lignin-Caprolactone Copolymer for Coating Metal Surfaces. *ACS Appl Polym Mater* **2020**, *2* (12), 5767–5778.

(118) Cao, Y. *et al*. Synthesis of Lignin-Based Polyols *via* Thiol-Ene Chemistry for High-Performance Polyurethane Anticorrosive Coating. *Compos B Eng* **2020**, *200*, 108295.

(119) Duval, A. *et al*. Scalable Single-Step Synthesis of Lignin-Based Liquid Polyols with Ethylene Carbonate for Polyurethane Foams. *Mater Today Chem* **2022**, *24,* 100793.

(120) Shomali, Z. *et al*. Carboxyalkylated Lignin Nanoparticles with Enhanced Functionality for Oil-Water Pickering Emulsion Systems. *ACS Sustain Chem Eng* **2022**, *10* (50), 16563–16577.

(121) Li, B. *et al*. Structure-Tunable Assembly of Lignin Sub-Micro Spheres by Modifying the Amphiphilic Interfaces of Lignin *via* n-Alkane. *Eur Polym J* **2020**, *126*, 109539.

(122) Agustin, M. B. *et al*. Lignin Nanoparticle-Decorated Nanocellulose Cryogels as Adsorbents for Pharmaceutical Pollutants. *J Environ Manage* **2023**, *330*, 117210.

(123) Sipponen, M. H. *et al*. All-Lignin Approach to Prepare Cationic Colloidal Lignin Particles: Stabilization of Durable Pickering Emulsions. *Green Chemistry* **2017**, *19* (24), 5831–5840.

(124) Agustin, M. B. *et al*. Laccase as a Tool in Building Advanced Lignin-Based Materials. *ChemSusChem* **2021**, *14* (21), 4615–4635.

(125) Mehra, R. et al. A Structural-Chemical Explanation of Fungal Laccase Activity. *Scientific Reports* **2018**, *8* (1), 17285.

(126) Longe, L. F. *et al*. Importance of Mediators for Lignin Degradation by Fungal Laccase. *ACS Sustain Chem Eng* **2018**, *6* (8), 10097–10107.

(127) Guan, Z. B. *et al*. Bacterial Laccases: Promising Biological Green Tools for Industrial Applications. *Cellular and Molecular Life Sciences* **2018**, *75* (19), 3569–3592.

(128) Liu, Y. *et al*. Advances in Thermostable Laccase and Its Current Application in Lignin-First Biorefinery: A Review. *Bioresour Technol* **2020**, *298*, 122511.

(129) Mattinen, M. L. *et al*. Enzymatically and Chemically Oxidized Lignin Nanoparticles for Biomaterial Applications. *Enzyme Microb Technol* **2018**, *111*, 48–56.

(130) Chen, S. *et al*. Synthesis of Lignin-Functionalized Phenolic Nanosphere Supported Ag Nanoparticles with Excellent Dispersion Stability and Catalytic Performance. *Green Chemistry* **2020**, *22* (9), 2879–2888.

(131) Zou, T. *et al*. Solvent-Resistant Lignin-Epoxy Hybrid Nanoparticles for Covalent Surface Modification and High-Strength Particulate Adhesives. *ACS Nano* **2021**, *15* (3), 4811–4823.

(132) Wu, Q. *et al*. Green and Stable Lignin-Based Nanofillers Reinforced Poly(l-Lactide) with Supertough and Strong Performance. *Int J Biol Macromol* **2022**, *221*, 1041–1052.

(133) Moreno, A. *et al*. Breathable Lignin Nanoparticles as Reversible Gas Swellable Nanoreactors. *Small* **2023**, *19* (7), 2205672.

(134) Moreno, A. *et al*. Unravelling the Hydration Barrier of Lignin Oleate Nanoparticles for Acid- and Base-Catalyzed Functionalization in Dispersion State. *Angewandte Chemie - International Edition* **2021**, *60* (38), 20897–20905.

(135) Sun, Z. *et al*. Bright Side of Lignin Depolymerization: Toward New Platform Chemicals. *Chem Rev* **2018**, *118* (2), 614–678.

(136) Dessbesell, L. *et al*. Global Lignin Supply Overview and Kraft Lignin Potential as an Alternative for Petroleum-Based Polymers. *Renewable and Sustainable Energy Reviews* **2020**, *123*, 109768.

(137) Kalami, S. *et al*. Replacing 100% of Phenol in Phenolic Adhesive Formulations with Lignin. *J Appl Polym Sci* **2017**, *134* (30),45124.

(138) Frazier, C. E. Adhesion and Adhesives. Solid Wood Processing. *Encyclopedia of Forest Sciences* **2004**.

(139) Huang, C. *et al*. Unlocking the Role of Lignin for Preparing the Lignin-Based Wood Adhesive: A Review. *Ind Crops Prod* **2022**, *187*, 115388.

(140) Wu, Q. *et al*. A Separable Paper Adhesive Based on the Starch—lignin Composite. *Carbohydr Polym* **2020**, *229*, 115488.

(141) El Hage, R. *et al*. Extraction, Characterization and Utilization of Organosolv Miscanthus Lignin for the Conception of Environmentally Friendly Mixed Tannin/Lignin Wood Resins. *Journal of Adhesion science and Technology* **2011**, *25* (13), 1549–1560.

(142) Kadla, J. F. *et al*. Lignin-Based Carbon Fibers for Composite Fiber Applications. *Carbon* **2002**, *40* (15), 2913–2920.

(143) Gordobil, O. *et al*. Lignin-Ester Derivatives as Novel Thermoplastic Materials. *RSC Adv* **2016**, *6* (90), 86909–86917.

(144) Wang, C. *et al*. Lignin-Based Thermoplastic Materials. *ChemSusChem* **2016**, *9* (8), 770–783.

(145) Chow, K. S. *et al*. Insights into Rubber Biosynthesis from Transcriptome Analysis of Hevea Brasiliensis Latex. *J Exp Bot* **2007**, *58* (10), 2429–2440.

(146) Yong, Q. *et al*. Synthesis of Galactoglucomannan-Based Latex *via* Emulsion Polymerization. *Carbohydr Polym* **2022**, *291,* 119565.

(147) Charleux, B. *et al*. Preparation of Hybrid Latex Particles and Core–Shell Particles Through the Use of Controlled Radical Polymerization Techniques in Aqueous Media. *Advances in Polymer Science* **2010**, 125–183.

(148) Nasiri, A. *et al*. The Use of Lignin in Emulsion-Based Pressure-Sensitive Adhesives. *Int J Adhes Adhes* **2020**, *100,* 102598.

(149) Engström, J. *et al*. Core–Shell Nanoparticle Interface and Wetting Properties. *Adv Funct Mater* **2020**, *30* (15), 1907720.

(150) Stutman, D. R. *et al*. Mechanism of Core/Shell Emulsion Polymerization. *Industrial & engineering chemistry product research and development* **1985**, 24 (3), 404–412.

(151) Leksawasdi, N. *et al*. Corn Starch Reactive Blending with Latex from Natural Rubber Using Na^+ Ions Augmented Carboxymethyl Cellulose as a Crosslinking Agent. *Scientific Reports* **2021**, *11* (1), 19250.

(152) Dayse, L. *et al*. Thermal and Mechanical Properties of Cationic Starch-Graft-Poly(Butyl Acrylate-Co-Methyl Methacrylate) Latex Film Obtained by Semi-Continuous Emulsion Polymerization for Adhesive Application. *Journal of Thermal Analysis and Calorimetry* **2021**, *146*, 143–152.

(153) Kimiaei, E. *et al*. Lignin Nanoparticles as an Interfacial Modulator in Tough and Multi-Resistant Cellulose–Polycaprolactone Nanocomposites Based on a Pickering Emulsions Strategy. *Adv Mater Interfaces* **2022**, *9* (27), 2200988.

(154) Moreno, A. *et al*. Access to Tough and Transparent Nanocomposites *via* Pickering Emulsion Polymerization Using Biocatalytic Hybrid Lignin Nanoparticles as Functional Surfactants. *Green Chemistry* **2021**, *23* (8), 3001–3014.

(155) Cao, Q. *et al*. Size-Controlled Lignin Nanoparticles for Tuning the Mechanical Properties of Poly(Vinyl Alcohol). *Ind Crops Prod* **2021**, *172,* 114012.

(156) Gan, D. *et al*. Plant-Inspired Adhesive and Tough Hydrogel Based on Ag-Lignin Nanoparticles-Triggered Dynamic Redox Catechol Chemistry. *Nat Commun* **2019**, *10* (1), 1487.

(157) Tedeschi, G. *et al*. Multifunctional Bioplastics Inspired by Wood Composition: Effect of Hydrolyzed Lignin Addition to Xylan-Cellulose Matrices. *Biomacromolecules* **2020**, *21* (2), 910–920.

(158) Wang, H. M. *et al*. Advanced and Versatile Lignin-Derived Biodegradable Composite Film Materials toward a Sustainable World. *Green Chemistry* **2021**, *23* (11), 3790–3817.

(159) Gioia, C. *et al*. Lignin-Based Epoxy Resins: Unravelling the Relationship between Structure and Material Properties. *Biomacromolecules* **2020**, *21* (5), 1920–1928.

(160) de Haro, J. C. *et al*. Lignin-Based Polymer Electrolyte Membranes for Sustainable Aqueous Dye-Sensitized Solar Cells. *ACS Sustain Chem Eng* **2021**, *9* (25), 8550–8560.

(161) Wang, Y. *et al*. Polyurethanes Based on Unmodified and Refined Technical Lignins: Correlation between Molecular Structure and Material Properties. *Biomacromolecules* **2021**, *22* (5), 2129–2136.

(162) Romhányi, V. *et al*. Correlations among Miscibility, Structure, and Properties in Thermoplastic Polymer/Lignin Blends. *ACS Sustain Chem Eng* **2018**, *6* (11), 14323–14331.

(163) Li, Q. *et al*. Enhancing the Multi-Functional Properties of Renewable Lignin Carbon Fibers *via* Defining the Structure–Property Relationship Using Different Biomass Feedstocks. *Green Chemistry* **2021**, *23* (10), 3725–3739.

(164) Andeme Ela, R. C. *et al*. Lignin Nanoparticle Morphology Depends on Polymer Properties and Solvent Composition: An Experimental and Computational Study. *ACS Appl Polym Mater* **2022**, *4* (10), 6925–6935.

(165) Schwanninger, M. *et al*. Klason Lignin: Modifications to Improve the Precision of the Standardized Determination. *Holzforschung* **2002**, *56* (2), 161–166.

(166) Maekawa, E. *et al*. An Evaluation of the Acid-Soluble Lignin Determination in Analyses of Lignin by the Sulfuric Acid Method. *Journal of wood chemistry and technology* **1989**, *9* (4), 549–567.

(167) Sundberg, A. *et al*. Determination of Hemicelluloses and Pectins in Wood and Pulp Fibres by Acid Methanolysis and Gas Chromatography. *Nord Pulp Paper Res J* **1996**, *11* (4), 216–219.

(168) Zinovyev, G. *et al*. Getting Closer to Absolute Molar Masses of Technical Lignins. *ChemSusChem* **2018**, *11* (18), 3259–3268.

(169) Korntner, P. *et al*. Characterization of Technical Lignins by NMR Spectroscopy: Optimization of Functional Group Analysis by ^{31}P NMR Spectroscopy. *Holzforschung* **2015**, *69* (6), 807–814.

(170) Granata, A. *et al*. 2-Chloro-4,4,5,5-Tetramethyl-1,3,2-Dioxaphospholane, a Reagent for the Accurate Determination of the Uncondensed and Condensed Phenolic Moieties in Lignins. *J Agric Food Chem* **1995**, *43* (6), 1538–1544.

(171) Meng, X. *et al*. Determination of Hydroxyl Groups in Biorefinery Resources *via* Quantitative ^{31}P NMR Spectroscopy. *Nat Protoc* **2019**, *14* (9), 2627–2647.

(172) Li, Z. *et al*. Cleavage of Ethers and Demethylation of Lignin in Acidic Concentrated Lithium Bromide (ACLB) Solution. *Green Chemistry* **2020**, *22* (22), 7989–8001.

(173) Zhang, L. *et al*. Quantitative 2D HSQC NMR Determination of Polymer Structures by Selecting Suitable Internal Standard References. *Magn Reson Chem* **2007**, *45* (1), 37–45.

(174) Balakshin, M. *et al*. Structural Analysis of Hardwood Native Lignins by Quantitative ^{13}C NMR Spectroscopy. *Holzforschung* **2016**, *70* (2), 95–108.

(175) Balakshin, M. *et al*. Comprehensive Structural Analysis of Biorefinery Lignins with a Quantitative ^{13}C NMR Approach. *RSC Adv* **2015**, *5* (106), 87187–87199.

(176) Capanema, E. A. *et al*. A Comprehensive Approach for Quantitative Lignin Characterization by NMR Spectroscopy. *J Agric Food Chem* **2004**, *52* (7), 1850–1860.

(177) Christiansen, A. W. *et al*. Differential Scanning Calorimetry of Phenol-Formaldehyde Resols. *J Appl Polym Sci* **1985**, *30* (6), 2279–2289.

(178) Xu, W. *et al*. Surface Engineered Biomimetic Inks Based on UV Cross-Linkable Wood Biopolymers for 3D Printing. *ACS Appl. Mater. Interfaces* **2019**, *11* (13), 12389–12400.

(179) Pylypchuk, I. V. *et al*. New Insight into the Surface Structure of Lignin Nanoparticles Revealed by ^{1}H Liquid-State NMR Spectroscopy. *ACS Sustain Chem Eng* **2020**, *8* (36), 13805–13812.

(180) Farooq, M. *et al*. Well-Defined Lignin Model Films from Colloidal Lignin Particles. Langmuir **2020**, *36* (51), 15592–15602.

(181) Xiong, F. *et al*. Preparation and Formation Mechanism of Renewable Lignin Hollow Nanospheres with a Single Hole by Self-Assembly. *ACS Sustain Chem Eng* **2017**, *5* (3), 2273–2281.

(182) Pang, T. *et al*. Lignin Fractionation for Reduced Heterogeneity in Self-Assembly Nanosizing: Toward Targeted Preparation of Uniform Lignin Nanoparticles with Small Size. *ACS Sustain Chem Eng* **2020**, *8* (24), 9174–9183.

(183) Zhang, L. *et al*. Lignin-Directed Control of Silver Nanoparticles with Tunable Size in Porous Lignocellulose Hydrogels and Their Application in Catalytic Reduction. *ACS Sustain Chem Eng* **2020**, *8* (33), 12655–12663.

(184) Christiansen, A. W. *et al*. Differential Scanning Calorimetry of Phenol-Formaldehyde Resoles. *J. Appl. Polym. Sci* **1985**, *30* (6), 2279–2289.

(185) Park, B. D. *et al*. Differential Scanning Calorimetry of Phenol-Formaldehyde Resins Cure-Accelerated by Carbonates. *Polymer* **1999**, *40* (7), 1689–1699.

(186) Vaishali Sethi, S. *et al*. Understanding the Role of Co-Surfactants in Microemulsions on the Growth of Copper Oxalate using SAXS. *Phys. Chem. Chem. Phys* **2019**, *21*, 17441.

(187) Liu, L. *et al*. Visualization of Film-Forming Polymer Particles with a Liquid Cell Technique in a Transmission Electron Microscope. *Analyst* **2015**, *140* (18), 6330–6334.

ISBN 978-952-12-4314-1